

國立交通大學

光電工程研究所

博士論文

Fabrication and Characterization of  
Advanced Fiber Bragg Gratings

先進光纖光柵之製作與特性量測



研究生：莊凱評

指導教授：賴暎杰 博士

中華民國九十三年六月

# Fabrication and Characterization of Advanced Fiber Bragg Gratings

## 先進光纖光柵之製作與特性量測

研究生：莊凱評

Student : Kai-Ping Chuang

指導教授：賴暎杰 博士

Advisor : Dr. Yinchieh Lai



國立交通大學 電機資訊學院  
光電工程研究所  
博士論文

A Dissertation  
Submitted in Partial Fulfillment of the Requirements  
for the Degree of Doctor of Philosophy in  
The Institute of Electro-Optical Engineering  
National Chiao-Tung University  
Hsin-Chu, Taiwan, R.O.C.

中華民國 九十三年 六月

# 先進光纖光柵之製作與特性量測

研究生：莊凱評

指導教授：賴暎杰 博士

國立交通大學 電機資訊學院

光電工程研究所

## 摘要

隨著光纖光柵在光纖通訊及光纖感測領域被發現有越來越多的應用，致力於改善光纖光柵的製作與特性量測對於製作具有特殊光學特性的濾波元件而言就顯得非常重要。在本論文中，我們利用逆散射之剝層 (layer-peeling) 法來設計先進的光纖光柵結構，並根據實驗的實際製作架構，使用最小方差逼近 (least-square fitting) 法來找出最佳的光纖光柵曝照參數。

在製作具有複雜結構之先進光纖光柵方面，我們提出了三個新的製作光纖光柵的方法。第一個方法我們稱之為偏振控制雙光束干涉法，第二個方法稱之為偏振控制相位光罩法，這兩個製作方法目的都是利用曝照光束偏振的特性，在製作光纖光柵逐段曝照過程中既可以任意控制光柵折射率 (ac-index) 的大小，同時又可以保持光柵不同位置的平均折射率 (dc-index) 為定值。藉著利用這些方法，具有低損耗及良好頻譜響應的濾波元件可以順利的被完成。第三個方法是干涉式側向繞射光柵位移監控的技術，我們提出這個光學監控方法來製作具有較長長度的光纖光柵元件。我們成功完成一些實驗的例子來證明這些方法的可行性，也利用 LabView 的自動控制

軟體來建立自動化的光柵曝照系統，藉此可以提升光纖光柵製作過程的準確性及重複性。

在光纖光柵特性量測方面，我們發展光纖式麥克森干涉儀（the balanced Michelson interferometer）的方法及側向繞射（side-diffraction）量測技術來分析光纖光柵完整的特性，包括光柵的複數反射係數及複數耦合係數等，這些係數代表著光纖光柵所有的光學和結構參數。當我們再結合逆散射之剝層法反推時，光纖光柵不同位置的平均折射率變化也可以求得。對未來先進光纖光柵製程的改善工作，這些特性的分析方法希望能夠有所幫助。



# Fabrication and Characterization of Advanced Fiber Bragg Gratings

Student: Kai-Ping Chuang

Advisor: Dr. Yinchieh Lai

Institute of Electro-Optical Engineering  
College of Electrical Engineering and Computer Science  
National Chiao-Tung University

## ABSTRACT

When the FBG devices begin to find a lot of applications in fiber communication and fiber sensing, it also becomes more important to further improve the FBG fabrication and characterization techniques for achieving more complex optical filter properties. In this thesis, in order to design the advanced fiber grating structures, the layer peeling inverse design method combined with the least square fitting method is developed. Based on these synthesis methods, the best experimental parameters for our sequential writing setup can be found.

For the fabrication of advanced fiber grating structures, we have also proposed three new exposure methods. One is the two-beam interferometer method with the polarization control, and another is the phase mask method with the polarization control. Both of them have the same purpose for achieving a controllable ac-index profile in a single scan, with the dc-index profile being kept constant during the scan. The spectral shapes with a steep edge, very low sidelobes, a flat top, and very little ripples can be achieved by the use of these methods. The third method is the interferometric side-diffraction position monitoring technique for writing long fiber Bragg gratings. Some examples are presented to demonstrate the feasibility of these

methods. The automation of the exposure system has also been setup for enhancing the accuracy and repetibility of the fabrication process.

In order to determine the complete characteristics of the fiber gratings, we develop the balanced Michelson interferometer method and the side-diffraction technique. The characteristics to be determined include the measurement of the complex reflection coefficient and the complex coupling coefficient of the grating. When the discrete layer peeling method is combined with these two measurement methods, we can get all of the information about the grating structure including the dc-index change. In addition, this analysis process may also be helpful for improving the fabrication processes of advanced FBGs.



## Acknowledgement

在這四年的攻讀博士生涯裏，實驗設備的從無到有以及到論文期刊的發表，指導教授賴暎杰博士的悉心教導與支持給了我研究過程中最大的幫助。記得在博二到博三的這段求學期間，因為新的實驗架構遲遲無法完成，以致於無法順利的發表文章，在心裡有點急的情況下求助於老師，記得當時老師的一句話“只要一天比一天實驗有所進展，就很好了。”，也是因為抱持著這樣的信念，能讓自己一步一步的完成博士學業。在此，由衷的感謝賴教授的細心教導。

光纖光柵實驗室的建立過程中，也多虧了所辦湯敏雄先生及實驗室學弟妹的幫忙，尤其是學弟妹孟璋、易霖、慧萍、夙鴻及淑慧在實驗上的幫助，實驗室才能夠建立的如此完善，在此一併致謝。此外，要特別感謝澄鈴學姊、許立根博士、瑞光、維巍及桂珠同學，除了在學業的討論上給了很大的幫助外，也給了我博士求學生涯中多采多姿的生活。

家，可以說是我的最後精神堡壘，非常感激我的父母和弟弟這四年來的全力支持，讓我無後顧之憂，得以專心的取得博士學位。女朋友虹雯的鼓勵與陪伴，使我這一路走來無怨無悔，伴我渡過最困難的時期。在此，將此論文獻給所有關心我的人。

# Contents

Chinese Abstract.....	I
English Abstract.....	III
Acknowledgement.....	V
Contents.....	VI
List of Figures.....	VIII
List of Acronyms.....	XIV
List of Symbols.....	XV

## Chapter 1. Introduction

1.1 Brief Review of Fiber Bragg Gratings.....	1
1.2 Motivation and Approach of the Research.....	3
1.3 Organization of the Dissertation.....	5

## Chapter 2. Synthesis of Fiber Bragg Gratings

2.1 Introduction.....	12
2.2 Fundamentals of Fiber Bragg Gratings.....	12
2.3 Different Types of Fiber Bragg Gratings.....	14
2.3.1 Uniform Fiber Bragg Gratings.....	15
2.3.2 Phase-shifted Fiber Bragg Gratings.....	15
2.3.3 Apodized Fiber Bragg Gratings.....	16
2.3.4 Chirped Fiber Bragg Gratings.....	16
2.4 Coupled-Mode Theory.....	17
2.5 Discrete Layer-Peeling Method.....	18
2.6 Least Square Method.....	21

2.7 Summary.....22

**Chapter 3. Characterization of Fiber Bragg Gratings**

3.1 Introduction.....34  
3.2 The Balanced Michelson Interferometer Method.....34  
3.3 The Side-Diffraction Technique.....36  
3.4 Characterization of Fiber Gratings.....39  
3.5 Summary.....43

**Chapter 4. Fabrication of Advanced Fiber Bragg Gratings**

4.1 Introduction.....67  
4.2 Setup of the Exposure System.....68  
4.3 Two-Beam Interferometer Method with Polarization  
Control.....70  
4.4 Phase Mask Method with Polarization Control.....75  
4.5 Interferometric Side-Diffraction Position Monitoring  
Technique for Writing Long Fiber Bragg Gratings.....80  
4.6 Summary.....85

**Chapter 5. Conclusions and Future Work**

5.1 Conclusions.....124  
5.2 Future Work.....126

**List of Publications.....127**

## List of Figures

Fig.2.1	The refractive-index modulation along the length of waveguides .....	26
Fig.2.2	The common types of fiber Bragg gratings; (a) uniform FBGs, (b) phase-shift FBGs, (c, d) apodized FBGs, and (e) chirped FBGs.....	27
Fig.2.3	(a) The spectra of three Bragg gratings with different coupling constants of 2, 4, and 8.; (b) time delay of the same gratings as in Fig. 2.3(a).....	28
Fig.2.4	A $\pi$ -phase shift uniform fiber Bragg grating. (the parameters are $kL=1.6$ and $L=5$ mm).....	29
Fig.2.5	(a) A Gaussian apodized FBG with non-constant dc index; (b) a pure apodization FBG with a Gaussian index profile.....	30
Fig.2.6	A chirped FBG with the grating length = 30 mm, chirped rate = 0.1667 nm/cm, and a tanh index profile. (a) The reflection and transmission spectra; (b) the phase and time delay.....	31
Fig.2.7	The description of the inverse and the forward methods for the synthesis and analysis of fiber gratings.....	32
Fig.2.8	A discretized model of the LP method.....	33
Fig.3.1	Fabry-Perot cavity consisting of a fiber Bragg grating and a reference reflector.....	47
Fig.3.2	Experimental setup of the balanced Michelson interferometer.	48
Fig.3.3	The interference $I_{inter}(\lambda)$ of combined signals.....	49
Fig.3.4	The inverse Fourier transform of $I_{inter}(\lambda)$ .....	49

Fig.3.5	The algorithm for finding the phase spectrum of the fiber grating.....	50
Fig.3.6	(a)The measured interference pattern $I_{\text{inter}}(\lambda)$ , (b)The calculated phase spectrum $\phi(\delta)$ . (cited from [12]).....	51
Fig.3.7	(a) Measured results using a commercial equipment “Advantest Q7760”, and (b) our measuring method. (cited from [12])....	52
Fig.3.8	The side-diffraction setup for measuring index modulation: M, reflection mirror; SL, spherical lens.....	53
Fig.3.9	The side-diffraction interference method for measuring grating period change: BS, beam splitter; M, reflection mirror; SL, spherical lens.....	54
Fig.3.10	The improved side-diffraction interference method for measuring the grating period variation and the ac-index modulation.....	55
Fig.3.11	Flow chart of the characterization method of fiber gratings.	56
Fig.3.12	The balanced Michelson interferometer setup used to measure the highly reflecting fiber gratings.....	57
Fig.3.13	The reflection spectrum and interference pattern by the use of the balanced Michelson interferometer method.....	58
Fig.3.14	The calculated phase information of the grating.....	59
Fig.3.15	(a) The Ac-index modulation from the DLP is compared with the side-diffraction method. (b) The Ac-index modulation from the DLP is compared with the side-diffraction interference method.....	60
Fig.3.16	The spatial grating phase is calculated from DLP method.....	61

Fig.3.17 The reflection spectra of the target and the calculated result from DLP method.....	62
Fig.3.18 The group time delays of the target and the calculated result from DLP method.....	63
Fig.3.19 The CCD interference period corresponds to the relative grating period.....	64
Fig.3.20 (a) dc-index amplitude $\Delta n_{dc}(z) = 0$ .....	65
Fig.3.20 (b) dc-index amplitude $\Delta n_{dc}(z) = \text{ac-index amplitude } \Delta n_{ac}(z) * 0.5$ .....	65
Fig.3.20 (c) dc-index amplitude $\Delta n_{dc}(z) = \text{ac-index amplitude } \Delta n_{ac}(z) * 1$ .....	66
Fig.3.20 (d) dc-index amplitude $\Delta n_{dc}(z) = \text{ac-index amplitude } \Delta n_{ac}(z) * 1.3$ .....	66
Fig.4.1 An auto-controlled FBG exposure system based on the two exposure methods of a phase mask and a two-beam interferometer.....	89
Fig.4.2 The way to flatten the dc-index of the fiber grating.....	90
Fig.4.3 The reflection and transmission spectra of the four channel FBG filter.....	91
Fig.4.4 Narrow-band filter by 100 sequences of step writing.....	92
Fig.4.5 (a) The reflection and transmission spectra, and (b) the phase and time delay of the simulated chirped FBG.....	93
Fig.4.6 The experimental result of a 10cm long chirped FBG.....	94
Fig.4.7 The Labview program for fabricating FBG.....	95
Fig.4.8 Schematic diagram of fiber Bragg grating fabrication system by	

	using two-beam interferometer method with polarization control.....	96
Fig.4.9	The refractive index profile at each sequential position of fiber .....	97
Fig.4.10	(a) The relation of the half-wave plate angle and the refractive index modulation amplitude along the FBG position and (b) experimental and theoretical results for the refractive index modulation versus the rotation angle of the half-wave plate...	98
Fig.4.11	The non-linear effect of refractive index change depends on a power law.....	99
Fig.4.12	(a) Reflection spectra of the $\cos^2$ pure apodized (experiment) and ordinarily apodized (simulation) FBGs and (b) reflection and transmission spectra of a $\pi$ -phase-shifted FBG.....	100
Fig.4.13	The reflection spectrum of pure gaussian-apodization FBG influences from the UV-induced birefringence.....	101
Fig.4.14	The Labview program is used to control the two-beam interferometer method with the polarization control.....	102
Fig.4.15	Experimental setup for writing complex fiber grating structures: s and f, slow and fast axes of half-wave plate.....	103
Fig.4.16	A constant dc-index structure and its reflection spectrum.....	104
Fig.4.17	A non-constant dc-index structure and its reflection spectrum	105
Fig.4.18	A non-constant dc-index structure and its reflection spectrum	106
Fig.4.19	The way of achieving a constant dc refractive index change...	107
Fig.4.20	The reflection spectra of a pure apodized FBG and an ordinary apodized FBG with non-constant dc index.....	108

Fig.4.21	Plots of the coupling coefficient reconstructed from a dispersionless reflection spectrum.....	109
Fig.4.22	Target and calculated reflection and group delay spectra from DLP.....	110
Fig.4.23	The normalized refractive-index profile and phase of the designed dispersionless FBG.....	111
Fig.4.24	The spectral response calculated from DLP before and after using the least square fitting.....	112
Fig.4.25	(a) The measured reflection and time delay spectra of the dispersionless FBG and (b) the simulated reflection and time delay spectra of the “standard” Gaussian-apodized FBG.....	113
Fig.4.26	The PMD and CD measurement of the dispersionless FBG...	114
Fig.4.27	The calculated birefringence from PMD and CD by equation (4.3).....	115
Fig.4.28	The Labview program is used to fabricate FBG by use of the phase mask method with the polarization control.....	116
Fig.4.29	Traditional position monitoring method.....	117
Fig.4.30	Experimental setup for fabricating and monitoring fiber grating: SL, spherical lens; M, reflecting mirror; BS, beam splitter; PBS, polarization beam splitter; HWP, half-wave plate; BC, beam combiner; $\theta_1$ , the angle of the FBG writing beams; $\theta_2$ , the input angle of the probe beam; $\theta_3$ , the interfering angle of the probe and the reference beams.....	118
Fig.4.31	The Labview program of side-diffraction monitoring method for fabricating long FBG.....	119

Fig.4.32 Algorithm for calculating the phase of interference pattern....120

Fig.4.33 A typical experimental interference pattern and the calculated phase distribution.....121

Fig.4.34 The overlap-step-scan exposure method.....122

Fig.4.35 The reflection and transmission spectra of a 75-mm long gaussian apodized FBG with a constant dc refractive index along the whole grating.....123



## List of Acronyms

<u>Acronyms</u>	<u>Descriptions</u>
FBG	Fiber Bragg Grating
GLM	Gel'fand-Levitan-Marchenko
LP	Layer Peeling
GA	Genetic Algorithms
EA	Evolutionary Algorithms
DLP	Discrete Layer Peeling
LS	Least Square
DFB	Distributed Feedback
FP	Fabry-Perot
OSA	Optical Spectrum Analyzer
PZT	Piezoelectric Translator



## List of Symbols

<u>Symbols</u>	<u>Descriptions</u>
$\lambda_B$	Bragg wavelength
$n_{eff}$	effective modal index
$\Lambda$	grating period
$\delta$	wavenumber detuning
$\beta$	propagation constant
$\theta(z)$	spatial grating phase
$\phi(\lambda)$	spectrum phase
$\Delta n(z)$	refractive index change
$\Delta n_{ac}(z)$	ac refractive-index change
$\Delta n_{dc}(z)$	dc refractive-index change
$\Delta\Lambda$	grating period change
$\bar{n}(x, y)$	the index change of the unperturbed fiber
$n(x, y, z)$	the index change of the perturbed fiber
$u(z)$	the envelope of the forward field
$v(z)$	the envelope of the backward field
$r$	reflection coefficient
$t$	transmission coefficient
$\rho_j$	complex reflection coefficient of the j-th section
$q(z)$	complex coupling coefficient
$\tau_g$	group delay time
$k$	grating vector
$h$	impulse response

$\Delta$	grating section distance
$A_m(z)$	the refractive index envelope of the m-th small gaussian beam
$w_s$	the width of the gaussian beam
$P_d$	the first-order diffraction power]



# Chapter 1. Introduction

## 1.1 Brief Review of Fiber Bragg Gratings

A fiber Bragg grating (FBG) is a section of the optical fiber in which the refractive index of the core is perturbed to form a periodic index modulation profile. When the reflection from a period of the grating is in phase with that from the next period, maximum mode coupling or reflection occurs and the Bragg condition is fulfilled:

$$\lambda_B = 2n_{eff} \Lambda \quad (1.1)$$

Here  $\lambda_B$  is the Bragg wavelength,  $n_{eff}$  is the effective modal index and  $\Lambda$  is the perturbation period.

The formation of permanent gratings by the photosensitivity in an optical fiber was first demonstrated by Hill et al. [1] in 1978. Here photosensitivity means that the exposure of UV lights will lead to a rise in the refractive index of certain doped glasses. Fiber gratings are usually fabricated by a variant of the transverse holographic method first proposed by Meltz et al. [2] in 1989. Afterward, the phase mask technique [3-5] has been widely used recently, which has the advantages of less-stringent requirements on the UV source, simplifying the manufacturing process and yet yielding fiber gratings with high performance. In order to write long, complex fiber gratings with advanced characteristics, the schemes of sequential writing have been proposed [6-8].

Because a fiber grating can be designed to have an almost arbitrary and complicated reflection response, it has a variety of applications as are well described by Hill and Meltz [9]. For telecommunication, the two most promising applications have been the wavelength selective devices [10-12] and the dispersion compensation devices [13-14]. FBGs have also

become popular as sensing devices in applications ranging from structural monitoring to chemical sensing [15-17]. Another noteworthy application of fiber gratings is to be used as the narrowband reflectors for fiber lasers [18-20].

In order to adopt fiber gratings for various applications, it is important to have tools for synthesis, fabrication and characterization of special fiber grating devices. The most common mathematical model that describes wave propagation in fiber gratings is the coupled-mode theory [21]. The synthesis problem of gratings amounts to finding the grating structure (grating amplitude and phase or equivalently the coupling constant) from a pre-specified, complex reflection or transmission spectrum. These popular inverse algorithms include Gel'fand-Levitan-Marchenko (GLM) inverse-scattering method [22-23], Layer-Peeling (LP) inverse-scattering algorithms [24-26], Genetic Algorithm (GA) method [27] and Evolutionary Algorithms (EA) [28-29].

The increasing complexity and more-demanding specifications of fiber gratings for these applications require increasingly precise measurement of the grating parameters. Characterization of FBGs means to determine the complex reflection coefficient or the complex coupling coefficient of the grating. Indirect methods for characterizing fiber-grating profiles based on the measured reflection and transmission spectra can be achieved by the inversion techniques [22-29]. Although in principle such techniques are very powerful, their inherent limitations (due to noise, for example) as well as the demonstration of their practical application have yet to be shown. In addition, such methods are not necessarily efficient in determining the precise nature and the location of the defects in the written grating structure. The direct methods are usually based on interferometry [30-33], side-diffraction [34-36] or heat-scan method [37]. In Ref.31, a simple interferometric approach was used to characterize the weak fiber gratings. The group delay of the grating (or grating phase) can be obtained from measurement of the interference fringes from the grating and a reference reflector. By

using the side-diffraction or heat-scan technique, the grating index amplitude and period change can be obtained. One can also combine the inverse algorithms methods with the direct characterization methods to find the complex coupling coefficient of the grating [38]. With these powerful tools, the design, fabrication and characterization of advanced fiber gratings can be achieved for various practical applications.

## **1.2 Motivation and Approach of the Research**

Advanced fiber Bragg gratings with special structures have become popular for various practical applications in modern fiber communication systems. Design, fabrication and characterization techniques of fiber gratings must be developed to meet the stringent requirements of fiber communication. In this work, for the design of advanced fiber gratings, the problem will be treated by the layer-peeling inverse synthesis method. The method is fast and accurate, and amounts to finding the grating structure (grating amplitude and phase) from a specified, complex spectrum. In this respect we will refer to the results achieved by Skaar et. al. [26]. He simplified the discrete layer-peeling (DLP) synthesis method proposed by Feced et. al. [24] to improve its clarity and efficiency. In order to meet the requirement of practical fabrication, the Least Square (LS) method [39] has been utilized to find the best experimental parameters for our sequential writing setup.

In particular, the FBGs can act as the channel multiplexer-demultiplexers or the dispersion compensators in dense wavelength division multiplexing (DWDM) systems, in which the requirements for the optical filter properties are very stringent. The spectral shape of these optical filters needs to have a steep edge, very low sidelobes, and a flat top with very little ripples. For FBG filters to meet these requirements, it is important to apodize the FBG structure such that its dc-index change remains a constant across the whole grating (pure

apodization). For more advanced FBGs like dispersionless FBGs, multiple  $\pi$ -phase shifts are also required. After we find the structure parameters of these fiber gratings from the DLP technique, the practical fabrication method for implementing these structures will become the most important issue. In the literature, several fabrication methods for these so-called pure apodized and/or phase-shifted FBGs have been developed. The double-UV exposure methods [40-42] need a two-stage exposure process and the variable-diffraction-efficiency phase mask method [4] needs a special designed mask. The phase mask dithering method [5] adopts mask dithering to achieve a constant dc refractive-index change during a single scan, but it will more easily induce extra vibration for the interferometric control of the relative position between the fiber and the phase mask. Recently it was shown that the apodized FBGs with constant average index and phase shifts can be fabricated by using a phase mask polarization control method [6]. However, in this method the FBG length is limited by the size of the phase mask and the precision adjustment of the fiber-to-phase-mask distance and the polarizer alignment are needed. In order to practically achieve the purposes of pure apodization index profiles, multiple  $\pi$ -phase shifts and long fiber grating length, in this work we propose and demonstrate three new methods which are capable of fabricating FBGs with these complex structures. The first method is based on the two-beam interferometer technique with the polarization control on one of the interfering beams. The second method is also based on the polarization control of the exposure UV beam, and can be combined with the sequential writing setup based on either the two-beam interference or the phase-mask approach to produce pure apodized complicated FBGs in a single scan. The third method is based on the side-diffraction interference technique, which is capable of monitoring the fiber grating position without the accumulative error due to the drift of the interferometer and inaccurate grating period.

The increasing complexity and more-demanding specifications of fiber gratings for

various applications require increasingly precise measurement of the grating parameters. For the characteristics measurement of fiber gratings, we develop two direct methods to measure the important grating parameters including the grating phase ( ), the refractive index change ( $\Delta n$ ) and the grating period change ( $\Delta \Lambda$ ). The two methods are the balanced Michelson interferometer technique for measuring the spectrum phase information and the side-diffraction technique for measuring the refractive index change and the grating period change. These methods are efficient in determining the precise nature and the location of the defects in the written grating structure. The accurate measurement of grating parameters is useful for the design and fabrication of FBGs. The causal relationship among characterization, design and fabrication will be helpful for finding the system error of the FBG exposure setup. Eventually this system error may also be taken into account in the design of the FBG structure from the beginning [43].



### **1.3 Organization of the Dissertation**

The main organization of this thesis can be divided into three parts, which include the theoretical analyses, the characterization methods and the fabrication methods of the fiber gratings. In the introductory chapter, we describe the history of the fiber gratings and the purposes of this thesis research. It contains the review of the previous works and the challenges of the proposed methods. The chapter 2 describes the synthesis of fiber gratings, which include a short introduction on various types of fiber gratings and the developed methods for the design of complex fiber grating structures. In chapter 3, we improve the measurement methods based on the balanced Michelson interferometer method and the side-diffraction technique for the characterization of fiber gratings. The complex reflection spectrum and the complex coupling coefficient can be obtained by using the proposed

analysis process. In chapter 4, we setup the auto-controlled fabrication system and propose three new fabrication methods to actually fabricate advanced fiber gratings with the desired complex grating structures. The proposed methods can be based on the phase mask or the two-beam interferometer setups to write long, complex fiber gratings. We also develop the Labview program to control the fabrication process. So that the accuracy and repetibility of the fabrication process can be enhanced. Finally, in chapter 5 we draw a conclusion of this research and provide directions for performing further research related to this topic.



## References for Chapter 1:

- [1] K. O. Hill, Y. Fujii, D. C. Johnsen, and B. S. Kawasaki, "Photosensitivity in optical fiber waveguide: Application to reflection filter fabrication," *Appl. Phys. Lett.*, vol. 32, pp.647-649, 1978.
- [2] G. Meltz, W. W. Morey, and W. H. Glenn, "Formation of Bragg gratings in optical fibers by a transverse holographic method," *Opt. Lett.*, vol. 14, pp. 823-825, 1989.
- [3] K. O. Hill, B. Malo, F. Bilodeau, D. C. Johnson, and J. Albert, "Bragg gratings fabricated in monomode photosensitive optical fiber by UV exposure through a phase mask," *Appl. Phys. Lett.*, vol. 62, pp.1035-1037, 1993.
- [4] J. Albert, K. O. Hill, B. Malo, S. Theriault, F. Bilodeau, D. C. Johnson, and L. E. Erickson, "Apodisation of the spectral response of fiber Bragg gratings using a phase mask with variable diffraction efficiency," *Electron. Lett.*, vol. 31, pp. 222-223, 1995.
- [5] W. H. Loh, M. J. Cole, M. N. Zervas, S. Barcelos, and R. I. Laming, "Complex grating structures with uniform phase masks based on the moving-scanning beam technique," *Opt. Lett.*, vol. 20, pp. 2051-2053, 1995.
- [6] J. B. Jensen, M. Plougmann, H. -J. Deyerl, P. Varming, J. Hubner, and M. Kristensen, "Polarization control method for ultraviolet writing of advanced Bragg gratings," *Opt. Lett.*, vol. 27, pp. 1004-1006, 2002.
- [7] A. Asseh, H. Storoy, B. E. Sahlgren, S. Sandgren, and R. Stubbe, "A writing technique for long fiber Bragg gratings with complex reflectivity profiles." *J.Lightwave Tech.*, vol. 15, pp. 1419-1423, 1997.
- [8] I. Petermann, B. Sahlgren, S. Helmfrid, A. T. Friberg, and P.-Y. Fonjallaz, "Fabrication of advanced fiber Bragg gratings by use of sequential writing with a continuous-wave ultraviolet laser source," *Appl. Opt.*, vol. 41, pp. 1051-1056, 2002.
- [9] K. O. Hill, G. Meltz, "Fiber Bragg Grating Technology: Fundamentals and Overview," *J.*

Lightwave Tech., vol. 15, pp. 1263-1276, 1997.

- [10] I. Baumann, J. Seifert, W. Nowak, and M. Sauer, "Compact all-fiber add-drop multiplexer using fiber Bragg gratings," *IEEE Photon. Technol. Lett.*, vol. 8, pp. 1331-1333, 1996.
- [11] M. Ibsen, R. Feced, P. Petropoulos and M. N. Zervas, "99.9% reflectivity dispersion-less square-filter fibre Bragg gratings for high speed DWDM networks," *Optical Fiber Communication Conference*, pp. 230-232, 2000.
- [12] M. Ibsen, "Advanced fibre Bragg grating design and technology," *Optical Communication, ECOC'01 27<sup>th</sup> European Conference*, vol. 5, pp. 181-182, 2001.
- [13] J. A. R. Williams, K. S. I. Bennion, and N. J. Doran, "Fiber dispersion compensation using a chirped in-fiber Bragg grating," *Electron. Lett.*, vol. 30, pp. 985-987, 1997.
- [14] W. H. Loh, F. Q. Zhou, and J. J. Pan, "Sampled fiber grating based dispersion slope compensator," *IEEE Photon. Technol. Lett.*, vol. 11, pp. 1280-1282, Oct. 1999.
- [15] A. D. Kersey, M. A. Davis, H. J. Patrick, M. LeBlanc, K. P. Koo, C. G. Askins, M. A. Putnam, and E. J. Friebele, "Fiber grating sensors," *J. Lightwave Tech.*, vol. 15, pp. 1442-1463, 1997.
- [16] Youlong Yu, Hwayaw Tam, Wenghong Chung, and Muhtesem Suleyman Demokan, "Fiber Bragg grating sensor for simultaneous measurement of displacement and temperature," *Opt. Lett.*, vol. 25, pp. 1141-1143, 2000.
- [17] Sarfraz Khaliq, Stephen W. James, and Ralph P. Tatam, "Fiber-optic liquid-level sensor using a long-period grating," *Opt. Lett.*, vol. 26, pp. 1224-1226, 2001.
- [18] J. T. Kringlebotn, J. L. Archambault, L. Reekie, and D. N. Payne, "Er<sup>3+</sup>:Yb<sup>3+</sup>-codoped fiber distributed-feedback laser," *Opt. Lett.* 19, pp. 2101-2103, 1994.
- [19] W. H. Loh, B. N. Samson, L. Dong, G. J. Cowle, and K. Hsu, "High Performance Single Frequency Fiber Grating-Based Erbium:Ytterbium-Codoped Fiber Lasers," *J. Lightwave*

- Tech., vol. 16, pp. 114-118, 1998.
- [20] M. Ibsen, S. Y. Set, G. S. Goh, and K. Kikuchi, "Broad-Band Continuously Tunable All-Fiber DFB Lasers," *IEEE Photon. Technol. Lett.*, vol. 14, pp. 21-23, 2002.
- [21] T. Erdogan, "Fiber Grating Spectra," *J. Lightwave Tech.*, vol. 15, pp.1277-1294, 1997.
- [22] G-W. Chern and L. A. Wang, "Analysis and design of almost-periodic vertical-grating-assisted codirectional coupler filters with nonuniform duty ratios," *Appl. Opt.*, vol. 39, pp. 4926-4937, 2000.
- [23] G. H. Song, "Toward the ideal codirectional Bragg filter with an acoustooptic-filter design," *J. Lightwave Tech.*, vol. 13, pp.470-480, 1995.
- [24] R. Feced, M. N. Zervas, and M. A. Muriel, "An efficient inverse scattering algorithm for the design of nonuniform fiber Bragg gratings," *IEEE J. Quantum Electron.*, vol. 35, pp. 1105-1115, 1999.
- [25] L. Poladian, "Simple grating synthesis algorithm," *Opt. Lett.*, vol. 25, pp. 787-789, 2000.
- [26] J. Skaar, L. Wang, and T. Erdogan, "On the synthesis of fiber Bragg gratings by layer peeling," *IEEE J. Quantum Electron.*, vol. 37, pp.165-173, 2001.
- [27] J. Skaar and K. M. Risvik, "A genetic algorithm for the inverse problem in synthesis of fiber gratings," *J. Lightwave Tech.*, vol. 16, pp. 1928-1932, 1998.
- [28] Thomas Back, "Evolutionary Algorithms in Theory and Practice," Oxford, New York, 1996.
- [29] Cheng-Ling Lee and Yinchieh Lai, "Evolutionary programming synthesis of optimal long-period fiber Bragg filters for EDFA gain flattening," *IEEE Photon. Technol. Lett.*, vol. 14, pp. 1557-1559, 2002.
- [30] Mark Froggatt, "Distributed measurement of the complex modulation of a photoinduced Bragg grating in an optical fiber," *Appl. Opt.*, vol. 35, pp. 5162-5164, 1996.
- [31] J. Skaar, "Measuring the group delay of fiber Bragg gratings by use of end-reflection

interference”, *Opt. Lett.*, vol. 24, pp.1020-1022, 1999.

- [32] E. Ingemar Petermann, Johannes Skaar, Bengt E. Sahlgren, Raoul A. H. Stubbe, and Ari T. Friberg, “Characterization of Fiber Bragg Gratings by Use of Optical Coherence-Domain Reflectometry,” *J. Lightwave Tech.*, vol. 17, pp. 2371-2378, 1999.
- [33] Shay Keren and Moshe Horowitz, “Interrogation of fiber gratings by use of low-coherence spectral interferometry of noiselike pulses,” *Opt. Lett.*, vol. 26, pp. 328-330, 2001.
- [34] L. M. Baskin et al., “Accurate Characterization of Fiber Bragg Grating Index Modulation by Side-Diffraction Technique”, *IEEE Photon. Technol. Lett.*, vol. 15, pp. 449-451, 2003.
- [35] F. El-Diasty, A. Heaney, and T. Erdogan, “Analysis of fiber grating by a side-diffraction interference technique,” *Appl. Opt.*, vol. 40, pp. 890–896, 2001.
- [36] P. A. Krug, R. Stolte, and R. Ulrich, “Measurement of index modulation along an optical fiber Bragg grating,” *Opt. Lett.*, vol. 20, pp. 1767-1769, 1995.
- [37] S. Sandgren, B. Sahlgren, A. Asseh, W. Margulis, F. Lrurell, R. Stubbe, and A. Lidagrd, “Characterisation of Bragg gratings in fibres with the heat-scan technique,” *Electron. Lett.*, vol. 31, pp. 665-666, 1995.
- [38] Ph. Giaccari, H. G. Limberger, and R. P. Salathé, “Local coupling-coefficient characterization in fiber Bragg gratings,” *Opt. Lett.*, vol. 28, pp. 598-600, 2003.
- [39] W. H. Press, S. A. Teukolsky, W. T. Vetterling, and B. P. Flannery, *Numerical Recipes in C* (Cambridge University Press, New York, 1992).
- [40] B. Malo, S. Theriault, D.C. Johnson, F. Bilodeau, J. Albert, and K.O. Hill, “Apodised in-fibre Bragg grating reflectors photoimprinted using a phase mask,” *Electron. Lett.*, vol. 31, pp. 223-225, 1995.
- [41] H. Singh, and M. Zippin, “Apodized fiber Bragg gratings for DWDM applications using uniform phase mask,” in *Proceedings of the 24<sup>th</sup> European Conf. on Optical Communication* (Lerko Print S.A., Madrid, Spain), vol. 1, pp. 189-190, 1998.
- [42] C. Yang, and Y. Lai, “Apodised fiber Bragg gratings fabricated with uniform phase mask

using low cost apparatus,” *Electron. Lett.*, vol. 36, pp. 655-657, 2000.

[43] Alexander V. Buryak and Dmitrii Yu. Stepanov, “Correction of systematic errors in the fabrication of fiber Bragg gratings,” *Opt. Lett.*, vol. 27, pp. 1099-1101, 2002.



# Chapter 2. Synthesis of Fiber Bragg Gratings

## 2.1 Introduction

The synthesis of fiber Bragg gratings amounts to finding the grating structure from a specified, complex spectrum. The purpose of synthesis is helpful for finding the optimal experimental parameters and for the characterization of already fabricated gratings. The objective of this chapter is to understand the characteristics of fiber gratings and then to use the layer-peeling method to find the grating structure for the required filter properties. The content of this chapter is arranged as follows: In section 2.2, we introduce the fundamentals of fiber Bragg gratings which include a short introduction on the grating structure and the photosensitivity of a fiber. In section 2.3, various types of fiber Bragg gratings are discussed, which include uniform FBGs, phase-shifted FBGs, apodized FBGs and chirped FBGs. The theoretic model and the synthesis method of fiber gratings are described in section 2.4 and 2.5. In order to practically implement the ideal grating structure constructed from the layer-peeling method by the sequential writing setups, we use the least square method to find the experimental parameters and the procedure is described in section 2.6. Finally, a summary for this chapter is given in section 2.7.

## 2.2 Fundamentals of Fiber Bragg Gratings

Fiber Bragg gratings have almost periodic structures consisting of a variation of the refractive index along the propagation direction, as shown in Fig. 2.1. We assume that the unperturbed fiber has a refractive index profile  $\bar{n}(x, y)$  and the perturbed fiber has the  $z$ -dependent index

$n(x, y, z)$ . The  $z$ -dependence of the index perturbation is approximately quasi-sinusoidal in the sense that it can be written as

$$n^2 - \bar{n}^2 = \Delta\varepsilon_{r,ac}(z) \cos\left(\frac{2\pi}{\Lambda} z + \theta(z)\right) + \Delta\varepsilon_{r,dc}(z) \quad (2.1)$$

where  $\Lambda$  is a chosen design period so that  $\theta(z)$  becomes a slowly varying function of  $z$  when compared to the grating period  $\Lambda$ . The functions  $\Delta\varepsilon_{r,ac}(z)$  and  $\Delta\varepsilon_{r,dc}(z)$  are real functions and are slowly varying. They also satisfy

$$|\Delta\varepsilon_{r,ac}(z)| \ll n_{co}^2, \quad |\Delta\varepsilon_{r,dc}(z)| \ll n_{co}^2 \quad (2.2)$$

Note that since the index perturbation is small, (2.1) can be written as

$$\Delta n(z) = n - \bar{n} = \Delta n_{ac}(z) \cos\left(\frac{2\pi}{\Lambda} z + \theta(z)\right) + \Delta n_{dc}(z) \quad (2.3)$$

where  $\Delta n_{ac}(z)$  and  $\Delta n_{dc}(z)$  are the ‘‘ac’’ and ‘‘dc’’ index changes, respectively. We have also used the approximation  $n^2 - \bar{n}^2 \approx 2n_{co}(n - \bar{n})$ .  $\theta(z)$  is the spatial grating phase. One can also say that  $(n + \Delta n_{dc}(z))$  is the effective refractive index  $n_{\text{eff}}$ .

The typical index modulation values of a fiber grating are about  $10^{-6} \sim 10^{-3}$ , which are dependent on the dopants in the fiber and the UV-exposure condition. For commercial photosensitive fibers, germanium and boron co-doped fibers have been demonstrated to be excellent for increasing the photosensitivity of the silica fibers. Some examples are like FberCore PS-1500 and 3M GF-3 fibers [1]. The high-pressure hydrogen loading of the fiber also gives great help for increasing the photosensitivity to reduce the exposure time [1-2]. Other schemes to increase photosensitivity have also been suggested, including the codoping of the perform core with materials such as aluminum [3], tin [4], and phosphorus [5]. Another important property of the photo-induce refractive index change is its anisotropy. This characteristic property can be easily observed by irradiating the fiber from the side with the UV light polarized perpendicular to the fiber axis. The anisotropy in the photo-induce

refractive index change results in the birefringence of the fiber. The magnitude of the birefringence proportionally to the total induced index change was measured to be as smaller as 0.2% and as larger as 8% of the total index change [6]. The effect is useful for fabricating polarization mode converting devices or rock filters [7].

The magnitude of the refractive index change also depends on the UV-exposure condition, such as the wavelength, intensity, and total dosage of the irradiating lights. Various continuous wave (CW) and pulsed laser light sources with the wavelength ranging from the visible to the UV have been used to photo-induce the refractive index changes in the optical fiber [8-10]. In practice, the most commonly used light sources are KrF and ArF excimer lasers that generate 248 and 193 nm optical pulses. In this thesis, we use CW 244 nm Argon Ion SHG UV laser source as the exposure light.

## 2.3 Types of Fiber Bragg Gratings



The optical properties of a fiber grating are determined by the variation of refractive index  $\Delta n(z)$  along the fiber axis  $z$ . In equation (2.3), the parameters of  $\Delta n(z)$  are what can be controlled in a fiber grating. They include the ac-index change  $\Delta n_{ac}(z)$ , the dc-index change  $\Delta n_{dc}(z)$  (or effective index  $n_{eff}$ ), the grating period  $\Lambda$ , and the grating phase  $\phi(z)$ . Fig. 2.2 illustrates the common types of fiber Bragg gratings which include uniform FBGs, phase-shift FBGs, apodized FBGs, and chirped FBGs. The discussion of this section will describe the difference among these grating types and the important parameters for the design and fabrication of these FBGs.

### 2.3.1 Uniform Fiber Bragg Gratings

The variation of refractive index  $\Delta n(z)$  for a uniform FBG is shown in Fig. 2.2(a). For this grating structure, the index modulation  $\Delta n_{ac}(z)$  and the effective index  $n_{\text{eff}}$  are keeping constant along the grating length. The grating period is also fixed along the whole grating. The quantities of interest are the reflection spectrum and the time delay. Fig. 2.3(a) shows the spectra of three Bragg gratings with different coupling constants of 2, 4, and 8. These gratings have the fixed finite grating length, but with different index modulation amplitudes. One can see that a uniform period and index-modulation grating will produce side lobes at the shorter and longer wavelength bands. The time delay spectra of these gratings are shown in Fig. 2.3(b). They are calculated by

$$\tau_g = -\frac{\lambda^2}{2\pi c} \frac{d\phi(\lambda)}{d\lambda} \quad (2.4)$$

Near the edge of the band stop, strong dispersion can be seen with the increasing strength of the grating. At the center of the stop band, the time delay is minimum.

### 2.3.2 Phase-shifted Fiber Bragg Gratings

For many applications, the transmission characteristics of a fiber Bragg grating attracted more attention. For examples, the applications of distributed feedback (DFB) fiber lasers [11-12] and superstructure band-pass filters [13] are becoming more popular. The single  $\lambda/4$  (or  $\lambda/2$ ) phase-shifted DFB structure has a pass-band in the middle of the stop band as shown in Fig. 2.2(b). It is like a Fabry-Perot (FP) resonator, which works in the same way as a bulk FP interferometer expect that the grating is a narrow-band distributed reflector. The example spectra of a grating with a  $\lambda/4$ -phase shift in the middle of the grating length is shown in Fig. 2.4 the grating has a uniform index shape with a grating length of 5 mm and the coupling

coefficient of 1.6. There is a transmission peak appeared in the middle of the stop band.

### 2.3.3 Apodized Fiber Bragg Gratings

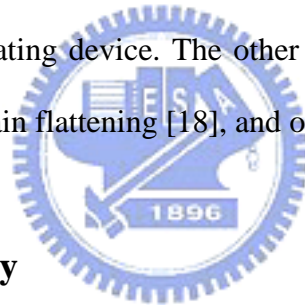
“Apodization” is a word often encountered in filter design. Its meaning can be described as designing a special index envelope shape to improve the spectral properties. The commonly used apodization functions are as follows: Gaussian, Tanh, Sinc, and Raised cosine etc.. The apodization can be achieved through controlling the parameters of  $\Delta n_{ac}(z)$  in equation (2.3). The beneficial effects of apodization are not only in the smoothness of the reflection spectrum, but also in the dispersion characteristics. One simple method to apodize a FBG is to make the profile of  $\Delta n_{ac}(z)$  to be one of the apodization functions. In this case due to the usual fabrication procedure, the value of  $\Delta n_{ac}(z)$  may not be constant along the whole grating as shown in Fig. 2.2(c). The reflection spectrum of this grating has large side lobes in the shorter wavelength band, which is shown in Fig. 2.5(a). This kind of filters cannot be used in the DWDM systems which require a steep edge, very low sidelobes, and a flat top with very little ripples. In order to meet the requirement, the dc-index change  $\Delta n_{dc}(z)$  must be kept constant throughout the grating when the ac-index change  $\Delta n_{ac}(z)$  is apodized. This type of gratings are called the pure (or true) apodized FBGs. The Gaussian apodized grating index profile is shown in Fig. 2.2(d), and the corresponding reflection and transmission spectra are shown in Fig. 2.5(b). One can see that there are very low side lobes on both sides of the central wavelength.

### 2.3.4 Chirped Fiber Bragg Gratings

“Chirp” is the high-pitched varying sound emitted by certain birds and bats. Gratings that

have a non-uniform period along the whole grating are called to be chirped. Chirped gratings have many different forms which may be linear [14], quadratic [15], or random along the grating [16]. Besides, the most important property of chirped gratings is the phase information, which can be contributed from the dc-index change, phase shift and period change terms. The chirped FBGs can be fabricated by controlling one of these parameter terms. In general, the period-chirped FBG has the structure of different period along the grating, which is shown in Fig. 2.2(e). The spectra of one example chirped FBG is shown in Fig. 2.6. The simulation is done with the grating length = 30 mm, chirped rate = 0.1667 nm/cm, and a tanh index profile. Fig. 2.6(a) shows the reflection and transmission spectra, and the Fig. 2.6(b) shows the phase and time delay spectra.

Chirped gratings have many applications. In particular, the linearly chirped grating can act as the dispersion compensating device. The other applications include the chirped pulse amplification [17], amplifier gain flattening [18], and optical sensing [19].



## 2.4 Coupled-Mode Theory

The relation between the spectral response of a fiber grating and the corresponding grating structure is usually calculated by the coupled-mode theory. The fiber is assumed to be lossless and single-mode in the wavelength range of interest. In other words, we consider only one forward and one backward propagating modes. Moreover, the fiber is assumed to be weakly guiding. That is the difference between the refractive indices in the core and the cladding is very small. Under this assumption the electric and magnetic fields are approximately transverse to the fiber axis, and one can ignore all the polarization effects due to the fiber structure and consider solely the scalar wave equation [20].

The coupled-mode equations can be written as

$$\begin{aligned}\frac{du}{dz} &= +i\delta u + q(z)v \\ \frac{dv}{dz} &= -i\delta v + q^*(z)u\end{aligned}\quad (2.5)$$

In these equations, we ignore the terms that are rapidly oscillating since they contribute little to the growth and decay of the modes. The fields of  $u$  and  $v$  correspond to the forward and backward propagating amplitudes. In (2.5) the wavenumber detuning  $\delta = k - k_0$  and the coupling coefficient  $q$  of the grating is given by :

$$q(z) = i\kappa(z)\exp(-2i\int_0^z \sigma(z')dz') \quad (2.6)$$

where  $\kappa(z)$  is a complex, slowly varying function of  $z$  and  $\sigma(z')$  is a real, slowly varying function that accounts for the dc index variation from  $\Delta\varepsilon_{r,dc}(z)$ . Here  $q(z)$  is related to the index modulation by :

$$\begin{aligned}|q(z)| &= \frac{\eta\pi\Delta n_{ac}(z)}{\lambda} \\ \arg q(z) &= \theta(z) - 2\eta k \int_0^z \Delta n_{dc}(z')dz' + \frac{\pi}{2}\end{aligned}\quad (2.7)$$

The modulus of  $q$  is proportional to the ac-index modulation amplitude. The term  $\theta(z)$  is the spatial grating phase and the integral term in (2.7) is the modification to the spatial phase due to the increased dc index.

## 2.5 Discrete Layer-Peeling Method

This layer-peeling method for synthesis of fiber gratings comes from an inherently discrete model [21]. It was first developed by geophysicists like Goupillaud and Robinson, and was extended by Bruckstein et. al. [22,23]. In this thesis, the described discrete layer-peeling (DLP) method was developed by J. Skaar et. al. [24]. This method is an inverse method for finding the structure parameters of the complex coupling coefficient of a fiber grating from the

complex reflection spectrum. The description of the inverse and the forward methods for the synthesis of fiber gratings. are summarized in Fig. 2.7.

The discretized LP method can be described as shown in Fig. 2.8. The starting point for the numerical modeling of FBGs is based on the transfer matrix formulation, which connects the field at point  $z+$  with the field at  $z$  by the following relation :

$$\begin{bmatrix} u(z + \Delta, \delta) \\ v(z + \Delta, \delta) \end{bmatrix} = \begin{bmatrix} \cosh(\gamma\Delta) + i \frac{\delta}{\gamma} \sinh(\gamma\Delta) & \frac{q}{\gamma} \sinh(\gamma\Delta) \\ \frac{q^*}{\gamma} \sinh(\gamma\Delta) & \cosh(\gamma\Delta) - i \frac{\delta}{\gamma} \sinh(\gamma\Delta) \end{bmatrix} \begin{bmatrix} u(z, \delta) \\ v(z, \delta) \end{bmatrix} = [T] \begin{bmatrix} u(z, \delta) \\ v(z, \delta) \end{bmatrix} \quad (2.8)$$

Here  $u(z, \delta)$  and  $v(z, \delta)$  are the slowly varying amplitudes of the forward and backward propagating fields, and  $\gamma^2 = |q|^2 - \delta^2$ , where  $q$  is the coupling coefficient and  $\delta = \beta - \beta_B$  is the wavenumber detuning compared to a Bragg design wavenumber  $\beta_B$ . We refer to (2.8) as the piecewise uniform model since the grating is considered uniform in the interval  $[z, z+$

]. The matrix  $T$  can be replaced by the product of two transfer matrixes  $T_\Delta * T_\rho$ . Here

$$T_\Delta = \begin{bmatrix} \exp(i\delta\Delta) & 0 \\ 0 & \exp(-i\delta\Delta) \end{bmatrix} \quad (2.9)$$

is the pure propagation transfer matrix obtained by letting  $q \rightarrow 0$ , and

$$T_\rho = \left(1 - |\rho_j|^2\right)^{-1/2} \begin{bmatrix} 1 & -\rho_j^* \\ -\rho_j & 1 \end{bmatrix} \quad (2.10)$$

is the discrete reflector matrix obtained by letting  $q \rightarrow$  and holding  $q$  constant. The discrete reflection coefficient is given by

$$\rho_j = - \tanh \left( |q_j| \Delta \right) \frac{q_j^*}{|q_j|}. \quad (2.11)$$

It is straightforward to show that the result of transferring the fields using  $T_\Delta \cdot T_\rho$  is equivalent to the recursive formulation given below

$$r_{j+1}(\delta) = \exp(-2i\delta\Delta) \cdot \frac{r_j(\delta) - \rho_j}{1 - \rho_j^* r_j(\delta)} \quad (2.12)$$

Here  $r_j(\delta) = v_j(\delta)/u_j(\delta)$ .

To obtain an explicit expression for the determination of  $\rho_1$  by the inverse Fourier transform, we note that the spectrum  $r_1(\delta)$  can be written as a discrete-time Fourier transform of the impulse response  $h_1(\tau)$ ,

$$r_1(\delta) = \sum_{\tau=0}^{\infty} h_1(\tau) \exp(i\delta\tau 2\Delta) \quad (2.13)$$

Since the impulse response for  $\tau = 0$  is the same as if only the first reflector is present, we can see that  $\rho_1$  is simply the zeroth order Fourier coefficient of the series in (2.13) :

$$\rho_1 = h_1(0) = \frac{\Delta}{\pi} \int_{-\pi/2\Delta}^{\pi/2\Delta} r_1(\delta) d\delta \quad (2.14)$$

For numerical implementation, the spectral dependence must also be discretized, and hence the calculation of  $\rho_1$  by the inverse Fourier transform of  $r_1(\delta)$  can be achieved by the discrete Fourier transform

$$\rho_1 = \frac{1}{M} \sum_{m=1}^M r_1(m) \quad (2.15)$$

Here  $r_1(m)$  denotes a discretized version of the spectrum  $r_1(\delta)$  in the range  $|\delta| \leq \pi/2\Delta$ , and  $M$  is the number of wavelengths in the spectrum. After determining  $\rho_j$ , we can get the complex coupling constant  $q(z)$  by

$$\begin{cases} |q_j| = \frac{1}{2\Delta} \ln \left( \frac{1 - |\rho_j|}{1 + |\rho_j|} \right) \\ \arg q_j = -\arg \rho_j \end{cases} \quad (2.16)$$

## 2.6 The Least Square Method

From the DLP method, the normalized refractive-index modulation amplitude and phase profiles can be reconstructed from the target spectrum. In order to realize this complicated FBG by the proposed fabrication methods, it is important to include the overlap-step-scan effects in the design [25]. We use the least square (LS) fitting method [26] to find the best experimental exposure parameters.

In our experiment we will use a small gaussian beam to fabricate fiber gratings by an overlap-step-scan exposure method. It is assumed that  $A_{id}(z)$  is the refractive index envelope reconstructed from the Layer-Peeling method and  $A_m(z)$  is the refractive index envelope of the  $m$ -th small gaussian beam. Therefore the following merit function can be used for determining the optimum parameters of the overlap-step-scan exposure.

$$\sigma(\{C_m\}) = \int \left[ A_{id}(z) - \sum_m A_m(z) \right]^2 dz \quad (2.17)$$

where  $C_m$  represents the amplitude of the  $m$ -th small gaussian beam, and  $A_m(z)$  can be expressed as

$$A_m(z) = C_m \cdot \exp\left(-\frac{(z - z_m)^2}{w_s^2}\right) \quad (2.18)$$

In the above expression  $w_s$  is the width of the gaussian beam and  $z_m$  is the central position of the  $m$ -th exposure gaussian beam. We want to let  $\sum_m A_m(z)$  be as close to  $A_{id}(z)$  as possible.

This can be achieved by the least square method, which solves the following equations to find the optimum values.

$$\frac{\partial \sigma}{\partial C_m} = -2 \int \left[ A_{id}(z) - \sum_m A_m(z) \right] \cdot \exp\left(-\frac{(z - z_m)^2}{w_s^2}\right) dz = 0 \quad (2.19)$$

## 2.7 Summary

In this chapter we have described the characteristics of fiber Bragg gratings with various types of refractive index profiles. It is helpful for the design of various complex FBG structures. The discrete layer-peeling method has been adopted for the design of advanced fiber gratings. We also combine this synthesis method with the least square method to find the best experimental parameters for sequential UV exposure. These developed methods will be applied to the design of advanced FBG structures and can be realized by using the proposed fabrication methods to be described in the following chapter.



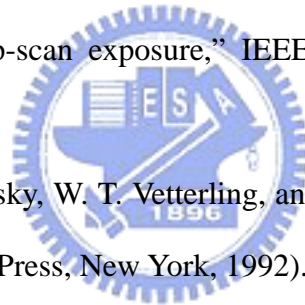
## References for Chapter 2:

- [1] P. L. Swart, M. G. Shlysgin, A. A. Chtcherbakov, and V. V. Spirin, "Photosensitivity measurement in optical fibre with Bragg grating interferometers," *Electron. Lett.*, vol. 38, pp. 1508-1510, 2002.
- [2] P. J. Lemaire, R. M. Atkins, V. Mizrahi, and W. A. Reched, "High pressure H<sub>2</sub> loading as a technique for achieving ultrahigh UV photosensitivity and thermal sensitivity in GeO<sub>2</sub> doped optical fibers," *Electron. Lett.*, vol. 29, pp. 1191-1193, 1993.
- [3] G. Meltz and W. W. Morey, *SPIE*, vol. 1515, pp. 185, 1991.
- [4] L. Dong, J. L. Cruz, L. Reekie, M. G. Xu and D. N. Payne, "Enhanced photosensitivity in tin-codoped germanosilicate optical fibers," *IEEE Photon. Technol. Lett.*, vol. 7, pp. 1048-1050, 1995.
- [5] Thomas A. Strasser, "photosensitivity in phosphorus fibers," in *OFC'96*, invited TuO1.
- [6] T. Erdogan and V. Mizrahi, "Characterization of UV-induced birefringence in photosensitive Ge-doped silica optical fibers," *J. Opt. Soc. Am. B*, vol. 11, pp. 2100-2105, 1994.
- [7] K. O. Hill, F. Bilodeau, B. Malo, and D. C. Johnson, "Birefringent photosensitivity in monomode optical fiber: Application to the external writing of rocking filters," *Electron. Lett.*, vol. 27, pp. 1548-1550, 1991.
- [8] K. O. Hill, Y. Fujii, D. C. Johnson, and B. S. Kawasaki, "Photosensitivity in optical fiber waveguides: Application to reflection filter fabrication," *Appl. Phys. Lett.*, vol. 32, pp. 647-649, 1978.
- [9] C. G. Askins, T.-E. Tsai, G. M. Williams, M. A. Putnam, M. Bashkansky, and E. J. Friebele, "Fiber Bragg reflectors prepared by a single excimer pulse," *Opt. Lett.*, vol. 17, pp. 833-835, 1992.
- [10] D. C. Psaila and C. Martijn de Sterke, "Fabrication of rocking filters at 193 nm," *Opt.*

Lett., vol. 21, pp. 1550-1552, 1996.

- [11] H. A. Haus and C. V. Shank, "Anti-symmetric type of distributed feedback lasers," *J. Quantum Electron*, vol. 12, pp. 532-539, 1976.
- [12] R. Kashyap, P. E. McKee, and D. Armes, "UV written reflection grating structures in photosensitive optical fibres using phase-shifted phase-mask," *Electron. Lett.*, vol. 30, pp. 1977-1978, 1994.
- [13] L. Wei and W. Y. Lit, "Phase-shifted Bragg grating filters with symmetrical structures," *IEEE J. Lightwave Tech.*, vol. 15, pp. 1405-1410, 1997.
- [14] K. C. Byron, K. Sugden, T. Bircheno, and I. Bennion, "Fabrication of chirped Bragg gratings in photosensitive fibre," *Electron. Lett.* vol. 29, pp. 1659, 1993.
- [15] B. Eggleton, P. A. Krug, and L. Poladin, "Dispersion compensation by using Bragg grating filters with self induced chirp," in *Tech. Digest of Opt. Fib. Comm. Conf., OFC'94*, pp. 227.
- [16] F. Ouellette, "The effect of profile noise on the spectral response of fiber grating," in *Bragg Gratings, Photosensitivity, Poling in Glass Fibers and Waveguides: Applications and Fundamentals*, vol. 17, OSA Technical Digest Series (Optical Society of America, Washington, DC, 1997), paper BMG13, pp. 222-224.
- [17] A. Boskovic, M. J. Guy, S. V. Chernikov, J. R. Taylor, and R. Kashyap, "All-fiber diode pumped, femtosecond chirped pulse amplification system," *Electron. Lett.*, vol. 31, pp. 877-879, 1995.
- [18] R. Kashyap, R. Wyatt, and P. F. McKee, "Wavelength flattened saturated erbium amplifier using multiple side-tap Bragg gratings," *Electron. Lett.*, vol. 29, pp. 1025, 1993.
- [19] A. D. Kersey and M. A. Davis, "Interferometric fiber sensor with a chirped grating distributed sensor element," *Proc. OFS'94*, pp. 319-322, Glasgow UK, 1994.

- [20] A. W. Snyder and J. D. Love, *Optical Waveguide Theory* (Chapman & Hall, 1983).
- [21] R. Feced, M. N. Zervas, and M. A. Muriel, "An efficient inverse scattering algorithm for the design of nonuniform fibre Bragg gratings," *J. Quantum El.*, vol. 35, pp. 1105-1115, 1999.
- [22] A. M. Bruckstein and T. Kailath, "Inverse scattering for discrete transmission-line models," *SIAM Rev.*, vol. 29, pp. 359-389, 1987.
- [23] A. M. Bruckstein, B. C. Levy and T. Kailath, "Differential methods in inverse scattering," *SIAM J. Appl. Math.*, vol. 45, pp. 312-335, 1995.
- [24] J. Skaar, L. Wang, and T. Erdogan, "On the synthesis of fiber Bragg gratings by layer peeling," *IEEE J. Quantum Electron.*, vol. 37, pp.165-173, 2001.
- [25] L. G. Sheu, K. P. Chuang, and Y. Lai, "Fiber Bragg grating dispersion compensator by single-period overlap-step-scan exposure," *IEEE Photon. Technol. Lett.*, vol. 15, pp. 939-941, 2003.
- [26] W. H. Press, S. A. Teukolsky, W. T. Vetterling, and B. P. Flannery, *Numerical Recipes in C* (Cambridge University Press, New York, 1992).



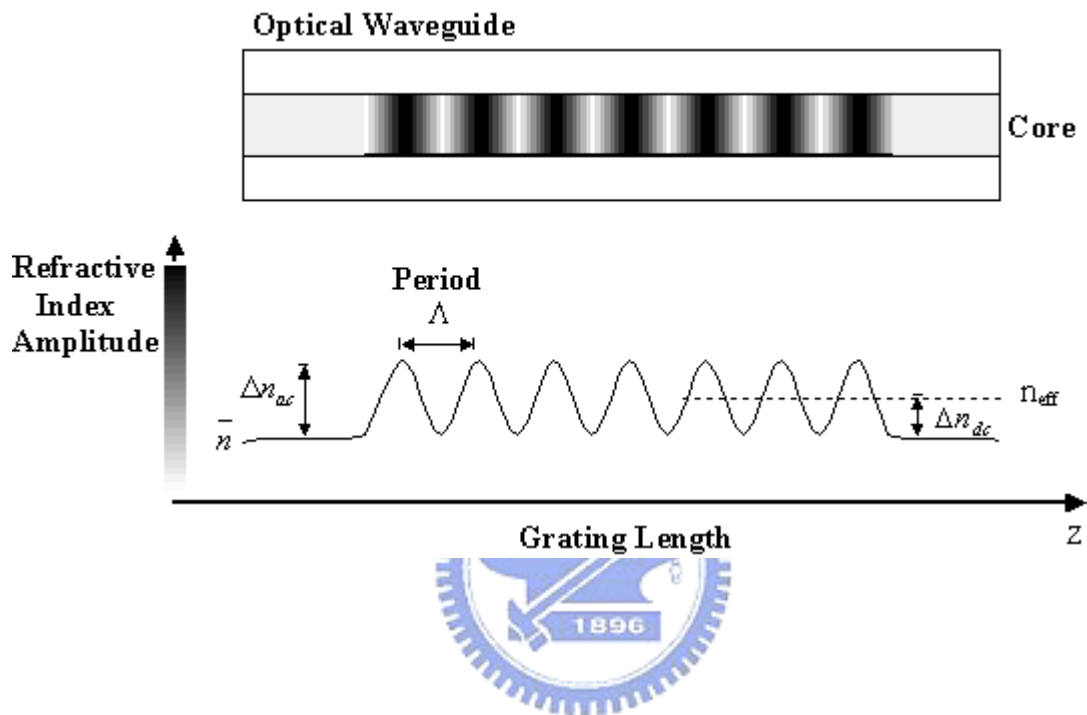


Fig. 2.1 The refractive-index modulation along the length of waveguides.

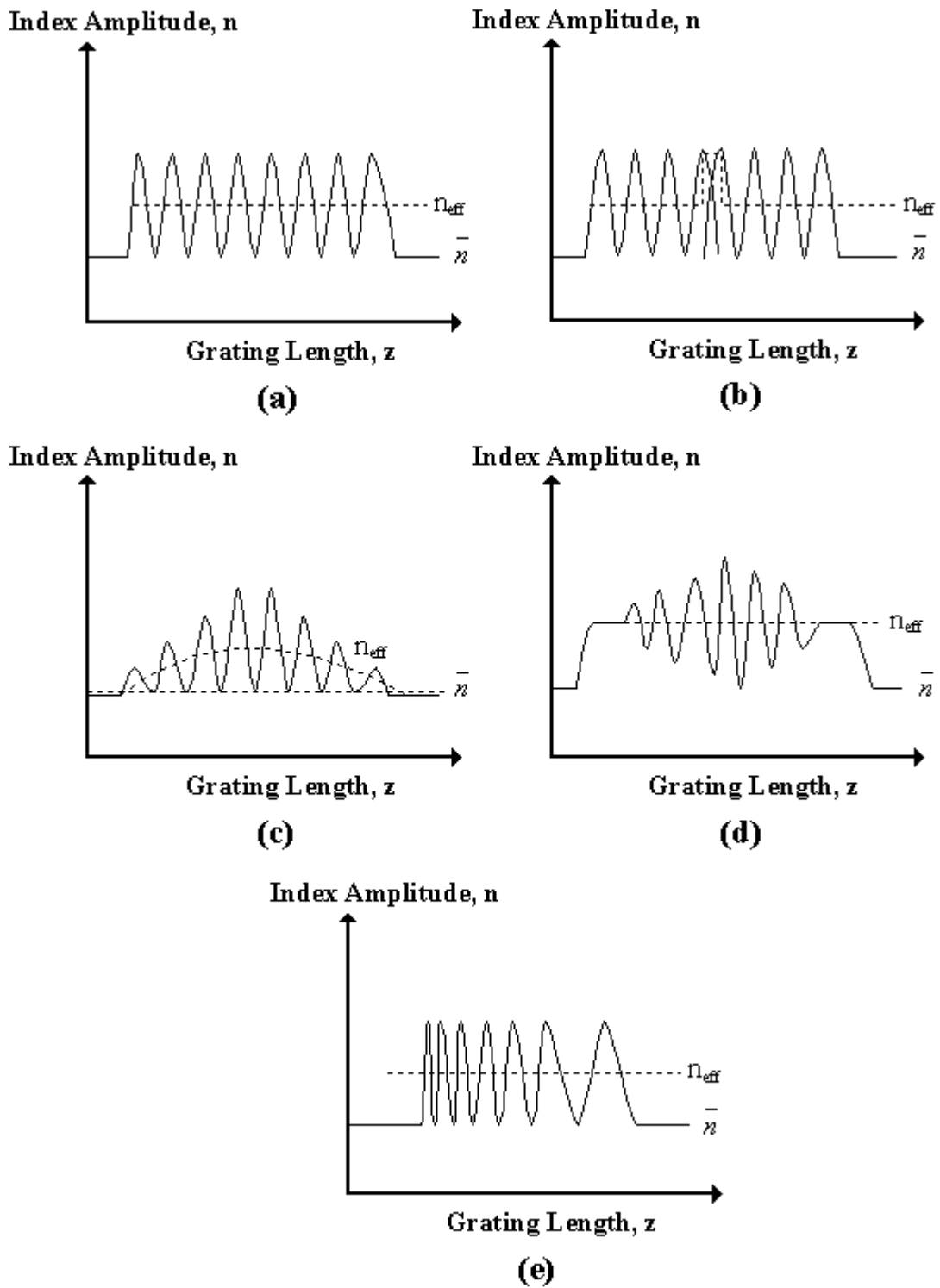


Fig. 2.2 The common types of fiber Bragg gratings; (a) uniform FBGs, (b) phase-shift FBGs, (c, d) apodized FBGs, and (e) chirped FBGs.

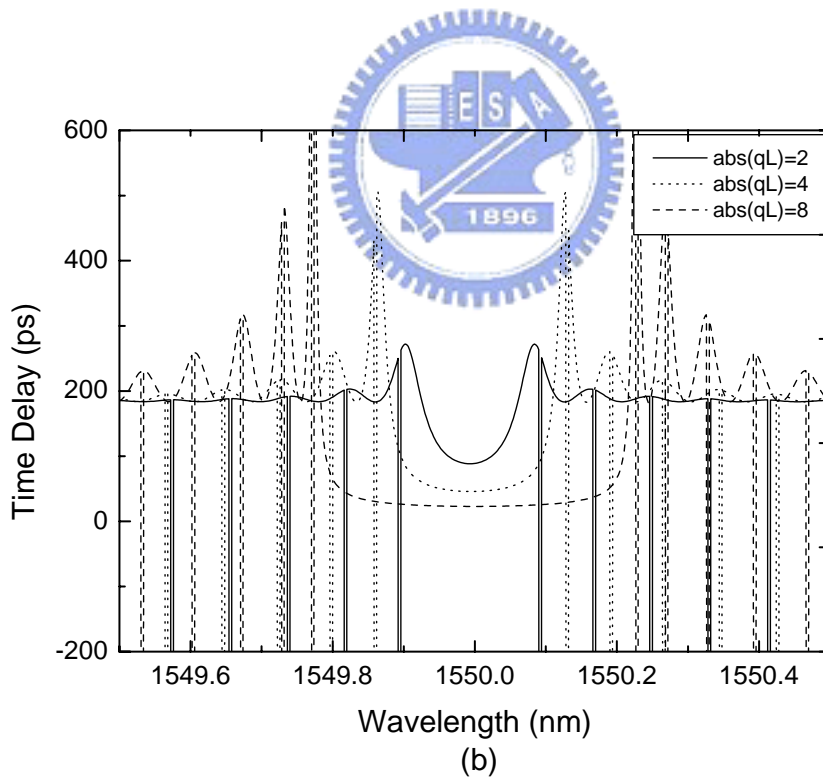
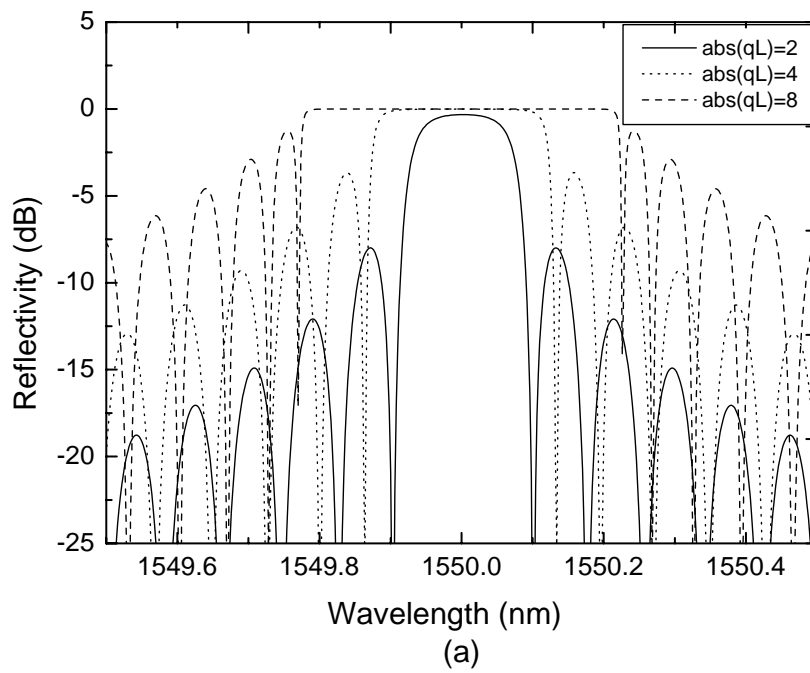


Fig. 2.3 (a) The spectra of three Bragg gratings with different coupling constants of 2, 4, and 8.; (b) time delay of the same gratings as in Fig. 2.3(a).

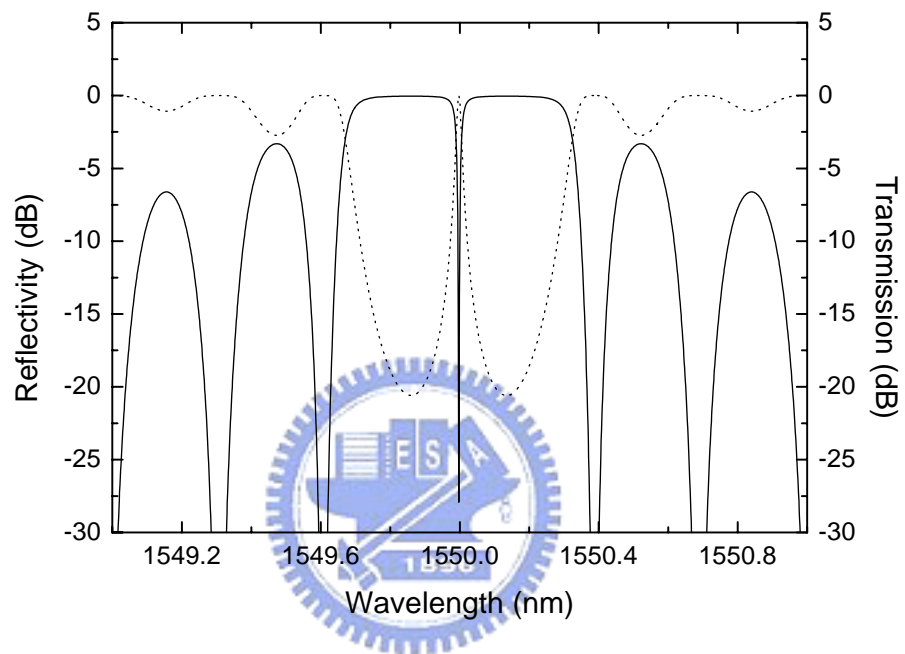
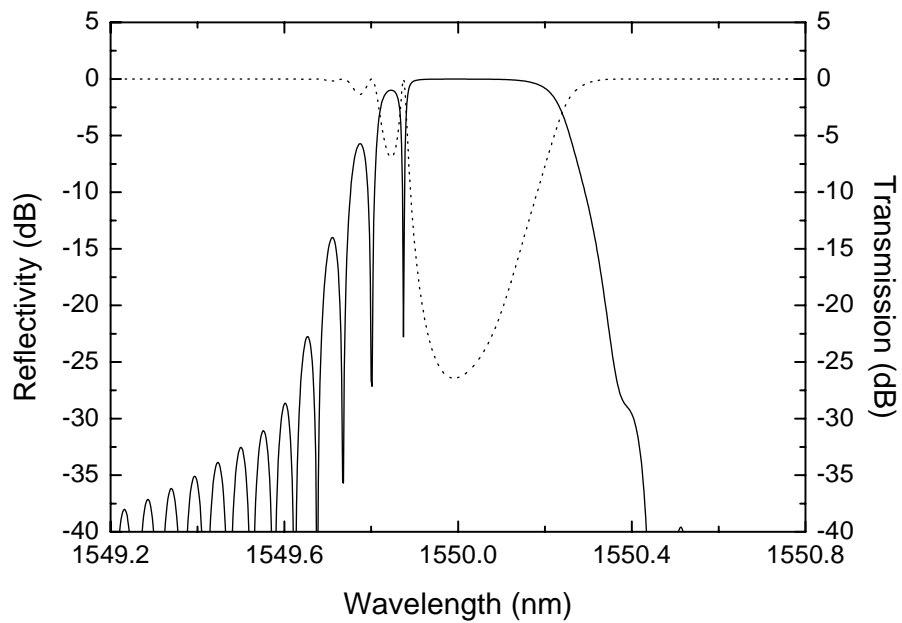
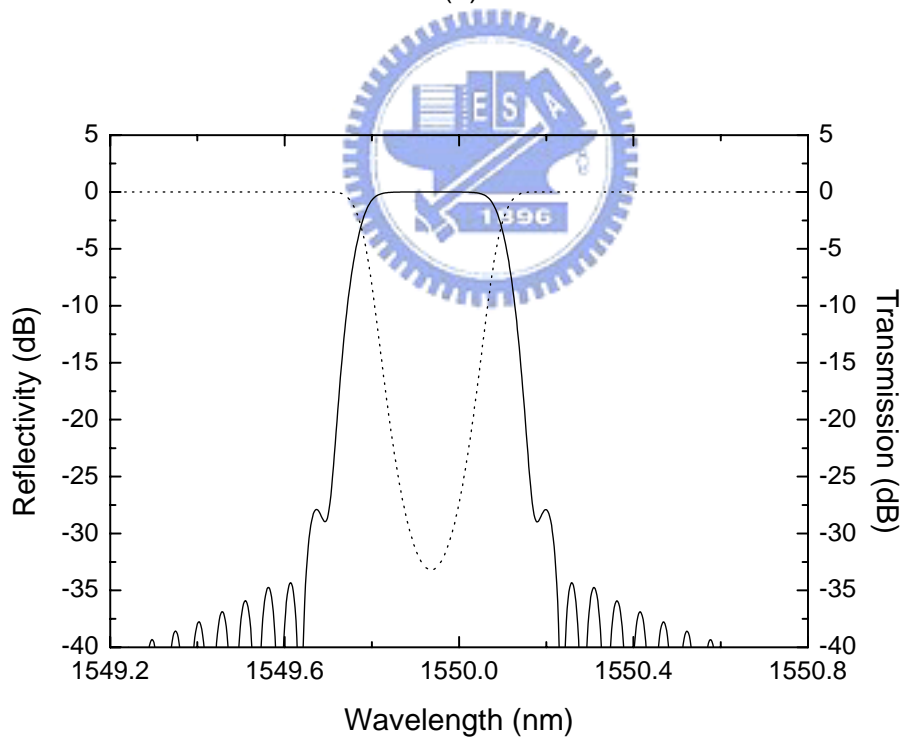


Fig. 2.4 A  $\pi$ -phase shift uniform fiber Bragg grating. (the parameters are  $\text{abs}(qL)=1.6$  and  $L=5$  mm)



(a)



(b)

Fig. 2.5 (a) A Gaussian apodized FBG with non-constant dc index; (b) a pure apodization FBG with a Gaussian index profile.

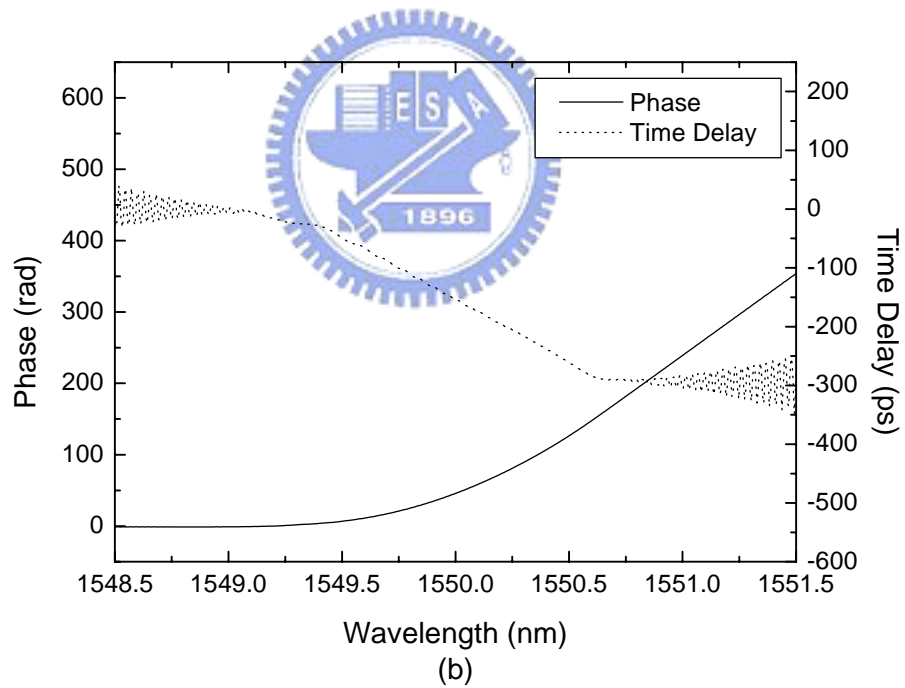
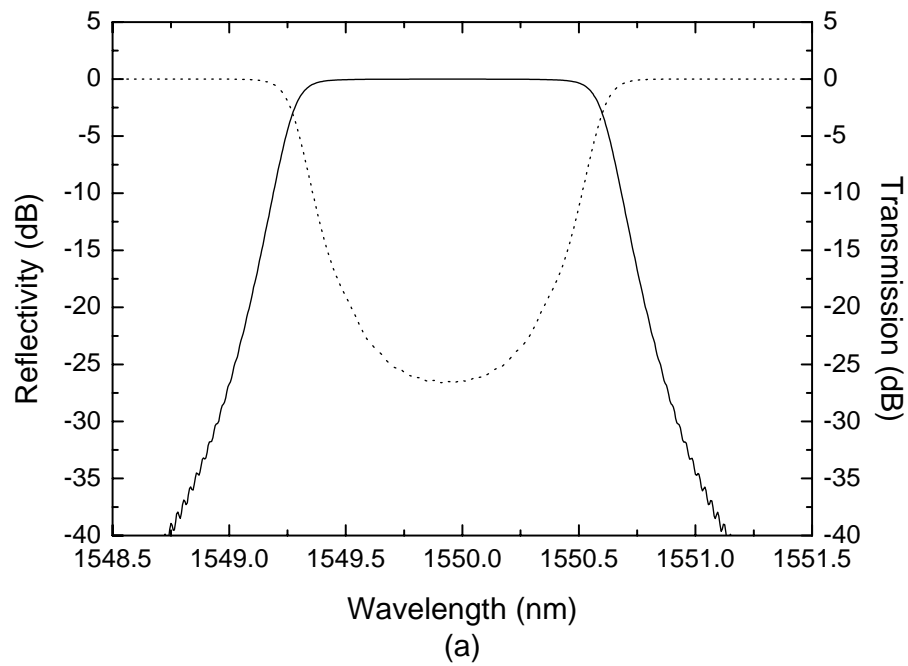


Fig. 2.6 A chirped FBG with the grating length = 30 mm, chirped rate = 0.1667 nm/cm, and a tanh index profile. (a) The reflection and transmission spectra; (b) the phase and time delay.

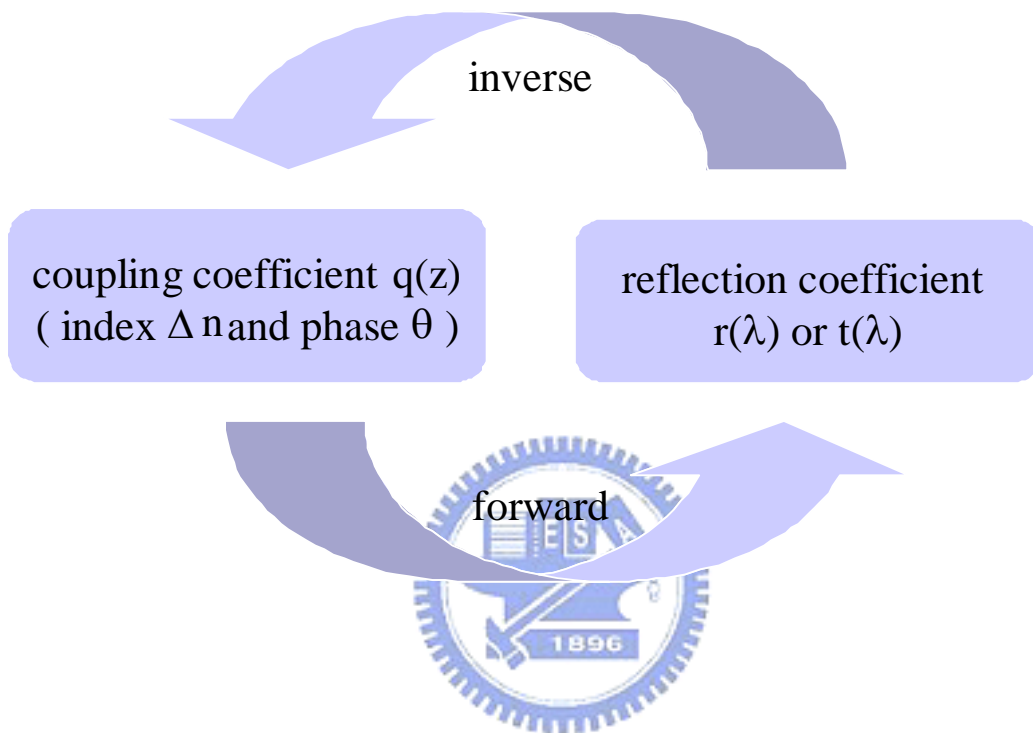


Fig. 2.7 The description of the inverse and the forward methods for the synthesis and analysis of fiber gratings.

## Optical Waveguide

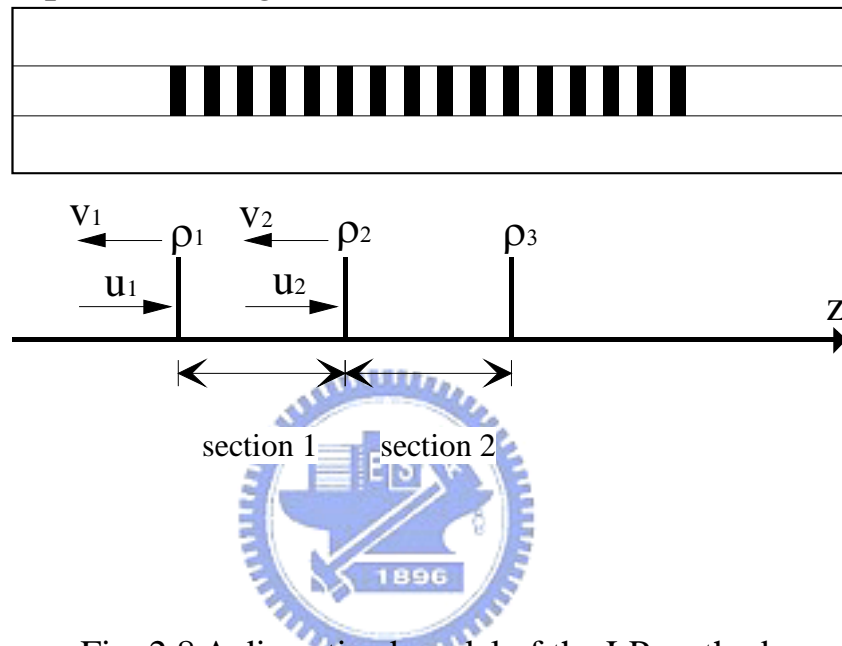


Fig. 2.8 A discretized model of the LP method.

## **Chapter 3. Characterization of Fiber Bragg Gratings**

### **3.1 Introduction**

The characterization of a fiber Bragg grating involves the determination of the complex reflection coefficient or the complex coupling coefficient of the grating. The mostly direct method for finding FBG reflection and transmission spectra is by using the optical spectrum analyzer (OSA). This measurement can help us to find the performances of a fiber grating initially and is not enough to get the grating structures for improving the design and fabrication of advanced fiber gratings. Accurate characterization of the amplitude (refractive-index modulation) and phase (dispersion) of FBGs are needed for many applications. In the literature, there have been a lot of different approaches based on the interferometry [1-4], side-scattering [5-7], heat-scan [8-9] or phase modulation methods [10-11]. In this chapter, we describe two measurement methods that we developed for measuring the spectral phase, index amplitude and period change of the FBGs. The two methods are based on the balanced Michelson interferometer technique for measuring the spectral phase information and the side-diffraction technique for measuring the refractive index change and the grating period change.

### **3.2 The Balanced Michelson Interferometer Method**

The characterization of fiber Bragg gratings is very important for their applications in high-bit rate fiber communication systems. It is not easy to measure the phase information of a fiber grating. In reference 4, Skaar used a lossless Fabry-Perot-like system consisting of two reflectors, where one reflector has known characteristics, and the other has not. The first

reflector is a FBG with unknown characteristics, and the other reflector is quite broad-band when compared to the FBG as shown in Fig. 3.1. They obtained the complex reflection spectrum of the FBG, or equivalently the reflectivity and group delay spectra, from the measurement of the reflectivity of the Fabry-Perot structure.

In this paper, we analyze a similar structure, namely a balanced Michelson interferometer consisting of two general reflectors, where one of them is the FBG to be characterized, and the other is a reference reflector [12]. The experimental setup is shown in Fig. 3.2 and can be analyzed as follows. In the FBG path, we obtain the path 1 signal

$$\tilde{E}_1(\lambda) = E_1(\lambda) \cdot \exp(i \frac{2\pi}{\lambda} L_1 + i\phi(\lambda)) \quad (3.1)$$

where  $\phi(\lambda)$  is the phase information of the FBG, and  $L_1$  is the path length from coupler. In the reference path, we obtain the path 2 signal

$$\tilde{E}_2(\lambda) = E_2(\lambda) \cdot \exp(i \frac{2\pi}{\lambda} L_2) \quad (3.2)$$

where  $L_2$  is the path length from coupler. When these two signal are combined at the output port of the coupler which is connected to an Optical Spectrum Analyzer (OSA), the measured output signal spectrum can be expressed as

$$I_{inter}(\lambda) = I_{grating} + I_{reference} + 2 \cdot \sqrt{I_{grating} \cdot I_{reference}} \cdot \cos(\frac{2\pi}{\lambda} \ell + \phi(\lambda)) \quad (3.3)$$

where  $\ell = L_1 - L_2$ ,  $I_{grating} = |\tilde{E}_1|^2$  and  $I_{reference} = |\tilde{E}_2|^2$ .

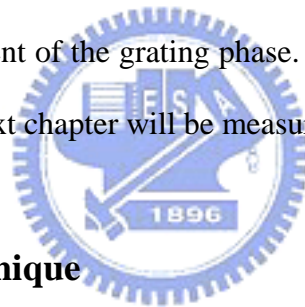
From equation (3.3) the interference spectrum  $I_{inter}(\lambda)$  will look like that in Fig. 3.3. One can take the inverse Fourier transform of  $I_{inter}(\lambda)$  to get the result shown in Fig. 3.4. By multiplying the result by a filtering window function centered at the peak corresponding to the angular frequency  $\omega$  and then taking a Fourier transform back to the spectral domain, we can get the phase response  $\phi(\lambda)$  from the result and the group delay  $\tau_g = d\phi/d\omega$  can also be calculated. The whole algorithm is summarized in Fig. 3.5.

In order to test our algorithm, we analyze a structure consisting of a gaussian apodized,

linear chirped FBG with the length  $L=5\text{mm}$ , the chirp rate =  $0.5\text{ (nm/cm)}$ , and the maximum grating reflection =  $96.84\%$ . The measured interference pattern  $I_{\text{inter}}(\lambda)$  is shown in Fig. 3.6(a). Fig. 3.6(b) shows the result of the calculated phase spectrum  $\phi(\lambda)$ .

We have also calculated the group delay time  $\tau_g=d\phi/d\lambda$  from the result of the phase response  $\phi(\lambda)$ . For comparison, we experimentally measure the group delay of this grating sample using a commercial dispersion measurement equipment (“Advantest Q7760”). The measured result (Fig. 3.7(a)) is compared with the result from our measuring method (Fig. 3.7(b)). One can see that we can get good measured results and the measurement resolution is about  $5\text{ ps}$ , which is probably limited by the resolution of the OSA as well as the environmental vibration.

The presented method has been carried out experimentally, and has been shown to be easy and accurate for the measurement of the grating phase. Some of the fabricated advanced fiber Bragg gratings shown in the next chapter will be measured by using this method.



### 3.3 The Side-Diffraction Technique

The spatial quality of a FBG will strongly affect the performance of the FBG device. By using the side-diffraction technique, we can directly measure the refractive index modulation and the grating period profile. In this section we describe how this side-diffraction method can be used to get the information of grating index and period changes. And we also proposed an improved method for increasing the measuring resolution when compared with the prior methods in the literature.

The side-diffraction technique can be divided into two categories of without/with interference as shown in Fig. 3.8 and Fig. 3.9. First, a side-diffraction method for measuring the refractive index modulation is shown in Fig. 3.8. A He-Ne laser as a probe beam is

focused through the side of the fiber into its core. The first-order Bragg diffraction of the probe beam occurs at the Bragg condition:

$$2 \cdot \Lambda \cdot \sin \theta_i = \lambda \quad (3.4)$$

where  $\theta_i$  is the input angle of the probe beam in air,  $\Lambda$  is the local grating period, and  $\lambda$  is the free-space wavelength of the probe beam which is 632.8 nm in our case. The FBG index structure can be expressed as

$$n(z) = n_{dc} + \Delta n \sin Kz, \quad (3.5)$$

where  $n_{dc}$  is the dc refractive index,  $K$  is the grating vector and  $\Delta n$  is the refractive index modulation. We can express the first-order diffracted power  $P_d$  by means of a scattering cross section  $\sigma_i$  in the form of

$$P_d = \sigma_i \times \hat{p}_i, \quad \eta = P_d / P_i \quad (3.6)$$

where  $P_i$  is the total input power and  $\eta$  is the diffracted efficiency. The scattering cross section can be express as

$$\sigma_i \approx 1.66 \left( \frac{2\pi}{\lambda} \right) a^3 \omega \Delta n^2 \sin^2 \gamma / \cos^2 \theta_i \quad (3.7)$$

where  $a$  is the core diameter of the fiber,  $\omega$  is the waist of the probe beam, and  $\gamma$  is the angle of polarization vector with respect to the diffraction plane. When the s-polarized light is used for the probe beam (i.e. the electric vector is perpendicular to the plane,  $\gamma = \pi/2$ ), the amount of the diffracted energy is maximum. From equation (3.5)~(3.7), we can get the refractive index modulation  $\Delta n$  with respect to the first-order diffracted power  $P_d$ , which has the relation of

$$\Delta n \propto \sqrt{P_d}. \quad (3.8)$$

The side-diffraction method provides a very accurate measurement of the index profile which have demonstrated simultaneous measurement of the fiber grating refractive index modulation with accuracy of  $2 \cdot 10^{-6}$  [7].

The other method is the side-diffraction interference method as shown in Fig. 3.9. We can measure the grating period change and the refractive-index modulation at the same time [see Ref. 6]. If we use the CCD camera to record the interference pattern, the intensity distribution of the interference fringe can be express as

$$I = I_r + I_d + 2(I_r I_d)^{1/2} \cos(2\pi f x), \quad (3.9)$$

$$\text{and } \alpha = 2 \sin^{-1}(\lambda f / 2)$$

where  $I_r$  and  $I_d$  are the intensities of reference and the first-order diffracted beams,  $f$  is spatial frequency of the interference fringe pattern (i.e.  $dx = 1/f$  as shown in Fig. 3.9), and  $\alpha$  is the angle between the reference and the first-order diffracted beams. Based on the phase match condition, the local grating period can be written as

$$\Lambda = \frac{\lambda}{[\sin \theta_i + \sin(\theta_i + \alpha)]}, \quad (3.10)$$

which, when  $\alpha \ll 1^0$  (i.e.  $\alpha \approx \lambda \cdot f$ ), can be approximated as

$$\Lambda \approx \frac{\lambda}{[2 \sin \theta_i - \lambda f \cdot \cos \theta_i]} \quad (3.11)$$

The local grating period  $\Lambda$  with respect to the central period can also be expressed as

$$\Lambda \approx \Lambda_0 \cdot \left[ 1 + \frac{\lambda f}{2 \tan \theta_i - \lambda f} \right]$$

$$\text{or } \Delta\Lambda \approx \frac{\lambda f}{2 \tan \theta_i - \lambda f} \quad (3.12)$$

From equation (3.12), we can find that the grating period variation  $\Delta\Lambda$  can be got from the spatial frequency of the interference pattern.

From equation (3.8), we can find that the refractive-index modulation  $\Delta n$  is proportion to  $\sqrt{P_d}$  or  $\sqrt{I_d}$ . In order to get the intensity information of the first-order diffracted beam  $I_d$ , we take the Fourier transform of the interference pattern  $I$  expressed in equation (3.9) to get the amplitude of the positive beating frequency pattern. The positive beating frequency

amplitude is proportion to  $2(I_r I_d)^{1/2}$ . By using this method, we can measure the distribution of the refraction-index modulation along the whole grating.

Fig. 3.10 shows the improved side-diffraction interference method for measuring the grating period variation and the ac-index modulation. In order to improve the resolution of both measured parameters, we use a single-polarization He-Ne laser with a larger output power of 25mW as a light source. We used a CCD camera to record the interference pattern. When a larger interference period is used, we can have a better period change resolution. For example, if the grating period  $\Lambda_0=535\text{nm}$ , the wavelength of a He-Ne laser  $\lambda=632.8\text{nm}$ , the interference angle  $\theta_i=36.2^\circ$ , the interference period on CCD camera  $dx=100\text{pixels}=1/f$  (where one pixel width = 7.15um), we can calculate the resolution of the measured grating period change to be about 0.0032nm. If the  $dx=50\text{pixels}=1/f$  is used, the resolution of the measured grating period change is about 0.0128nm.

### 3.4 Characterization of Fiber Gratings

Complete characterization of fiber gratings including the complex reflection spectrum and the complex coupling coefficient is required for the analysis of fiber grating properties or for improving the fabrication methods. In this section, we propose an analysis method for determining the complete characteristics of the fiber gratings including the dc-index modulation. This analysis method is based on the discrete layer peeling method (described in section 2.5), the balanced Michelson interferometer method (described in section 3.2) and the side-diffraction method (described in section 3.3). One example is proposed to demonstrate the applicability of this analysis method.

## I. Analysis Process

The flow chart of the proposed characterization method of fiber gratings is shown in Fig. 3.11. In general, if the grating structure has been known, one can use the transfer-matrix approach to compute the complex spectrum. Conversely, the complex coupling coefficient can be obtained from the complex spectrum by the use of the inverse scattering algorithm, like the discrete layer peeling method. For the inverse algorithm, when the reflectivity of the FBG is small ( $R < 30\%$ ), the structure of the FBG can be directly calculated from the complex reflection spectrum using a Fourier transform [13,14]. When the grating reflectivity is high, it does not give the accurate grating structure due to multiple reflections that propagate along the grating. An inverse scattering algorithm should be used for the fiber gratings with high reflectivities [15-18]. In our work the discrete layer-peeling algorithm [18] was used to extract the complex coupling coefficient of a fiber grating from the measured complex reflection spectrum. In the measurement of the complex reflection spectrum, we used the balanced Michelson interferometer method described in section 3.2. However, for highly reflecting fiber gratings, the forward propagating wave strongly attenuates along the grating and, therefore, the reflection from the region located close to the grating end is very low. Since the measured reflection signals contain noise, the reconstruction of the region located close to the grating end becomes inaccurate. In order to measure the accurate complex reflection spectrum using the balanced Michelson interferometer method, an improved method described in reference [19] can be used. The experimental setup is shown in Fig. 3.12. The complex reflection spectrum of the grating can be extracted by measuring the impulse response from both sides of the grating. Then the grating structure ( $|q(z)|$  and  $\arg q(z)$ ) can be calculated from the complex reflection spectrum by the use of the DLP algorithm. By using the side-diffraction technique described in section 3.3, we can measure the ac-index modulation

$\Delta n_{ac}$  and the grating period variation  $\Delta\Lambda$ . From the results of the DLP algorithm and the side-diffraction technique, we can get the grating structure parameters which include  $\Delta n_{ac}$ ,  $\Delta\Lambda$  and  $\Delta n_{dc}$ . In the above parameters, the  $\Delta n_{dc}$  distribution of the grating can be extracted from the equation (2.7) of  $\arg q(z)$ .

## II. Experimental Results

A chirped Bragg grating has been studied with the proposed analysis method. This chirped Bragg grating was fabricated by the use of a chirped phase mask with the chirp rate of 1 nm/cm which corresponds to the grating period change of 0.5 nm/cm. A frequency-doubled argon-ion laser launches a CW 244 nm single-polarization UV beam into a FBG fabrication system to write the grating. The grating with a gaussian-apodized index profile was written in a Fibercore photosensitive fiber, which has the maximum reflectivity of 5 dB. In order to get all of the grating structure parameters, we firstly used the balanced Michelson interferometer method to find the spectrum phase information of the grating. Fig. 3.13 shows the reflection spectrum and the interference pattern of the grating. From the interference pattern, we can calculate the spectral phase by using the algorithm as shown in Fig. 3.5. The calculated phase information of the grating is shown in Fig. 3.14. In the next step, we use the reflection spectrum and the spectral phase of the grating as a target spectrum to calculate the structure parameters of the grating by the use of the discrete Layer-peeling method. We choose the wavelength window to be 8 nm, which corresponds to the detuning window of about  $0.0305 \mu\text{m}^{-1}$ . Because the layer thickness  $\Delta$  and the detuning window  $\delta_w$  must be related by

$$\Delta = \frac{\pi}{\delta_w} \quad (3.13)$$

Thus  $\Delta \sim 100 \mu\text{m}$ . Furthermore, we choose the length of the grating to be  $L=2 \text{ cm}$ , which

therefore determines the number of layer  $N=L/\Delta$ . In the Fig. 3.15(a) and (b), the dot line curves show the ac-index modulation from the DLP simulation. For comparison we also use the side-diffraction methods which include the methods with/without interference to measure the ac-index modulation as shown in Fig. 3.15 (a) and (b). The results matches well. We also can find that the index profile of the interference method (Fig. 3.15 (b)) is broader than the diffraction method (Fig. 3.15 (a)). Therefore, the side-diffraction interference method has better resolution for the measurement of the index modulation. From the DLP method, we can get the spatial grating index ( shown in Fig. 3.15) and the spatial grating phase (shown in Fig. 3.16). By using these two grating structure parameters to calculate the grating spectra, the results match the target spectra of the DLP method very well, which are shown in Fig. 3.17 and Fig. 3.18. From the above algorithm, the spatial grating index and phase are obtained, and the index profiles of the simulation and experiment are matched well. In order to get the grating period distribution and the dc-index profile, we must extract the structure parameters of the spatial phase term  $\arg q(z)$ . Firstly, we use the side-diffraction interference method to determine the grating period change which can be calculated by the use of the equation 3.12 based on the interference period change on the CCD camera. Fig. 3.19 shows the measured CCD interference period and grating period distribution. Because the phase terms  $\arg q(z)$  and  $\theta(z)$  have been known, we can find the dc-index distribution  $\Delta n_{dc}(z)$  from the equation 2.7. Unfortunately, there are too many noises which come from the phase measurement process of the interferometer setup. Therefore, the reconstruction of the dc-index modulation is typically quite noisy and we cannot determine the accurate dc-index profile from this analysis process. However, another analysis process can be used to determine the dc-index profile for this simple case. Because this chirped fiber Bragg grating has the gaussian-apodized index profile, we can assume that the dc-index profile is the same with the ac-index profile, but is with a different amplitude value. From equation 2.7, we

calculate the grating period distribution, and compare the results with the measured grating period distribution from the side-diffraction interference method. From Fig. 3.20 (a)-(d), we can find that when the multiplication factor is about 1.3, we can get the same grating period distribution that can be compared with the experimental results. In general, the grating structure can be expressed as

$$n(z) = \Delta n_{dc} + \Delta n_{ac} \cdot \cos\left(\frac{2\pi}{\Lambda} z + \theta\right) \quad (3.14)$$

If the grating structure is with the grating visibility = 1, then the dc-index profile  $\Delta n_{dc}$  equals to the ac-index profile  $\Delta n_{ac}$ . But in this simulated example,  $\Delta n_{dc} = \Delta n_{ac} * 1.3$ , which is because that the  $\pm 1$  order diffraction efficiency of the chirped phase mask is not one hundred percent. After the measurement of this diffraction efficiency of our chirped phase mask, we find that the  $\pm 1$  order efficiency is about 65%, and the zero + higher order beams efficiency is about 15%. From these measured results, we can estimate the intensity ratio of the ac-index and the dc-index to be about  $I_{dc} = I_{ac} * 1.23$ . From the above analysis, the multiplication factor of 1.3 is reasonable for the presented example. To summarize, we can get all of the grating structure parameters by using the proposed analysis process. Although we cannot directly get the dc-index profile in the presented example, we believe that if the noises from the interferometer measurement can be reduced, the dc-index profile could also be measured accurately.

### 3.5 Summary

In this chapter we have proposed two improved methods for measuring the characteristics of the fiber gratings. When the side-diffraction interference method is combined with the balanced Michelson interferometer method, we can get all the characteristics of the fiber grating. In section 3.4 we have demonstrated that the complex reflection coefficient or the

complex coupling coefficient of the grating can be achieved by using the proposed methods. Based on the side-diffraction interference method, we will also propose a new method of monitoring the fiber grating position for fabricating long FBGs. These will be described in the following chapter.



### References for Chapter 3:

- [1] P. Lambelet, P. Y. Fonjallaz, H. G. Limberger, R. P. Salathé, C. Zimmer, and H. H. Gilgen, "Bragg grating characterization by optical lowcoherence reflectometry," *IEEE Photon. Technol. Lett.*, vol. 5, p. 565, 1993.
- [2] M. Volanthen, H. Geiger, M. J. Cole, R. I. Laming, and J. P. Dakin, "Low coherence technique to characterize reflectivity and time delay as a function of wavelength within a long fiber grating," *Electron. Lett.*, vol. 32, no. 8, pp. 757–758, 1996.
- [3] E. Ingemar Petermann, Johannes Skaar, Bengt E. Sahlgren, Raoul A. H. Stubbe, and Ari T. Friberg, "Characterization of Fiber Bragg Gratings by Use of Optical Coherence-Domain Reflectometry," *J. of Lightwave Tech.*, vol. 17, pp. 2371-2378, 1999.
- [4] J. Skaar, "Measuring the group delay of fiber Bragg gratings by use of end-reflection interference", *Opt. Lett.*, vol. 24, pp.1020-1022, 1999.
- [5] Peter A. Krug, Ralf Stolte and Reinhard Ulrich, "Measurement of index modulation along an optical fiber Bragg grating," *Opt. Lett.*, vol. 20, pp. 1767-1769, 1995.
- [6] Fouad El-Diasty, Alan Heaney, and Turan Erdogan, "Analysis of fiber Bragg gratings by a side-diffraction interference technique," *Appl. Opt.*, vol. 40, pp. 890-896, 2001.
- [7] L. M. Baskin, M. Sumetsky, P. S. Westbrook, P. I. Reyes, and B. J. Eggleton, "Accurate characterization of fiber Bragg grating index modulation by side-diffraction technique", *IEEE Photo. Tech. Lett.* vol15, no.3, pp.449-451, 2003.
- [8] W. Margulis, I. C. S. Carvalho, and P. M. P. Gouvea, "Heat scan: a simple technique to study gratings in fibers," *Opt. Lett.*, vol. 18, pp. 1016-1018, 1993.
- [9] S. Sandgren, B. Sahlgren, A. Asseh, W. Margulis, F. Lurell, R. Stubbe, and A. Lidagrd, "Characterisation of Bragg gratings in fibres with the heat-scan technique," *Electron. Lett.*, vol. 31, pp. 665-666, 1995.
- [10] S. Ryu, Y. Horiuchi, and K. Mochizuki, "Novel chromatic dispersion measurement

method over continuous gigahertz tuning range,” *J. Lightwave Technol.*, vol. 7, pp. 1177–1180, Aug. 1989.

[11] M. L. Rocha and R. Kashyap, “Characterization of fiber Bragg gratings: A study on accuracy and repeatability,” in *Dig. 4th Optical Fiber Measurement Conf.*, Teddington, U.K., pp. 14–17, 1997.

[12] 蔡孟璋，賴暎杰 “光纖光柵色散特性量測及光柵結構之反推” 國立交通大學光電所碩士論文， 2003。

[13] S. Huang, M. M. Ohn, M. Leblanc, and R. M. Measures, “Continuous arbitrary strain profile measurements with fiber Bragg gratings,” *Smart Mater. Struct.*, vol. 7, pp. 248–256, 1998.

[14] S. Keren and M. Horowitz, “Interrogation of fiber gratings by use of low-coherence spectral interferometry of noiselike pulses,” *Opt. Lett.*, vol. 26, pp. 328–330, 2001.

[15] R. Feced, M. N. Zervas, and M. A. Muriel, “An efficient inverse scattering algorithm for the design of nonuniform fiber Bragg gratings,” *IEEE J. Quantum Electron.*, vol. 35, pp. 1105–1115, 1999.

[16] E. Peral, J. Capmany, and J. Marti, “Iterative solution to the Gel’Fand–Levitan–Marchenko coupled equations,” *IEEE J. Quantum Electron.*, vol. 32, pp. 2078–2084, 1996.

[17] L. Poladian, “Simple grating synthesis algorithm,” *Opt. Lett.*, vol. 25, pp. 787–789, 2000.

[18] J. Skaar, L. Wang, and T. Erdogan, “On the synthesis of fiber Bragg gratings by layer peeling,” *J. Lightwave Technol.*, vol. 37, pp. 165–173, 2001.

[19] Shay Keren, Amir Rosenthal, and Moshe Horowitz, “Measuring the structure of highly reflecting fiber Bragg gratings,” *IEEE Photon. Technol. Lett.*, vol. 15, pp. 575–577, 2003.

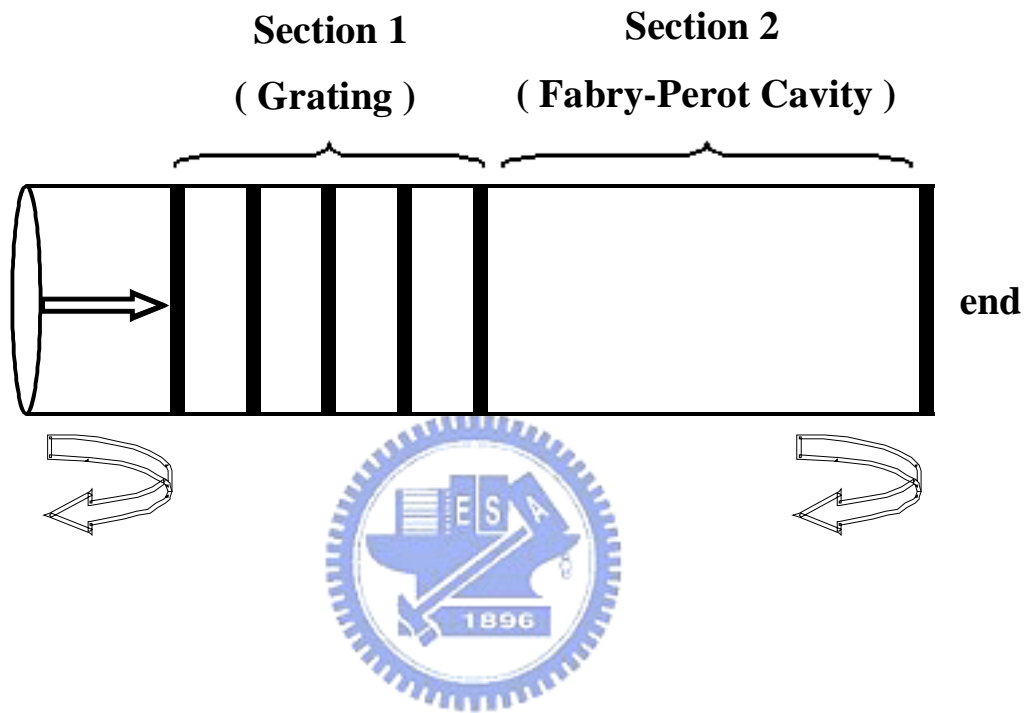


Fig. 3.1 Fabry-Perot cavity consisting of a fiber Bragg grating and a reference reflector.

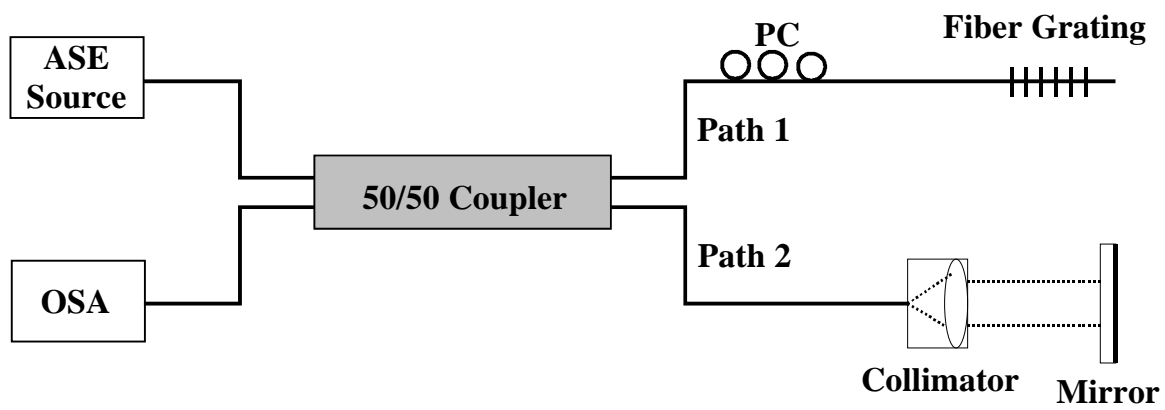


Fig. 3.2 Experimental setup of the balanced Michelson interferometer.

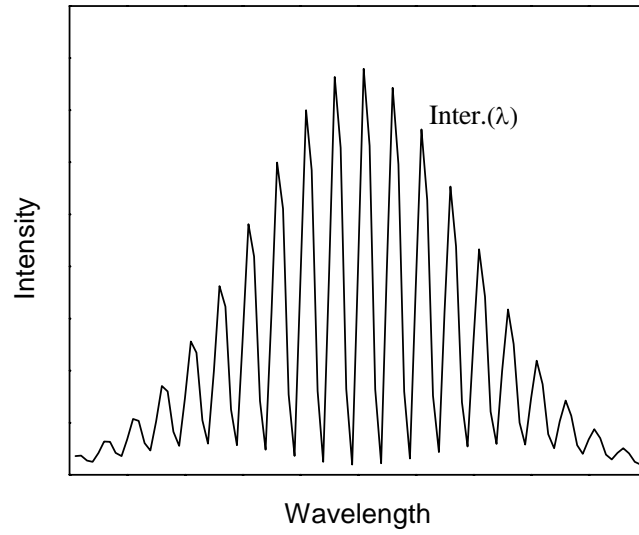


Fig. 3.3 The interference  $I_{\text{inter}}(\lambda)$  of combined signals.

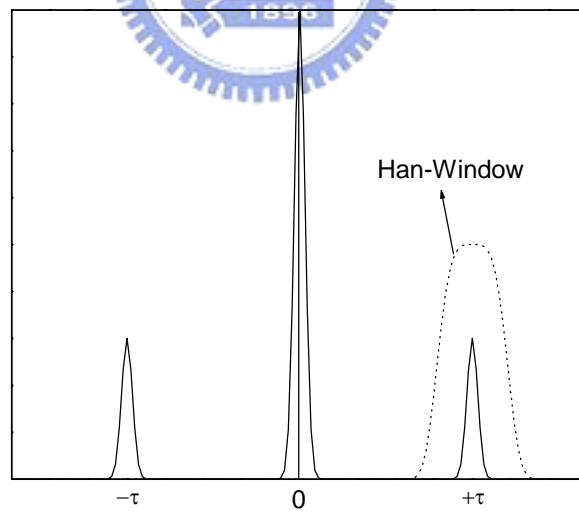


Fig. 3.4 The inverse Fourier transform of  $I_{\text{inter}}(\lambda)$ .

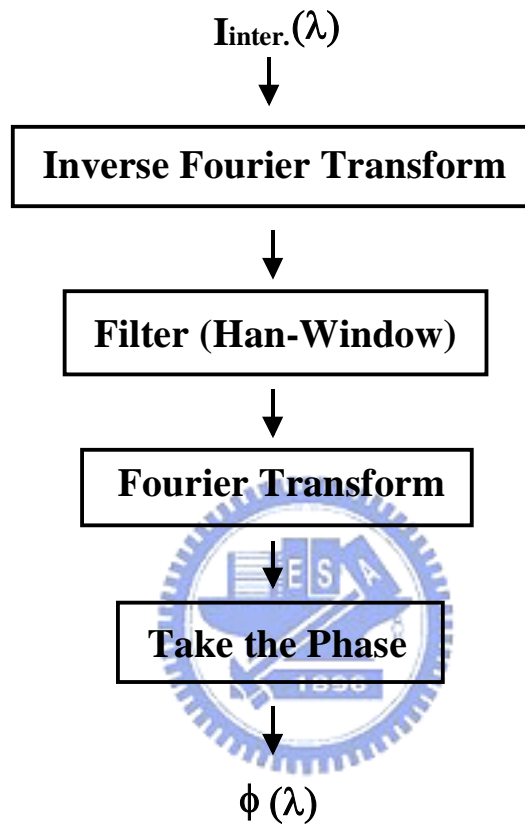
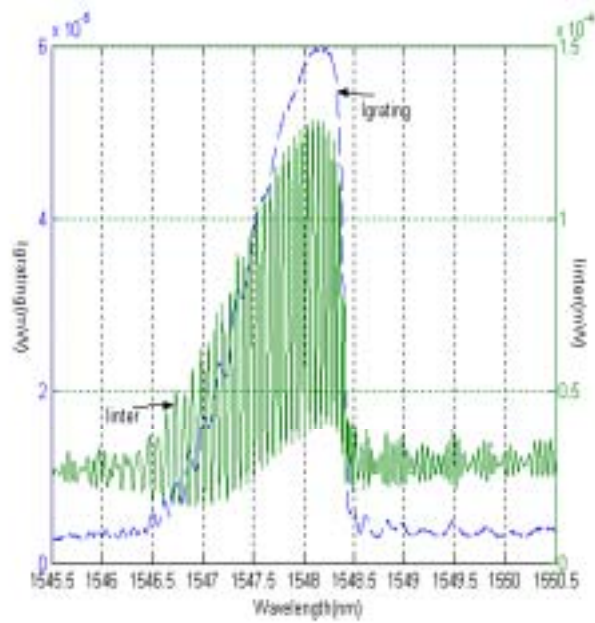
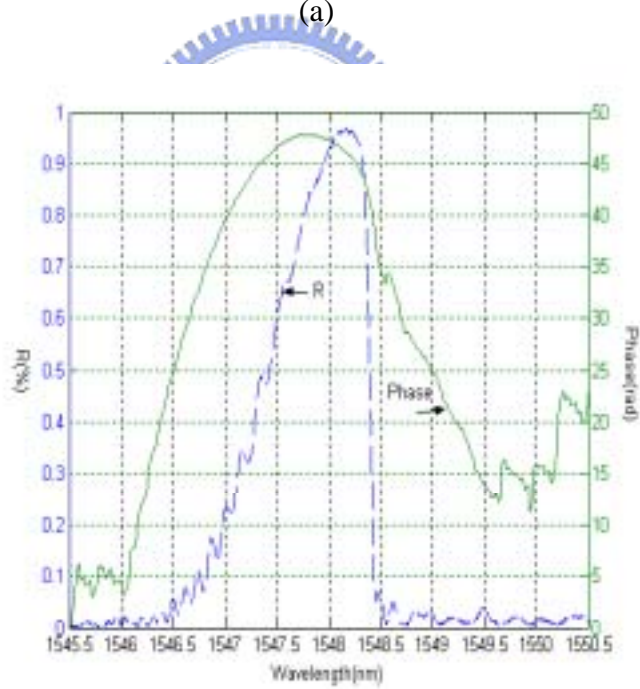


Fig. 3.5 The algorithm for finding the phase spectrum of the fiber grating.

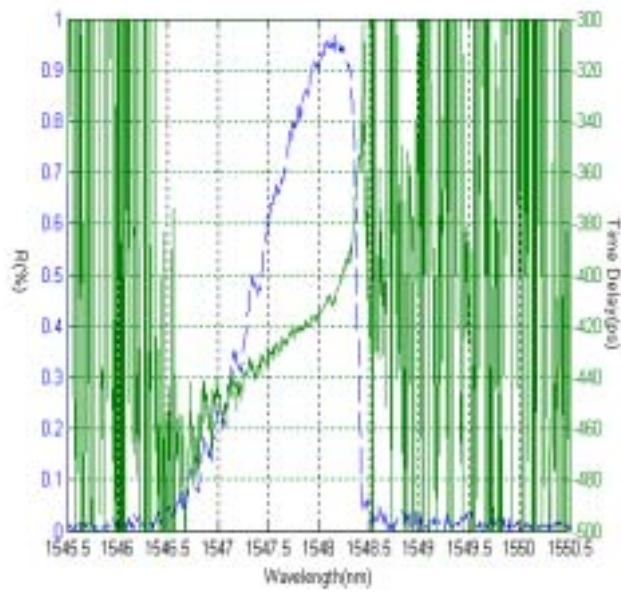


(a)

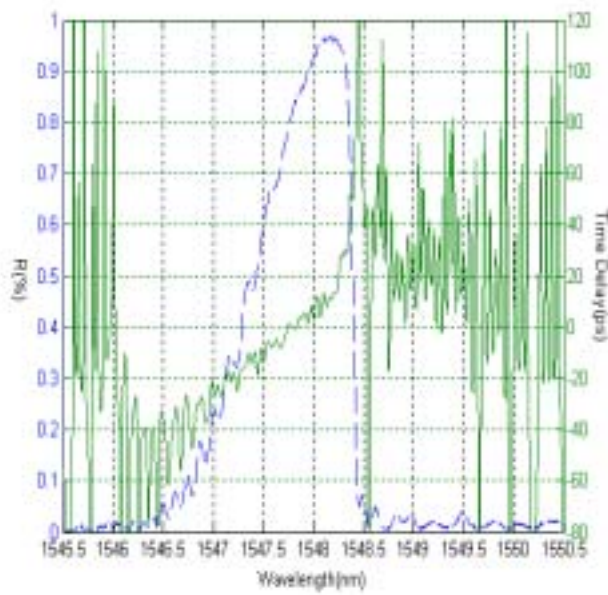


(b)

Fig. 3.6(a) The measured interference pattern  $I_{\text{inter}}(\lambda)$ , (b) The calculated phase spectrum  $\phi(\lambda)$ . (cited from [12])



(a)



(b)

Fig. 3.7 (a) Measured results using a commercial equipment “Advantest Q7760”, and (b) our measuring method. (cited from [12])

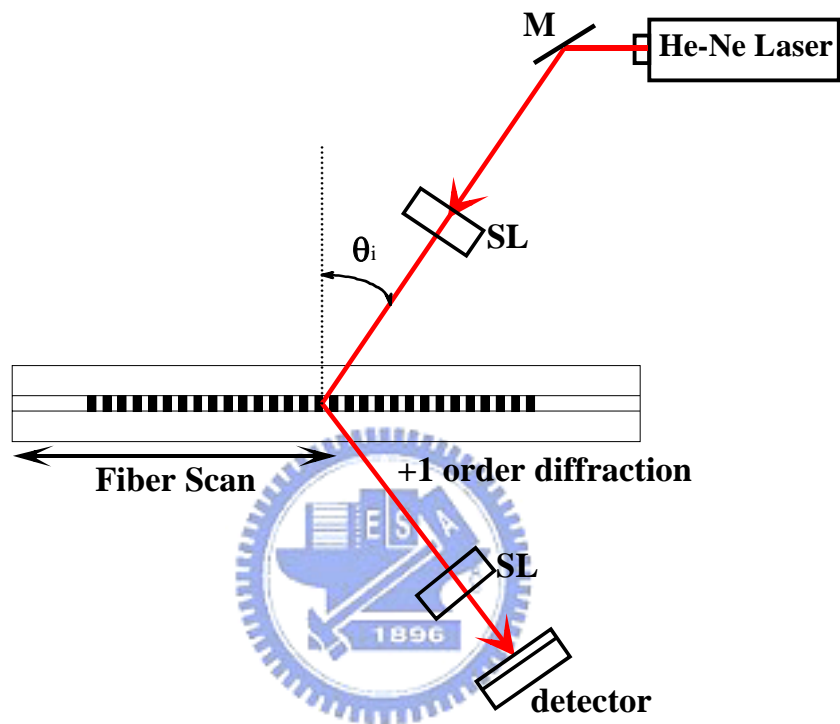


Fig. 3.8 The side-diffraction setup for measuring index modulation: M, reflection mirror; SL, spherical lens.

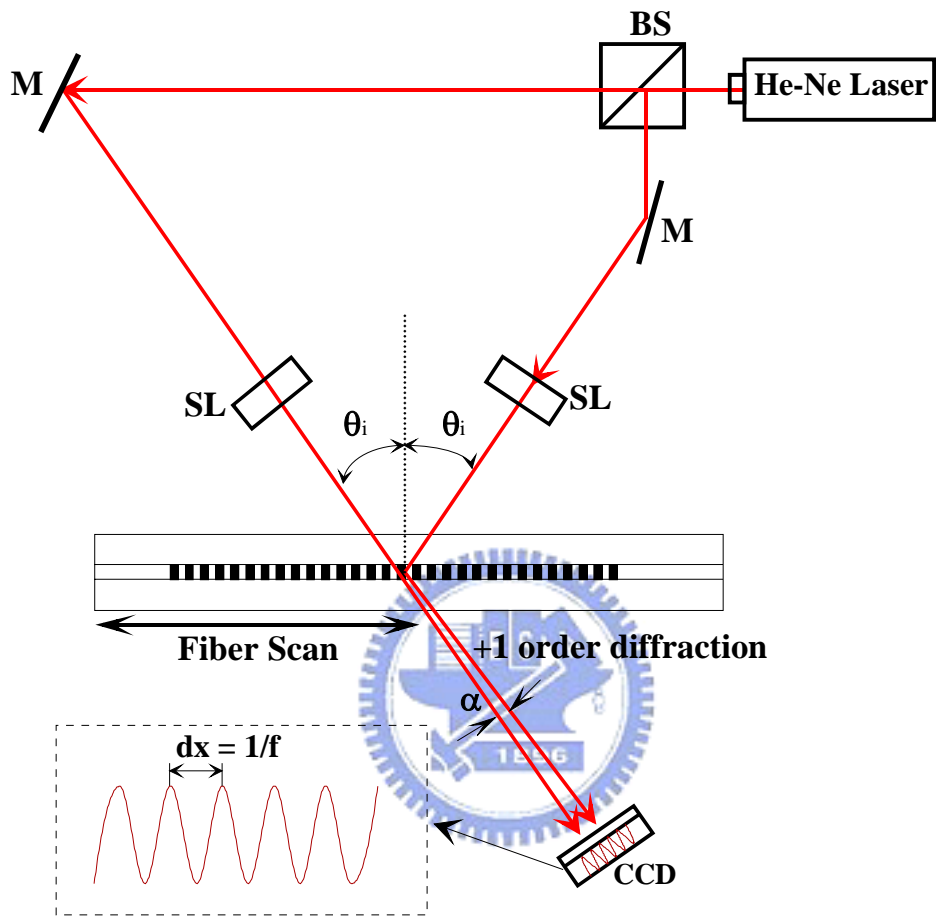


Fig. 3.9 The side-diffraction interference method for measuring grating period change: BS, beam splitter; M, reflection mirror; SL, spherical lens.

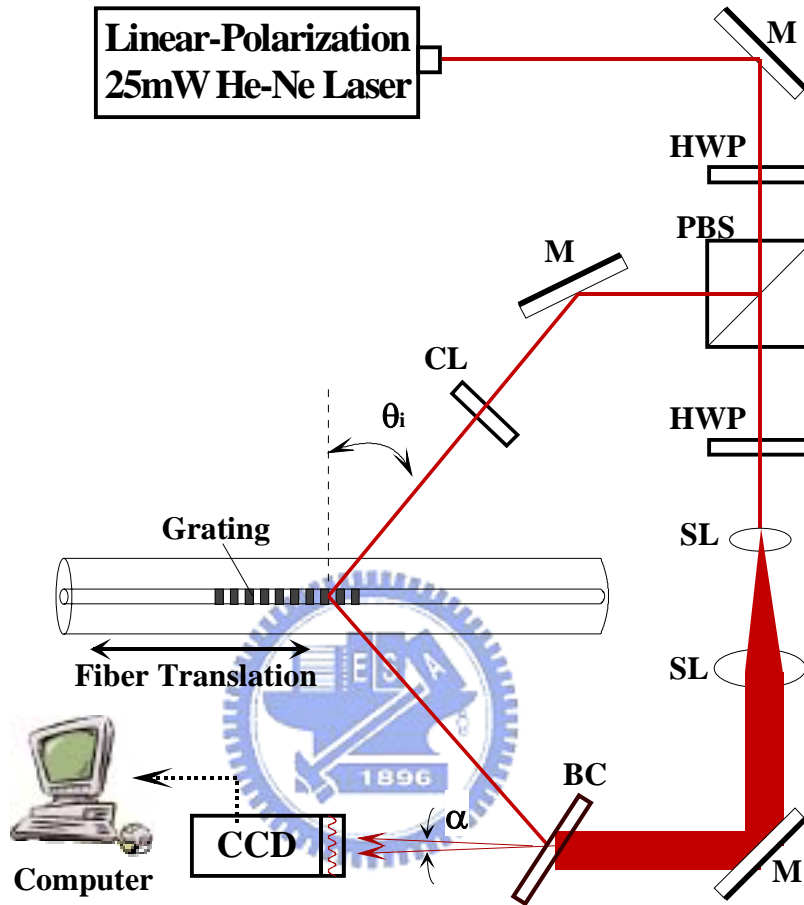


Fig. 3.10 The improved side-diffraction interference method for measuring the grating period variation and the ac-index modulation.

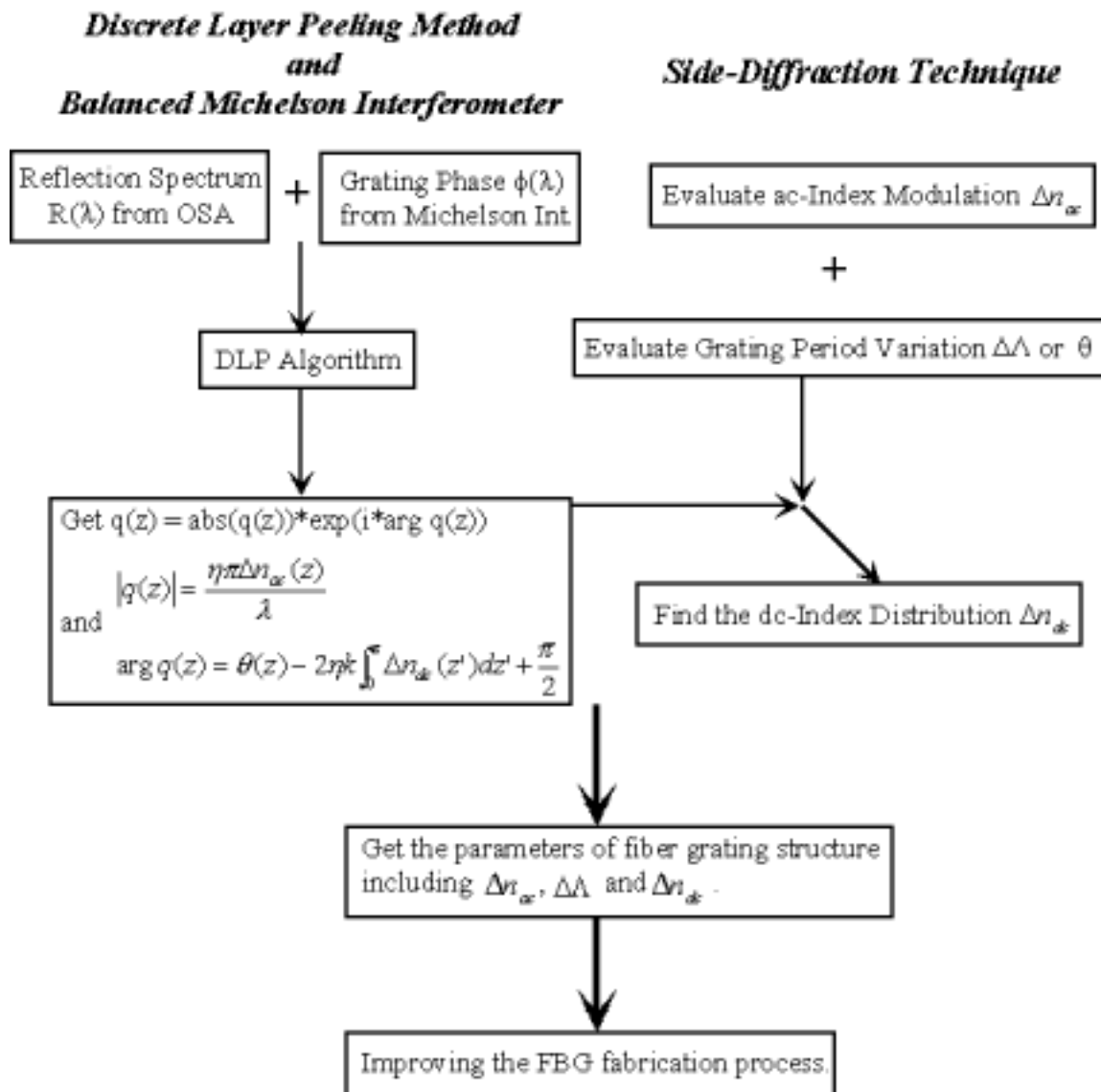


Fig. 3.11 Flow chart of the characterization method of fiber gratings.

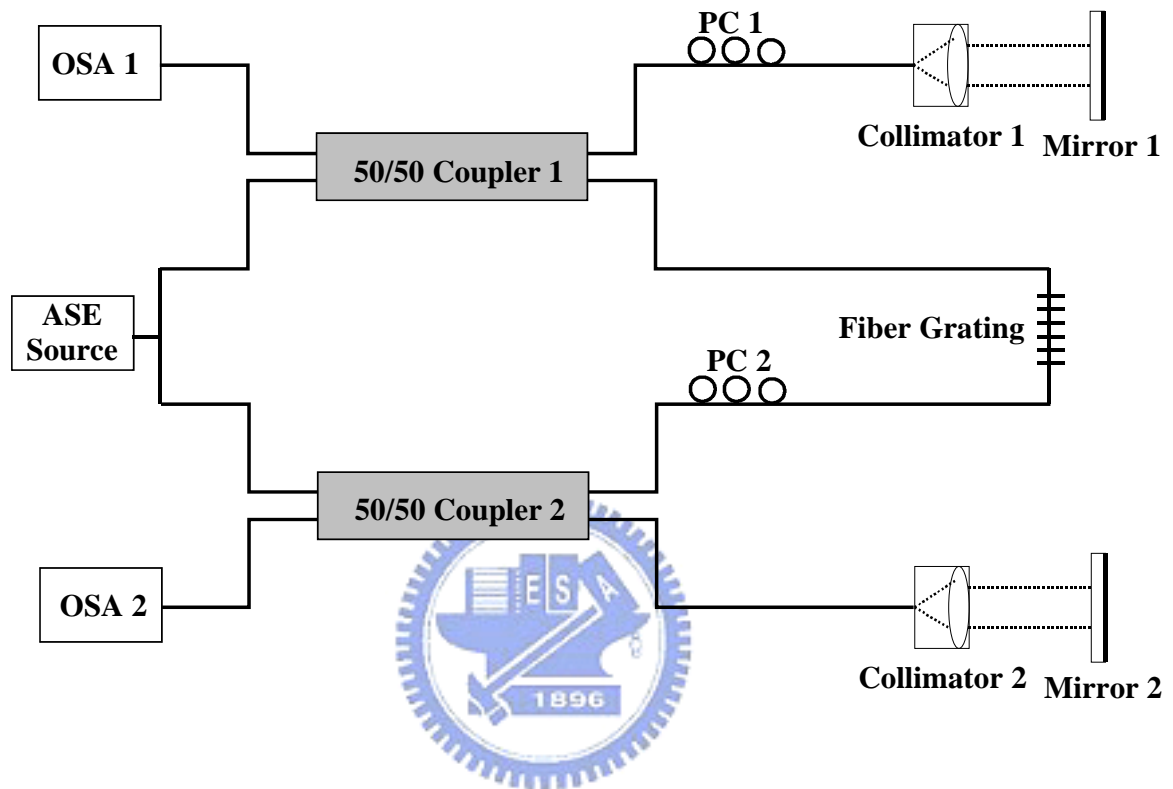


Fig. 3.12 The balanced Michelson interferometer setup used to measure the highly reflecting fiber gratings.

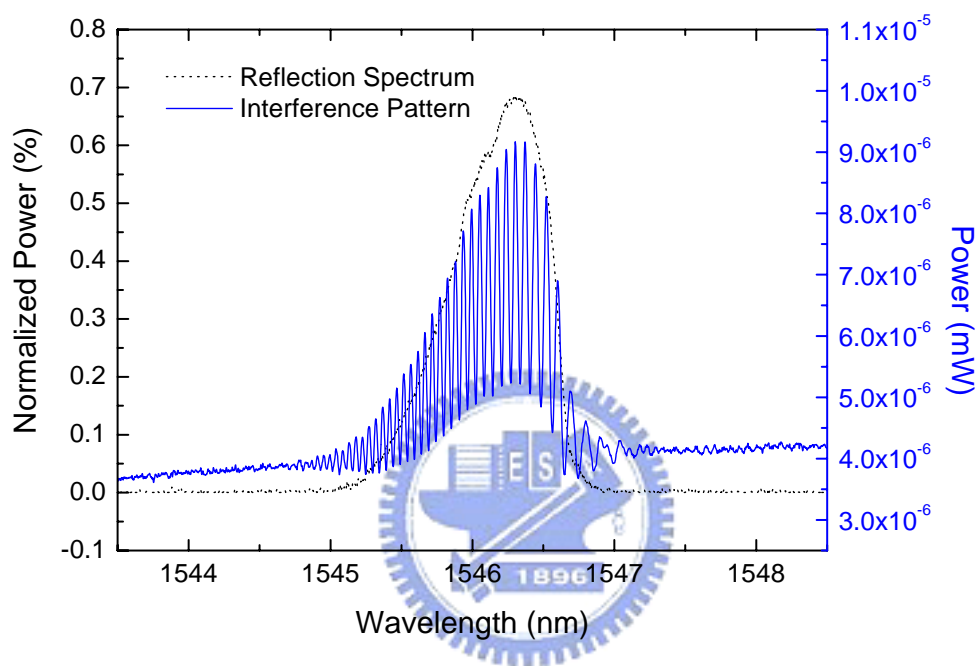


Fig. 3.13 The reflection spectrum and interference pattern by the use of the balanced Michelson interferometer method.

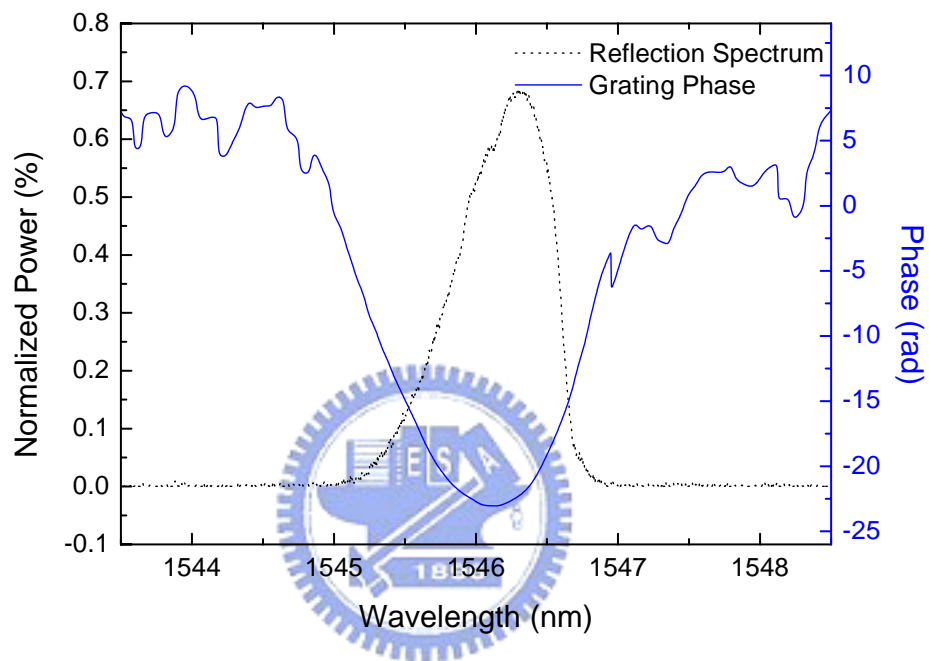
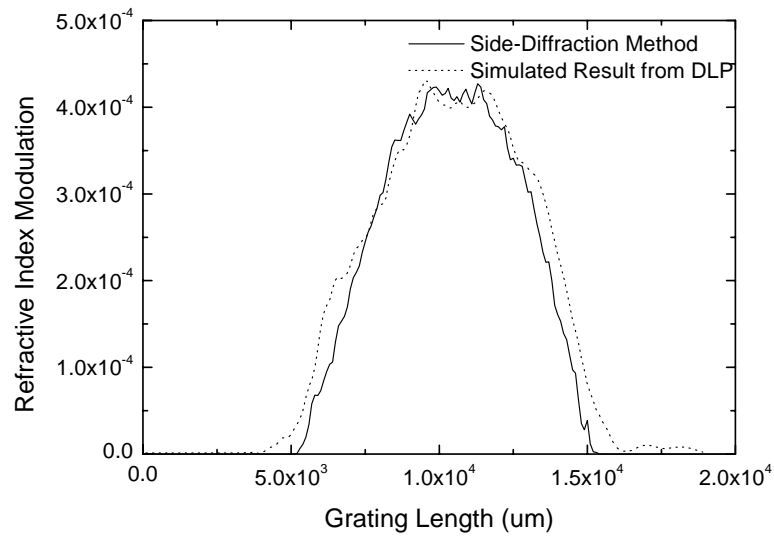
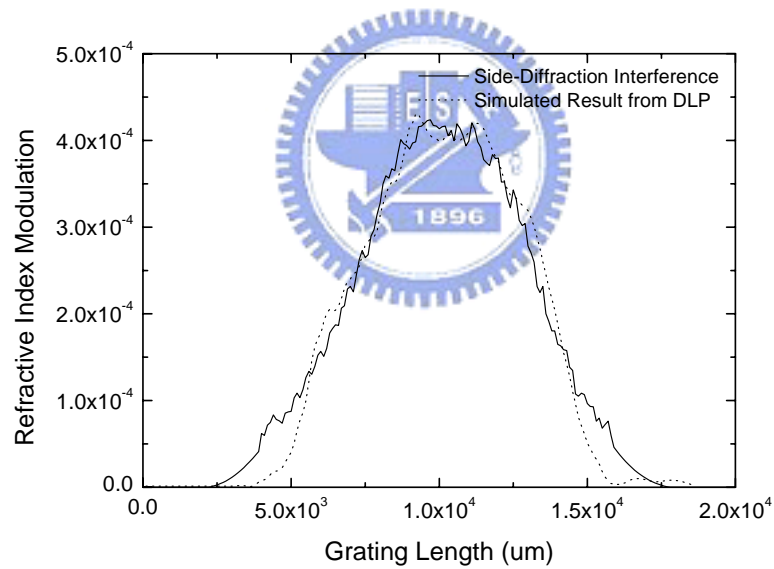


Fig. 3.14 The calculated phase information of the grating.



(a)



(b)

Fig. 3.15 (a) The Ac-index modulation from the DLP is compared with the side-diffraction method. (b) The Ac-index modulation from the DLP is compared with the side-diffraction interference method.

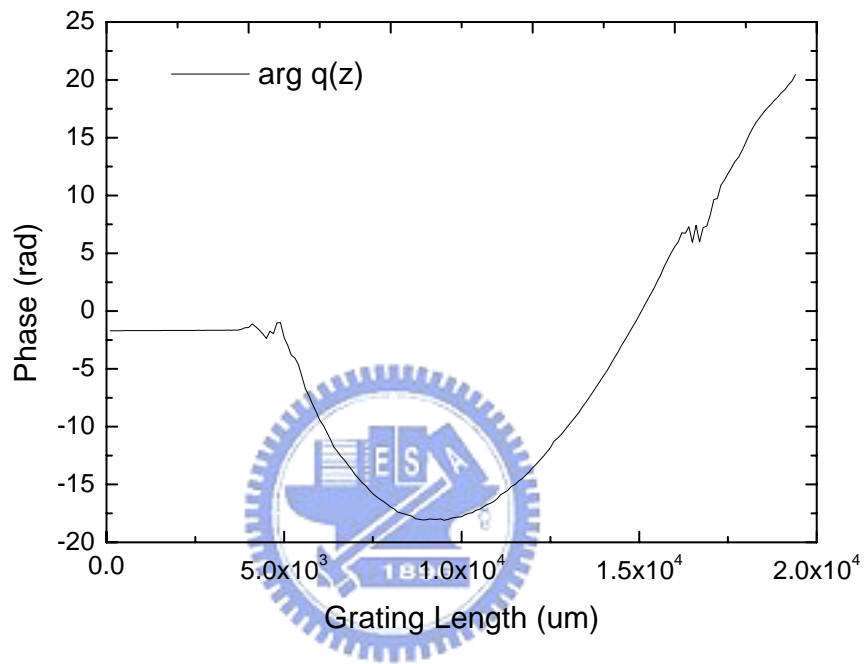


Fig. 3.16 The spatial grating phase is calculated from DLP method.

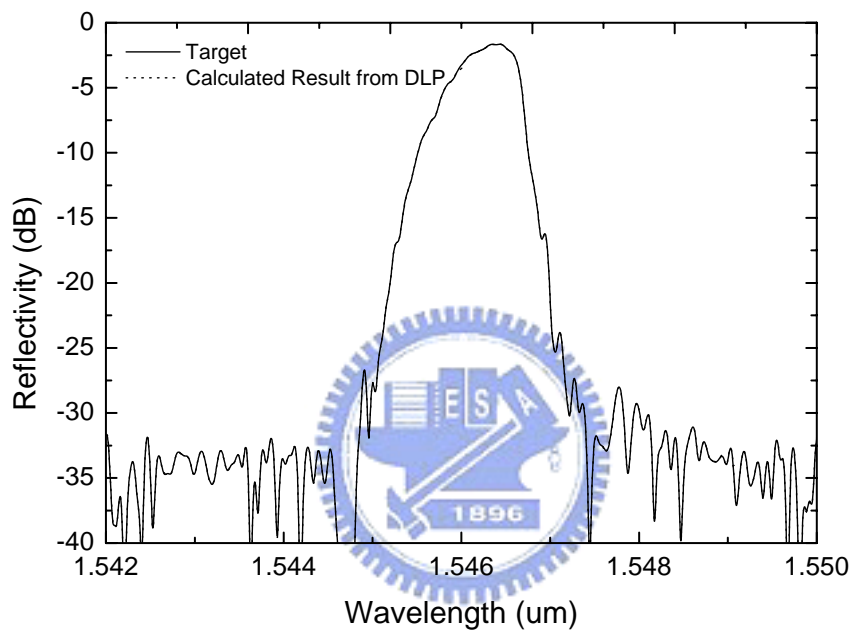


Fig. 3.17 The reflection spectra of the target and the calculated result from DLP method.

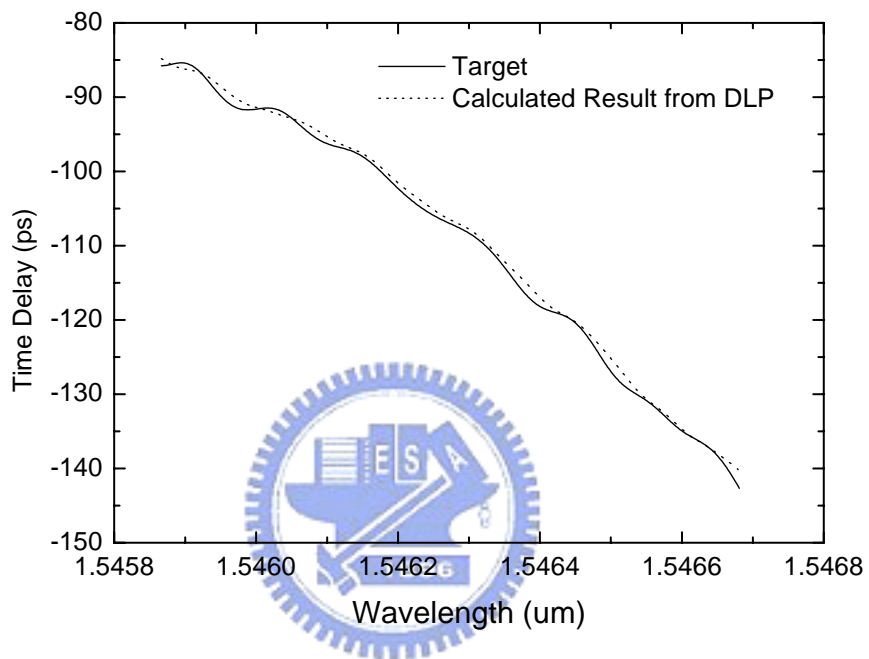


Fig. 3.18 The group time delays of the target and the calculated result from DLP method.

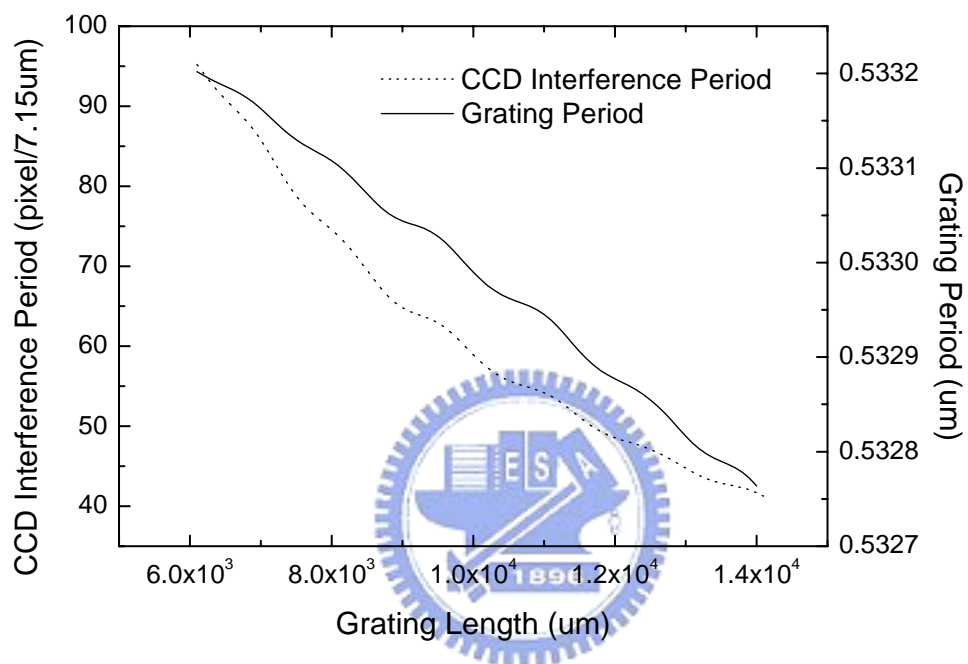


Fig. 3.19 The CCD interference period corresponds to the relative grating period.

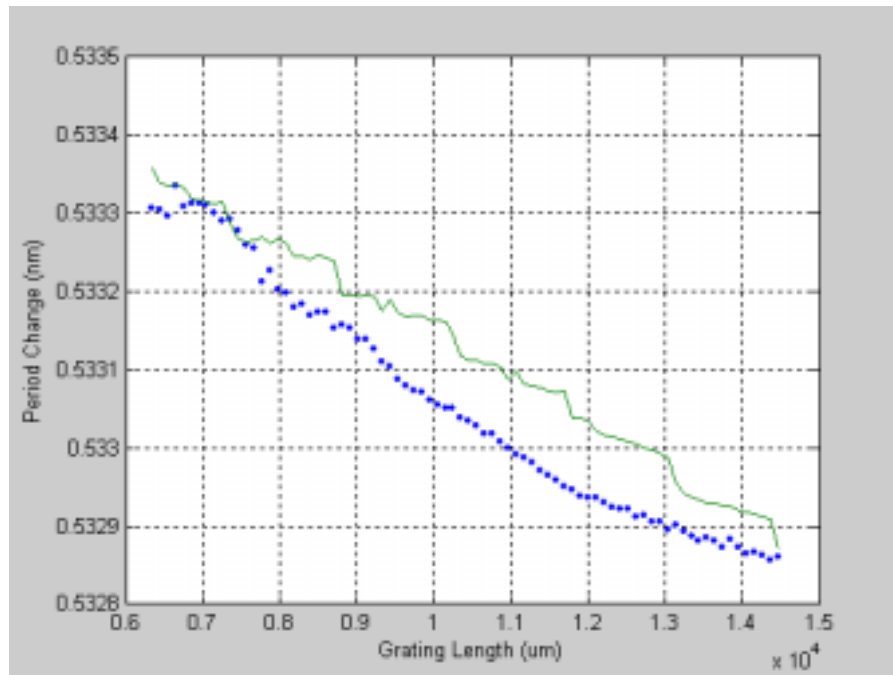


Fig. 3.20 (a) dc-index amplitude  $\Delta n_{dc}(z) = 0$ .

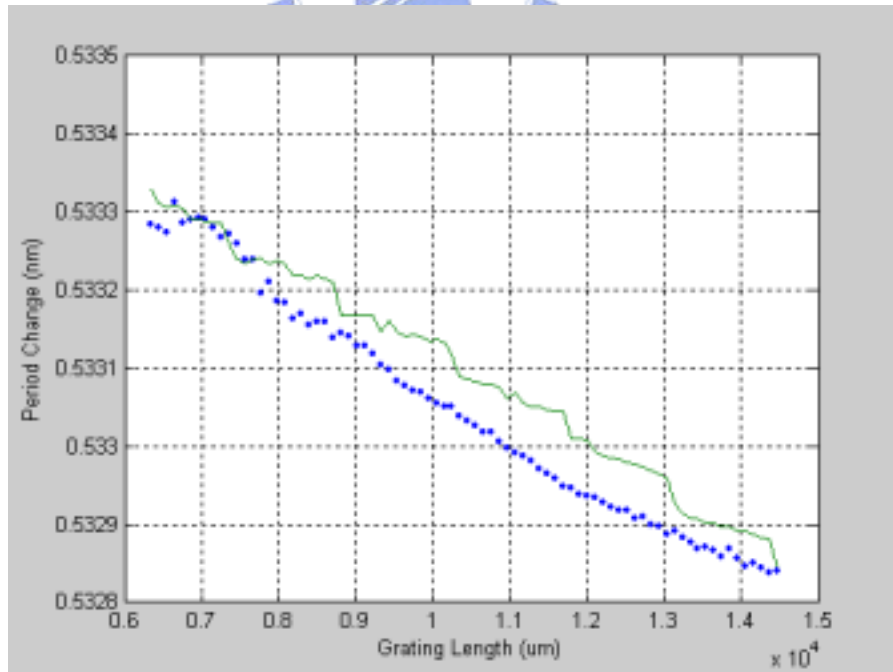


Fig. 3.20 (b) dc-index amplitude  $\Delta n_{dc}(z) = \Delta n_{ac}(z) * 0.5$ .

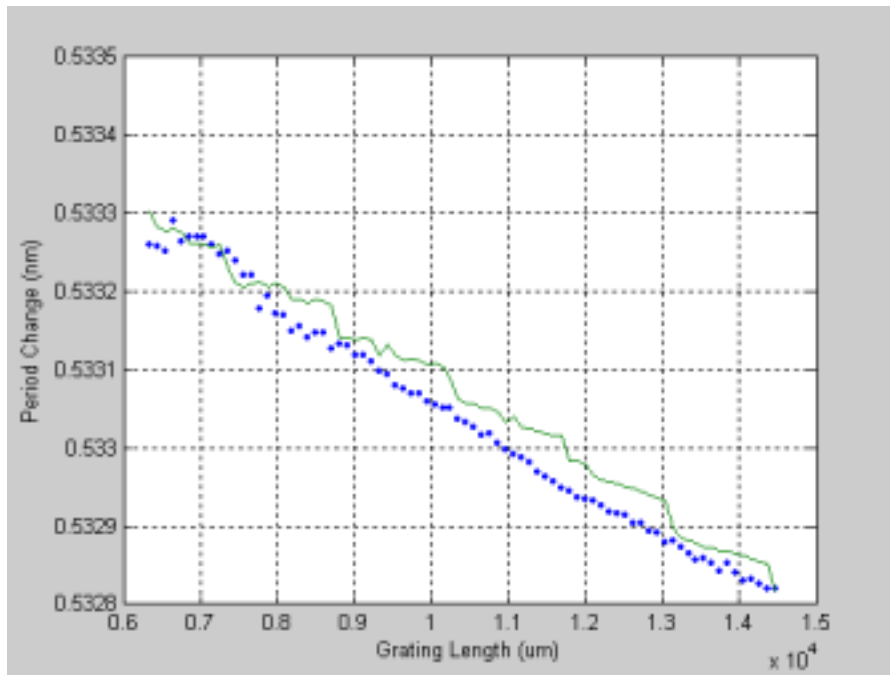


Fig. 3.20 (c) dc-index amplitude  $\Delta n_{dc}(z) = \text{ac-index amplitude } \Delta n_{ac}(z) * 1$ .

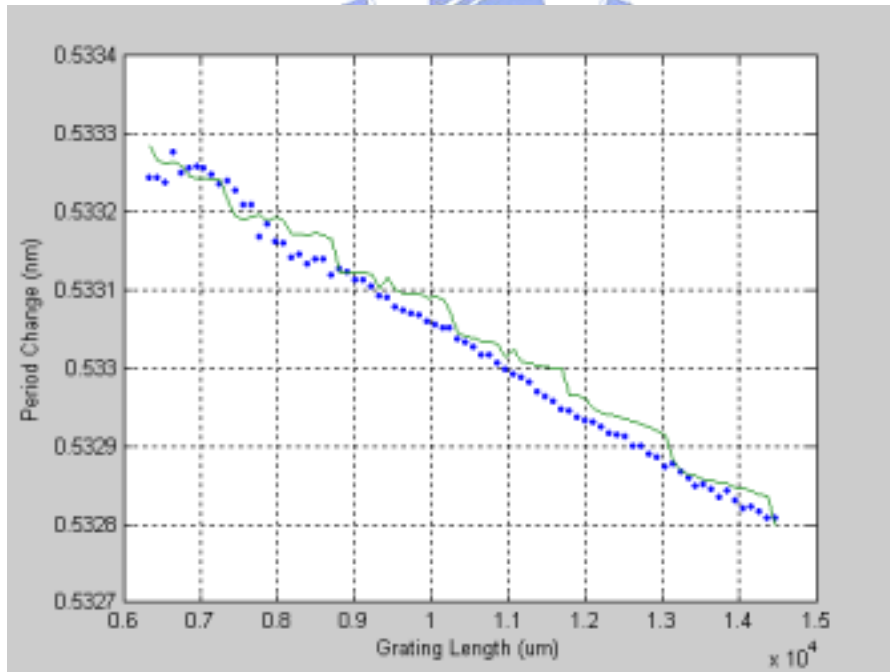


Fig. 3.20 (d) dc-index amplitude  $\Delta n_{dc}(z) = \text{ac-index amplitude } \Delta n_{ac}(z) * 1.3$ .

## Chapter 4. Fabrication of Advanced Fiber Bragg Gratings

### 4.1 Introduction

After the finding of the “Hill gratings” [1], the fabrication methods for fiber Bragg gratings fall into two categories: the holographic method [2] and the phase mask method [3]. In recent years, the fiber grating fabrication methods based on these two approaches have been developed rapidly. They can be used for the fabrication of advanced fiber Bragg gratings with complex structures from special design [4-7]. The applications of these advanced fiber Bragg gratings include the narrow band-pass filters [8], dispersion-free (dispersionless) FBGs [9], and DFB fiber lasers [10].

In this chapter we will describe some new methods for fabricating advanced fiber Bragg gratings, and will also demonstrate that these methods can be truly realized. In section 4.2 we describe the basic setup of our exposure system which is based on both the two-beam interferometer and the phase mask method. The automation of these methods is setup for fabricating long, complex FBGs. Some examples will be presented to demonstrate the performance of this exposure system. In section 4.3 we propose and demonstrate a new method which is capable of fabricating FBGs with not only pure apodization profiles but also  $\pi$ -phase shifts. This method is based on the two-beam interferometer technique with the polarization control on one of the interfering beams. In section 4.4 we propose another new approach based on the polarization control of the UV exposure beam. The method can be combined with the sequential writing setup based on either the two-beam interferometer or the phase-mask approach to produce pure apodized complex FBG structures in a single scan. Several experimental examples are also given to demonstrate the feasibility of the method. Within these new proposed methods, the connection of each grating section must be made for

forming a long, complex FBG structures. The phase error of each section connecting must be controlled under the acceptable range and thus the precision position monitoring of the fiber moving will become very important. We demonstrate a new method which is capable of monitoring the fiber grating position without the accumulative error due to the drift of the interferometer and the inaccurate grating period estimation. This monitoring method is based on the side-diffraction interference technique, which is shown in section 4.5. In section 4.6 we give a summary for this chapter.

## 4.2 Setup of the Exposure System

For the purpose of fabricating complex fiber grating structures, we have tried to setup an auto-controlled FBG exposure system based on the two exposure methods of phase mask and two-beam interferometer, which is as shown in Fig. 4.1. A frequency-doubled argon-ion laser launches a CW 244nm single-polarization UV beam into the exposure system that implements the phase mask exposure method or the two-beam interferometer exposure method. The fiber is placed in a holder mounted on a translation stage composed of a linear motor stage and a piezoelectric translator (PZT) stage with a position resolution of subnanometer. A He-Ne laser interferometer (Agilent 5529A system) with 2.5nm position resolution directly from the instrument is used for monitoring the fiber position. Sub-nm resolution can be achieved by time-averaging a certain number of the sample points. A shutter is placed after the UV laser in order to control the exposure time with an accuracy of 10ms. Specifically in the two-beam interferometer setup, a rotating reflecting mirror which controls the interference angle is used to change the period of the interference fringes. Because of the special symmetrical optical design, the induced angle changes for both beams will be the same and thus the UV standing wave pattern will not be angle-tilted with respect to the fiber. Although the overlap area

between the interfering beams will move orthogonally to the fiber, we do not need to re-do the alignment of the setup when the changed angle is small since the position sensitivity is less severe. Even when the changed angle is large, a simple 1-D translation can be easily implemented to adjust the fiber position. This feature is quite useful for establishing a flexible exposure platform.

The most important parameters of the fiber grating including the refractive index modulation amplitude and phase must be controlled very precisely. Under real fabrication conditions, these parameters of the fiber grating can be adjusted by the control of the exposure time, the grating period, and the relative grating position. To verify the precision of our setup, we have performed some preliminary experiments. We first use the two-beam interferometer method to fabricate a multi-band FBG filter with four channels at different fiber positions. Each FBG is fabricated with gaussian apodized index profile and 5mm long. The dc-index modulation can be flattened by changing the interference angle of the two UV beams with the fiber position at the non-interference region as shown in Fig. 4.2. Their results are showed in Fig. 4.3. Secondly we use 100 sequences of step writing with the UV beam diameter of 5mm, the scanning step size of 535um, and with the raised gaussian apodized index profile which the dc-index is keeping constant along the whole grating. The constant dc-index profile can be reached in this case by using the double-UV exposure method [11]. We can get the 3dB bandwidth of about 0.15nm and the side lobe suppression below 25dB as showed in Fig. 4.4.

Another example to verify this auto-controlled exposure system is to fabricate a 100mm long chirped FBG by using a 100mm chirped phase mask with a chirp rate of 0.003444 nm/mm. We simulated a 100mm tanh apodized chirped FBG with zero dc index profile and with the max index change of 0.0005 and the 3-dB bandwidth of 0.4nm. We also calculated the group delay time to be 1937 ps/nm. The spectra and time delay of the simulated results are shown in Fig. 4.5. We then used the double-UV exposure method to reach a constant dc-index

change. The experimental result is shown in Fig. 4.6. The group time delay of this example is measured by use of the proposed balanced Michelson interferometer method described in chapter 3.2. We can find that the experimental result matches the simulated result very well.

This auto-controlled exposure system with the developed Labview program as shown in Fig. 4.7 has been demonstrated to be able to fabricate long FBGs with various periods. But for fabricating complex grating structures with the constant dc-index profile in a single scan and with no accumulative phase error, new exposure methods still need to be developed for reaching these purposes. In the following sections, we will propose three new methods to overcome these problems. These new methods can be used not only with the phase mask method but also with the two-beam interferometer method. They can make the parameter control of fabricated fiber gratings become more easy and accurate.

### **4.3 Two-Beam Interferometer Method with Polarization Control**



For many FBG applications, it is important to apodize the FBG structure such that its dc index change remains a constant across the whole grating (i.e. pure apodization). For more advanced FBGs like dispersionless FBGs, multiple  $\pi$ -phase shifts are also required. In this section we propose and demonstrate a new method which is capable of fabricating FBGs with not only pure apodization profiles but also  $\pi$ -phase shifts. This method is based on the two-beam interferometer technique with the polarization control on one of the interfering beams. The FBG is exposed by a step-scan exposure method and the pure apodization profile as well as  $\pi$ -phase shifts can be achieved in a single scan.

## I. Experimental setup and working principle

The experimental setup is illustrated in Fig. 4.8. A frequency-doubled argon-ion laser launches a CW 244nm single-polarization UV beam into a two-beam interferometer with a half-wave plate in one of the two interfering beams. The fiber is placed in a holder mounted on a translation stage composed of a linear motor stage and a piezoelectric translator (PZT) stage. A He-Ne laser interferometer (Agilent 5529A system) with sub-nm position resolution is used for monitoring the fiber position. A shutter is placed at the entrance of the setup in order to control the UV exposure flux. A rotating reflecting mirror which controls the interference angle is used to change the period of the interference fringes. The function of the half-wave plate is to rotate the polarization of the UV beam. It has been well known that for a general azimuthal angle  $\theta$  between the input polarization and the waveplate axis, the half-wave plate will rotate the beam polarization by an angle  $2\theta$ . Since the two interfering beams have the same linear polarization before passing through the waveplate and the field components of orthogonal polarizations will not interfere, the maximum refractive-index modulation amplitude is obtained at  $\theta = 0^\circ$  and zero modulation amplitude occurs at either  $\theta = -45^\circ$  or  $45^\circ$ . The orthogonal polarization field component generated by the polarization rotation of the waveplate has no contribution to the ac-modulation index, but will contribute to the dc-index change. To be more explicit, the ac-refractive-index modulation amplitude will be a  $\cos^2(2\theta)$  function according to a simple derivation. Therefore, with this setup, the ac-index change of the exposed FBG section can be adjusted by changing the angle  $\theta$  as shown in Fig. 4.9. Moreover, by switching the fast and the slow axes of the waveplate with a 90 degree angle rotation, we can also keep the output polarization the same but introduce an additional  $\pi$  phase shift on to the UV beam. In this way we can easily and accurately produce  $\pi$ -phase-shifted interference fringes on the fiber for exposing the  $\pi$ -phase-shifted FBGs.

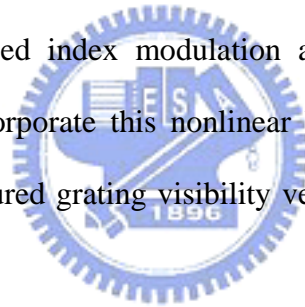
In our proposed method, the FBG is fabricated by an overlap-step-scan exposure approach [12]. We expose the fiber section-by-section and the adjacent sections overlap strongly to smooth out the random errors. The exposure time for each section is kept the same and the ac-index modulation of the FBG is controlled by changing the rotation angle of the half-wave plate. The dc-index change for each section exposure will be the same no matter what is the angle of the waveplate, as long as the exposure time for each section is fixed constant. One intuitive way to understand this is to notice that the total UV flux for each section exposure is always the same, independent of the waveplate angle. When the ac-index modulation is smaller (larger), the dc-index change created by the orthogonal field component becomes larger (smaller) and the net dc-index change remains the same as long as the exposure time is fixed. In this way we can achieve a flat dc-index change as illustrated in Fig. 4.10(a) after the exposure scan, as long as the step-scan size is much smaller than the beam width of the exposure UV beam.



## II. Experimental Results

In order to demonstrate that our new method can be truly applicable, we first expose single-section FBGs with different rotation angles of the waveplate and measure their corresponding refractive index modulation. By theoretically calculating the corresponding visibility for each rotating angle of the half-wave plate to obtain the theoretical value of the refractive index modulation versus the rotation angle of the half-wave plate, in Fig. 4.10(b) we verify that the experimental results match the theoretical predictions well. However in the figure it seems to show a systematic deviation between the theoretical curve and the experimental points. One of the possible causes is the non-linear behavior of the refractive index modulation versus the exposed energy [13]. We have tried to characterize the non-linear

behavior from our measurement data and to check numerically whether the deviation caused by the non-linear effects can be significant. The non-linear behavior of the refractive index modulation depends on a power law [13]. In Fig. 4.11, we calculate the deviation curve of FBG with non-linear effect depending on the power law, and we can see that its trend of deviation match the experimental results shown in Fig. 4.10(b) well. We find that for the FBGs with symmetric apodization profiles, the impacts are less significant (only sidelobes are larger). However, for FBGs with asymmetric apodization profiles (like the dispersionless FBGs), the impacts will be more significant (the spectral shape may be even changed). The non-linear behaviour of the refractive index change which both a function of fluence and intensity is important for fabricating more complex or asymmetric FBGs, and this effect must be concerned for all of the FBG fabrication method. In principle, in order to achieve more accurate control of the induced index modulation and to avoid the bad impacts of the nonlinear effects, we can incorporate this nonlinear behavior in the design with a careful calibration based on the measured grating visibility versus the waveplate angle for the fixed exposure energy.



We then proceed to fabricate a pure apodized FBG with a cosine<sup>2</sup> apodization function. The FBG is formed in a photosensitive fiber after 100-section sequential writing with a total grating length about 5 cm. It is fabricated by the overlap-step-scan exposure setup with the exposed UV beam diameter = 5.2 mm and the fiber scan step = 535  $\mu\text{m}$ . We uniformly rotated the half-wave plate azimuth angle from  $\theta = -45^{\circ}$  to  $45^{\circ}$  during the exposure scan to produce the required apodization. For comparison, we also show the theoretical reflection spectrum for the FBG with the same cosine<sup>2</sup> apodization function but also with a non-constant dc index change as in ordinarily apodized FBGs. In Fig. 4.12(a), we show the reflection spectra of both gratings. One can see that the cosine<sup>2</sup> “ordinarily” apodized FBG (dot line) will has much higher sidelobes than the purely apodized FBG (real line) on the shorter wavelength

side. The sidelobes of the “ordinarily” apodized cosine<sup>2</sup> FBG are mainly due to the self-chirp caused by the non-uniform dc-index along the grating length [14]. This is the main reason why pure apodization is usually needed for achieving high performance.

In Fig. 4.12(b) we show an example of the fabricated  $\pi$ -phase-shifted FBGs. It is a 3 cm long FBG with a raised-cosine<sup>2</sup> shape and the added  $\pi$ -phase shift is created by rotating an additional 90<sup>0</sup> angle of the half-wave plate after half of the scan. As expected, the  $\pi$ -phase shift induces a narrow transmission peak in the middle of the stop band. The measurement resolution of the transmission peak is limited by the 0.01 nm resolution of our optical spectrum analyzer. Multiple  $\pi$ -phase shifted FBGs also can be fabricated easily with the present method. This kind of  $\pi$ -phase shift fabrication technique should be very useful for producing advanced FBG devices as well as for the applications of distributed feedback (DFB) fiber lasers.

In the proposed method a linearly polarized UV beam is used for FBG fabrication. In reference [15] it has been shown that the UV polarization is the dominant cause of birefringence in the UV-induced index change. The birefringent effect always exists for the FBG fabrication processes with polarized beams. In the present polarization control method, the major difference compared to the other fabrication methods is that the present method induces the variation of the dc refractive index change along the fast and slow polarization axes of the whole grating. This effect will result in non-constant dc index change, which could affect the reflection response. In Fig. 4.13, if we consider the 8% birefringence of FBG [15], it can be seen that this effect for the reflection spectrum is very small to be neglected. In the present method, the highly isotropic fiber gratings can also be produced by exposure of the fiber to UV light polarized predominantly along the fiber axis [15]. The induced birefringence of our fabricated FBGs is estimated to be 1-2% of the index modulation, which is a reasonable value when the s-polarization UV beam is used [15]. This magnitude of

birefringence is numerically found to have very little effects on the reflection spectra for the designed FBG devices.

We have demonstrated that pure apodization and  $\pi$ -phase-shifted FBGs can be achieved through the combination of a novel two-beam interferometer with polarization control and the overlap-step-scan exposure method. By using the auto-control Labview program as shown in Fig. 14, the required ac refractive index modulation as well as  $\pi$ -phase-shifts can be achieved easily by rotating the half-wave plate during the scan and the dc-index change can be fixed at a constant simultaneously. This new technique should have the great potential to become a powerful tool for fabricating complicated FBG structures for different application purposes.

#### **4.4 Phase Mask Method with Polarization Control**



The formation of fiber Bragg gratings (FBGs) by side-illumination with two coherent UV beams was first demonstrated by Meltz et al. [2] in 1989. Afterwards, the invention of the phase mask approach [3] made the fabrication of FBG devices more repeatable due to the less stringent requirement on the UV source. Today the commercial FBG devices are almost based on the phase mask method. It is necessary to invent a FBG fabrication method based on the phase mask method for fabricating complex FBG structures easily. In this section we propose a new approach based on the polarization control of the UV beam. The method can be combined with the sequential writing setup based on either the two-beam interference or the phase-mask approach to produce pure apodized complicated FBGs in a single scan. Several experimental examples are also given to demonstrate the feasibility of the method.

## I. Experimental setup and working principle

Our experimental setup is illustrated in Fig. 4.15. A frequency-doubled argon-ion laser launches a CW 244 nm single-polarization UV beam into the fabrication system which uses the phase mask technique with the fiber mounted on a translation stage that is monitored by a He-Ne laser interferometer with nm position resolution. The key feature of the proposed method is that the two writing beams for creating the ac and dc refractive-index modulation respectively are generated by the combination of the half-wave plate and the polarization beam splitter. In this way the total energy of the writing beams is always constant as long as the exposed time is fixed. With such a setup the dc-index change can be kept constant even when the ac-index modulation is apodized through the rotation of the half-wave plate. The translation stage includes a PZT stage with a position resolution of subnanometer. This permits us to incorporate arbitrary phase shifts into the fiber grating during the writing scan. The function of the half-wave plate is to rotate the polarization of the UV beam. The polarization beam splitter separates the input UV beam into two orthogonal polarization beams, which will be used as the writing beams for the dc- and ac -index modulation respectively. In order to keep the net dc-index-change remaining constant for getting pure apodization FBG (like Fig. 4.16) when rotating the half-wave plate, we must make the two writing beams experience equal optical losses by adding the optical attenuator to one of the beam paths. If the optical losses on the two writing beams cannot be made equal, it will cause higher sidelobes at two wavelength sides of the stop band as shown in Fig. 4.17 and Fig. 4.18. Fig. 4.19 explains the way of achieving a constant dc-index change. The net UV-induced index modulation after the scan exposure can be described by

$$\Delta n(z) = \sum_m \eta S(z - z_m) \cdot \left[ 1 + \cos^2(2\theta_m) \cdot \cos\left(\frac{2\pi z}{\Lambda} + \phi_m\right) \right], \quad (4.1)$$

where  $\Lambda$  is the grating period,  $S(z)$  is the exposed UV distribution,  $z_m = m\Delta z$  is the

center position of the  $m$ -th exposure,  $\theta_m$  is the phase of the half-wave plate,  $\phi_m$  is the grating phase, and  $\eta$  is the photosensitivity factor. It can be seen that the net dc-term is independent of  $\theta_m$  and can be made to approach a constant distribution if the scan step-size  $\Delta z$  is chosen to be much smaller than the beam-width of  $S(z)$ . In this way, by simply programming the relative angle position of the half-wave plate, pure apodized FBGs with any structures can be created in a single scan.

## II. Experimental Results

To demonstrate that our new method can be truly applicable, we first design a pure apodized FBG with the ac-index modulation amplitude being a cosine<sup>2</sup> function. Such a profile can be easily achieved by uniformly rotating the waveplate azimuth angle from  $\theta = -45^\circ$  to  $45^\circ$ . We use the Fibercore photosensitive fibers (PS1500) with 7-day hydrogen loading at room temperature. A 30-mm FBG is fabricated by the overlap-step-scan exposure method [12] with the UV beam diameter about 2.4 mm and the scan-step about 240  $\mu\text{m}$ . We expose the fiber section-by-section and the adjacent sections overlap strongly to smooth out the random error. In Fig. 4.20 we verify that the experimental result (real line) matches the theoretical result (dash line) quite well and the sidelobe suppression level is down to -30 dB. As a comparison, the dot line shows the calculated spectrum for the FBG which has the same ac apodization index profile but also has a non-constant dc index change (as in the FBGs fabricated by ordinary exposure schemes). One can see that the spectral edge in the shorter wavelength side is much improved with pure apodization.

There are many applications which need one or multiple phase shifts in the FBGs, such as dispersionless FBGs and DFB fiber lasers. The requirements for dispersionless FBGs include the linear phase spectrum and the flat-top, nearly rectangular intensity spectrum. A

practical dispersionless FBG can be designed by using the discrete layer-peeling (DLP) method and the designed FBG will exhibit multiple  $\pi$ -phase shifts in the index profile. In our design example, we use the target spectrum described by the following “super-gaussian” function:

$$r(\delta) = \sqrt{R} \cdot \exp\left[-(\delta / \delta_{PB})^{20}\right] \quad (4.2)$$

Here  $\delta$  is the wavenumber detuning. The maximum reflectivity is  $R=0.99$  and the bandwidth parameter  $\delta_{PB} = 7.58 \times 10^{-4} \text{ um}^{-1}$ , which corresponds to a pass-band FWHM of 0.4 nm at a center wavelength of 1548.2 nm. The order of the super-gaussian function is chosen to be 20 to have a bandwidth utilization factor about 0.85, defined by ratio between the 1 dB reflection bandwidth and the 30 dB bandwidth. For this experiment, the length of the grating is chosen to be  $L=35$  mm. The results of simulation are shown in Fig. 4.21 and Fig. 4.22. In Fig. 4.21, the coupling coefficient of the fiber grating was reconstructed from a target of dispersionless reflection spectrum. From Fig.4.22 we show that we can get good results of reflection with a sidelobe suppression of below 30 dB and group delay spectra from the DLP method. In Fig. 4.23, the normalized refractive-index modulation amplitude and phase profiles reconstructed from the target spectrum are plotted. In order to realize this complicated FBG by our fabrication method, it is important to include the overlap-step-scan effects in the design. In this case, we assume that the diameter of the small gaussian index profile induced by the UV beam is 1 mm and the step-size is about 100 um. We use the least square (LS) fitting to find the best experimental exposure parameters. From the bottom picture of the Fig. 4.23, the refractive-index profile curve from the DLP method and the fitting curve from the LS method match very well. This indicates that the overlap-step-scan exposure scheme should be able to accurately produce the required index profile. Fig. 4.24 shows the reflectivity and group delay spectra calculated from the results after using the least square method. It can be seen that if the least square method is used to find the optimal experimental parameters, we can still get

good spectral response of the fiber grating.

We have experimentally succeeded in fabricating a dispersionless FBG based on the designed parameters in Fig. 4.23. The measured time delay and reflection spectrum of the fabricated FBG sample are shown in Fig. 4.25(a). As expected, an almost 0.4 nm bandwidth dispersionless FBG is realized. It is also confirmed that the standard deviation of the time delay is 6.8 ps inside the stopband. To compare the performance of the dispersionless FBG with an “ordinary” apodized FBG, a 3 cm long Gaussian-apodized\_grating with the same reflection bandwidth of 0.4 nm is simulated and is shown in Fig. 4.25(b). Both of them are spectrally similar but the time delay for the case of the “ordinary” apodized FBG shows a maximum variation of more than 100 ps within the stopband. The measured group delay ripples of our fabricated dispersionless FBG sample are still larger than the theoretical predictions from the design. This should be mainly due to the fiber position control errors during the exposure scan and can be further reduced by improving the scan setup. Nevertheless, from the measured results, very small group delay ripples can already be achieved even with the present setup. This demonstrates the feasibility of the proposed method.

In the proposed method a linearly polarized UV exposure light is used for the FBG fabrication. It has been shown in reference [15] that the linearly polarized UV exposure light will also induce birefringence in fiber core. From the polarization mode dispersion (PMD) and chromatic dispersion (CD) measurement of our dispersionless FBG as shown in Fig. 4.26, we estimate the birefringence is  $\Delta n = 1.0 \times 10^{-5}$  which is about 1-2% of the index change as shown in Fig. 4.27. The birefringence  $\Delta n$  is calculated by the equation as follow [16]

$$DGD = |C|2\Delta nP \quad (4.3)$$

where DGD is differential group delay of PMD (ps), C is chromatic dispersion (ps/nm),  $\Delta n$  is birefringence and P is the grating period (nm). This value of birefringence is reasonable

when the s-polarization UV beam is used [10]. It has also been shown that the induced birefringence can be reduced by a factor of 3-10 (depending on the fiber type) by using the p-polarization UV beam [10]. Therefore, for achieving lowest birefringence with the proposed method, the UV exposure beam should be in the p-polarization, even though the induced ac-index modulation will be reduced by a factor for fixed exposure energy. The reduction of the birefringence also helps to reduce the PDL and PMD ripples transferred from the reflectivity and the group delay ripples through the birefringence.

To conclude, we have proposed and demonstrated a new sequential writing technique with polarization control for fabricating complicated FBGs with pure apodization and phase shifts. We also use the DLP inverse design method and the LS fitting method to accurately determine the optimum experimental parameters for the sequential overlap-step-scan exposure method used in our experiment. Pure apodized FBGs with sidelobe suppression of 30 dB as well as dispersionless FBGs with small time delay variation have been demonstrated. Complicated FBG profiles with pure apodization can be stably and repeatedly fabricated with the present method and the developed auto-control Labview program as shown in Fig. 4.28. These advantages shall provide more flexible options to fabricate complicated fiber grating structures for different applications.

#### **4.5 Interferometric Side-Diffraction Position Monitoring Technique for Writing Long Fiber Bragg Gratings**

A fiber Bragg grating (FBG) is a fiber device with a periodic modulation of the refractive index inside the fiber core. Some advanced fiber Bragg gratings with complex grating structures of arbitrary phase and index profiles have become very important in many applications including the DWDM channel multiplexer- demultiplexers, the chromatic

dispersion compensator and the fiber laser [8, 12, 17, 18]. In the past few years, several methods that can realize long and complex FBG structures have been developed. They include the moving-fiber-scanning-beam technique [19] and the sequential writing techniques [7, 20]. In these methods, a He-Ne laser interferometer is required to monitor the fiber position for performing sequential UV-writing, which is shown in Fig. 4.29. However, in these methods the accumulative error of the fiber position due to the interference drift of the interferometer and the inaccurate grating period estimation also tends to seriously impact the fabrication of long fiber gratings. In the present letter we propose and demonstrate a new method which is capable of monitoring the fiber grating position without the accumulative error. This monitoring method is based on the side-diffraction interference technique, which was originally developed for measuring the variation of the grating period and the refractive-index modulation profile of the exposed FBGs [21].



## I. Experimental setup and working principle

Our experimental setup is shown in Fig. 4.30. The light source for position monitoring is a 25-mW single-polarization He-Ne laser and its output light is expanded by two spherical lenses to achieve the final beam diameter of about 4.5-mm. The expanded beam is then divided into one probe beam and one reference beam by a polarization beam splitter, and the intensity ratio of these two divided beams can be controlled by the use of the first half-wave plate. The second half-wave plate can rotate the polarization of the reference beam with respect to the probe beam. The probe beam is then focused by a spherical lens of 20-cm focal length and illuminates the fiber from the side. The first-order Bragg diffraction of the probe beam occurs at the phase-matching Bragg condition [22]

$$\sin \theta_2 = N_B \cdot \frac{\lambda}{\lambda_B}, \quad (4.4)$$

where  $\theta_2$  is the input angle of the probe beam in air,  $N_B$  is the effective index of the fiber at the Bragg wavelength  $\lambda_B$ , and  $\lambda$  is the wavelength of the probe beam. The diffracted probe beam and the reference beam are combined at the beam combiner with an interference angle of  $\theta_3$ . A 440x480 monochrome CCD camera of 7.15-um pixel width is used to record the interference pattern caused by the side-diffraction of the exposed FBG section. For the FBG exposure, a frequency-doubled argon-ion laser launches a CW 244-nm single-polarization UV beam into a two-beam interferometer with a half-wave plate in one of the two interfering beams for achieving pure apodization in a single scan [23]. The fiber is placed in a holder mounted on a translation stage composed of a linear motor stage and a piezoelectric translator (PZT) stage with sub-nm position resolution. A LabVIEW program as shown in Fig. 4.31 is used to analyze the interference patterns for determining the fiber position accurately.

The major working principle to monitor the fiber grating position is based on the phase-shift of the interference pattern in the CCD camera when the fiber is scanned along the fiber axis. We assume that the fiber grating to be measured is approximately uniform and has a sinusoidal index modulation  $n(z)$  along the fiber axial direction as

$$n(z) = n_0 + \Delta n \cdot \cos\left(\frac{2\pi z}{\Lambda} + \phi(z)\right), \quad (4.5)$$

where  $n_0$  is the average refractive index,  $\Delta n$  is the amplitude of refractive index variation,  $\Lambda$  is the grating period, and  $\phi(z)$  describes spatial grating phase. The first-order diffracted probe beam interferes with the reference beam in the CCD camera. The intensity of the first-order diffracted probe beam is denoted  $I_p$ , and the intensity of the reference beam is assumed to be  $I_r$ . The intensity distribution of the interference fringe along the x-axis which is perpendicular to the bisector of the two interfering beams is given by

$$I_{\text{int}} = I_p + I_r + 2\sqrt{I_p I_r} \cdot \cos(kx \cdot 2 \sin\left(\frac{\theta_3}{2}\right) + \Phi), \quad (4.6)$$

where  $k = 2\pi / \lambda$  is the wave vector,  $\theta_3$  is the interfering angle and  $\Phi$  is the phase

difference between the two interfering beams. From equation (4.6) the interference spectrum  $I_{int}$  can be processed by the Fourier transform to get the frequency response. By multiplying the spectral data by a filtering window function centered at the peak corresponding to the positive beating frequency and then taking an inverse Fourier transform back to the original domain, we can get the phase  $\Phi$  from the phase of the resulted data points. The whole algorithm is summarized in Fig. 4.32. In order to test our algorithm, we analyze the obtained experimental interference pattern by using the algorithm. A typical experimental interference pattern and the calculated phase distribution are shown in Fig. 4.33. One can see that the grating phase is readily retrieved. According to the phase distribution before and after the fiber moving, we can connect the exposed fiber grating section-by-section accurately. In our preliminary experimental setup, the measurement resolution is about one per-cent of the grating period, limited by the CCD resolution.



## II. Experimental Results

To demonstrate the feasibility, we fabricate one gaussian apodized FBG with the dc refractive-index modulation being kept constant along the whole grating. We use the photosensitive fiber (Fibercore PS1500) with 7-day hydrogen loading at room temperature. In order to ensure that the fiber cladding has not been damaged by use of the fiber stripper, the fiber is steeped in ethanol solution before removing the jacket. The FBG is fabricated by the overlap-step-scan exposure setup [12] and the two-beam interferometer method with polarization control [22]. The exposed UV beam diameter is about 5-mm and the fiber scan step is about 500- $\mu\text{m}$  (see Fig. 4.34). The FBG is formed in a photosensitive fiber after 150-section sequential writing with a total grating length about 75-mm. We rotate the half-wave plate azimuth angle from  $\theta = -45^0$  to  $45^0$  during the exposure scan to produce the

required apodized index profile. It is worthy of noting that we move the fiber distance about 500-um per step roughly by the translation stage, and then fine tune the accurate grating position by the PZT stage for connecting each grating section with zero phase shift based on the phase measurement from the side-diffraction. The graph in Fig. 4.35 shows the reflection and transmission spectra of the grating with the sidelobes suppression level below -25 dB, and the 1-dB bandwidth of the reflection spectrum about 0.1-nm. One can see that there is no dip in the stop-band, which indicates that the grating sections are connected accurately with no obvious phase error.

In the present monitoring method, the limited power level of the diffracted probe beam can limit the interference visibility on the CCD camera and then affect the accuracy of the phase measurement. In our experimental setup, a minimum detectable index modulation  $\Delta n$  of approximately  $5 \times 10^{-6}$  has been achieved. For the symmetric fiber grating structure of the present example, the index variation at the two end sides of grating length can be down to zero. But in the asymmetric fiber grating structure, like sinc structure, which may measure wrong phase information at the weak index position to fail to connect the grating layer by layer. But it may be solved by some methods, like replace with the high-power He-Ne laser to increase the diffracted probe beam intensity, or increase the sensitivity of the signal detection.

To conclude, we have demonstrated that the proposed new method can be experimentally applicable for fabricating long fiber grating. This method has several advantages including: (1) the accurate grating period need not to be calibrated in advance, and (2) there is no accumulative error of fiber position during the long scan. The method also has the ability to incorporate optional multiple phase shifts in different grating sections during the exposure scan for fabricating phase-shifted FBGs. We believe the present method can provide a new option to real-time monitor the grating position for increasing the accuracy of long fiber grating fabrication.

## 4.6 Summary

In this chapter, we introduced our auto-control exposure system which includes a high resolution position scanning system and other motorized control systems, which is combined with the use of the Labview program to achieve the higher accurate fabrication process. For the fabrication of long, complex fiber grating structures, we have developed three new exposure methods and demonstrated that these new methods can realize the designed complex fiber grating structures. These proposed fabrication methods could also be used in the phase mask or the two-beam interferometer setups. Therefore, the proposed methods provide more options for fabricating advanced fiber gratings.



## References for Chapter 4:

- [1] K. O. Hill, Y. Fujii, D. C. Johnson, and B. S. Kawasaki, "Photo-sensitivity in optical fiber waveguides: Application to reflection filter fabrication," *Appl. Phys. Lett.*, vol. 32, pp. 647–649, 1978.
- [2] G. Meltz, W. W. Morey, and W. H. Glenn, "Formation of Bragg gratings in optical fibers by a transverse holographic method," *Opt. Lett.*, vol. 14, pp. 823-825, 1989.
- [3] K. O. Hill, B. Malo, F. Bilodeau, D. C. Johnson, and J. Albert, "Bragg gratings fabricated in monomode photosensitive optical fiber by UV exposure through a phase mask," *Appl. Phys. Lett.*, vol. 62, pp.1035-1037, 1993.
- [4] W. H. Loh, M. J. Cole, M. N. Zervas, S. Barcelos, and R. I. Laming, "Complex grating structures with uniform phase masks based on the moving-scanning beam technique," *Opt. Lett.*, vol. 20, pp. 2051-2053, 1995.
- [5] A. Asseh, H. Storoy, B. E. Sahlgren, S. Sandgren, and R. Stubbe, "A writing technique for long fiber Bragg gratings with complex reflectivity profiles." *J.Lightwave Tech.*, vol. 15, pp. 1419-1423, 1997.
- [6] J. B. Jensen, M. Plougmann, H. –J. Deyerl, P. Varming, J. Hubner, and M. Kristensen, "Polarization control method for ultraviolet writing of advanced Bragg gratings," *Opt. Lett.*, vol. 27, pp. 1004-1006, 2002.
- [7] I. Petermann, B. Sahlgren, S. Helmfrid, A. T. Friberg, and P.-Y. Fonjallaz, "Fabrication of advanced fiber Bragg gratings by use of sequential writing with a continuous-wave ultraviolet laser source," *Appl. Opt.*, vol. 41, pp. 1051-1056, 2002.
- [8] T. Komukai, K. Tamura, and M. Nakazawa, "An Efficient 0.04-nm Apodized Fiber Bragg Grating and Its Application to Narrow-Band Spectral Filtering," *IEEE Photo. Tech. Lett.*, vol. 9, pp. 934-936, 1997.

- [9] M.Ibsen et al., "99.9% reflectivity dispersion-less square-filter fiber Bragg gratings for high speed DWDM system," In proc. to OECC/IOOC 2000, postdeadline paper PD2.1, 2000.
- [10] A. Asseh, H. Storøy, J. T. Kringlebotn, W. Margulis, B. Sahlgren, S. Sandgren, R. Stubbe, and G. Edwall, "10cm Yb<sup>3+</sup> + DFB fiber laser with permanent phase shifted grating," *Electron. Lett.*, vol. 31, p. 969, 1995.
- [11] B. Malo, S. Theriault, D.C. Johnson, F. Bilodeau, J. Albert, and K.O. Hill, "Apodised in-fibre Bragg grating reflectors photoimprinted using a phase mask," *Electron. Lett.*, vol. 31, pp. 223-225, 1995.
- [12] L. G. Sheu, K. P. Chuang, and Y. Lai, "Fiber Bragg grating dispersion compensator by single-period overlap-step-scan exposure," *IEEE Photon. Technol. Lett.*, vol. 15, pp. 939-941, 2003.
- [13] H. Patrick and S. L. Gilbert, "Growth of Bragg gratings produced by continuous-wave ultraviolet light in optical fiber," *Opt. Lett.*, vol. 18, pp.1484-1486, 1993.
- [14] H. Singh, and M. Zippin, "Apodized fiber Bragg gratings for DWDM applications using uniform phase mask," in *Proceedings of the 24<sup>th</sup> European Conf. on Optical Communication (Lerko Print S.A., Madrid, Spain)*, vol. 1, pp. 189-190, 1998.
- [15] T. Erdogan and V. Mizrahi, "Characterization of UV-induced birefringence in photosensitive Ge-doped silica optical fibers," *J. Opt. Soc. Am. B*, vol. 11, pp. 2100-2105, 1994.
- [16] M. Schiano and G. Zaffiro, in *Proceedings of Optical Communication European Conference (Madrid, Spain, 1998)*, pp. 403-404.
- [17] M. Ibsen, M. K. Durkin, M. J. Cole, and M. I. Laming, "Sinc-sampled fiber Bragg gratings for identical multiple wavelength operation," *IEEE Photon. Technol. Lett.* vol. 10, pp. 842-844, 1998.

- [18] M. Ibsen, S. Y. Set, G. S. Goh, and K. Kikuchi, "Broad-Band Continuously Tunable All-Fiber DFB Lasers," *IEEE Photon. Technol. Lett.* vol. 14, pp. 21–23, 2003.
- [19] M. J. Cole, W. H. Loh, R. I. Laming, M. N. Zervas and S. Barcelos, "Moving fiber/phase mask-scanning beam technique for enhanced flexibility in producing fibre gratings with uniform phase mask," *Elect. Lett.*, vol. 31, pp. 1488-1490, 1995.
- [20] A. Asseh, H. Storøy, B. E. Sahlgren, S. Sandgren, and R. A. H. Stubbe, "A writing technique for long fiber Bragg gratings with complex reflectivity profiles," *J. Lightwave Technol.*, vol. 15, pp. 1419–1423, 1997.
- [21] F. El-Diasty, A. Heaney, and T. Erdogan, "Analysis of fiber grating by a side-diffraction interference technique," *Appl. Opt.*, vol. 40, pp. 890–896, 2001.
- [22] P. A. Krug, R. Stolte, and R. Ulrich, "Measurement of index modulation along an optical fiber Bragg grating," *Opt. Lett.*, vol. 20, pp. 1767-1769, 1995.
- [23] K.-P. Chuang, L.-G. Sheu, and Y. Lai, "Pure apodized phase-shifted fiber Bragg gratings fabricated by a two-beam interferometer with polarization control," *IEEE Photon. Technol. Lett.*, vol. 16, pp. 834-836, 2004.

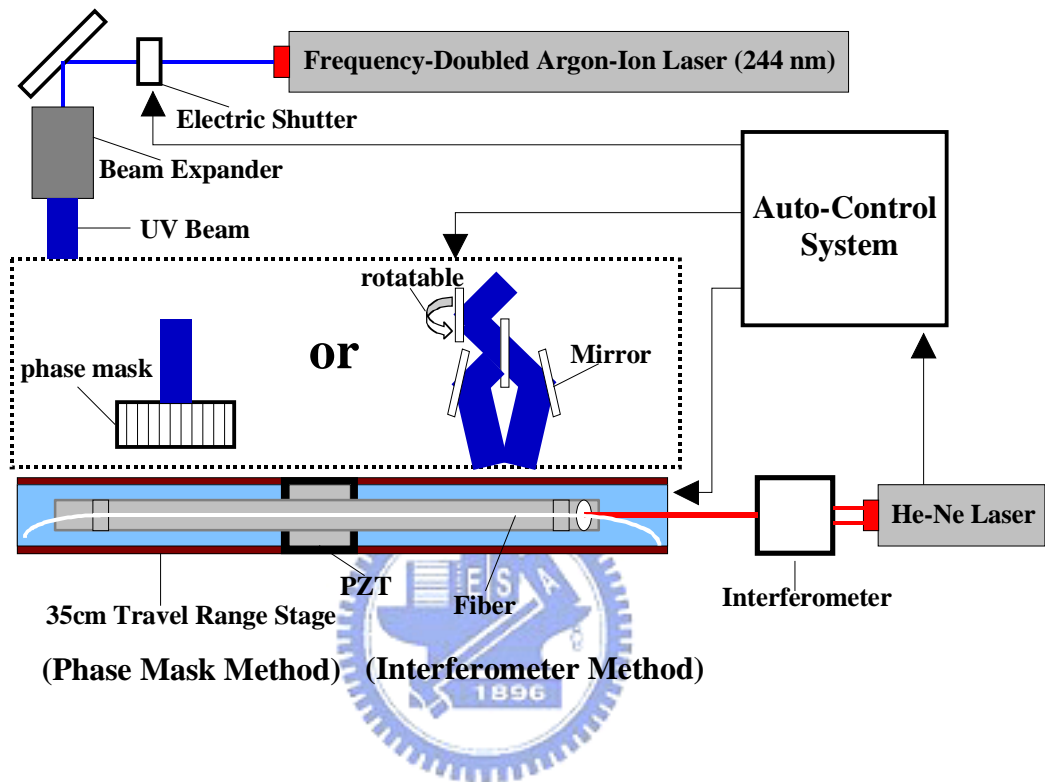


Fig. 4.1 An auto-controlled FBG exposure system based on the two exposure methods of a phase mask and a two-beam interferometer.

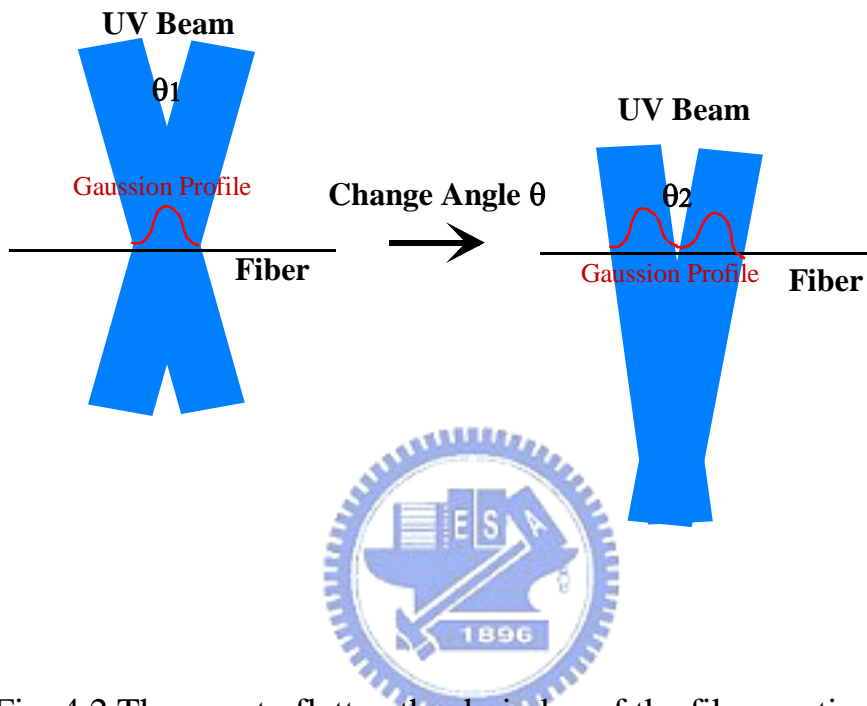


Fig. 4.2 The way to flatten the dc-index of the fiber grating.

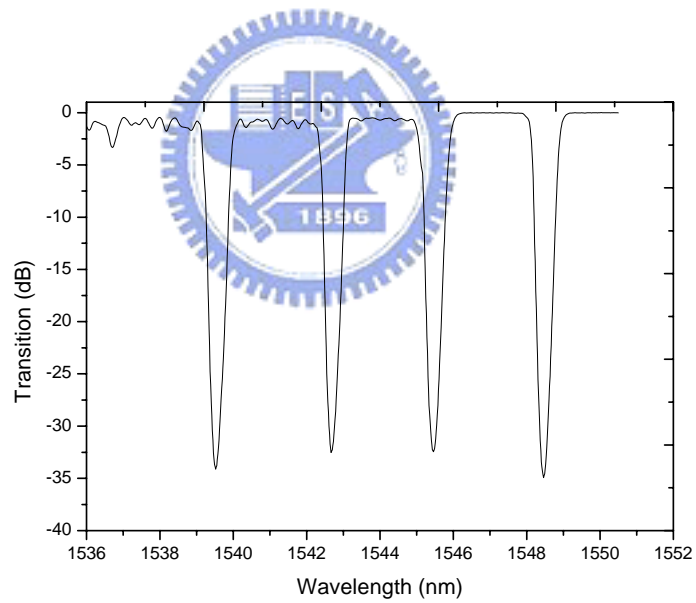
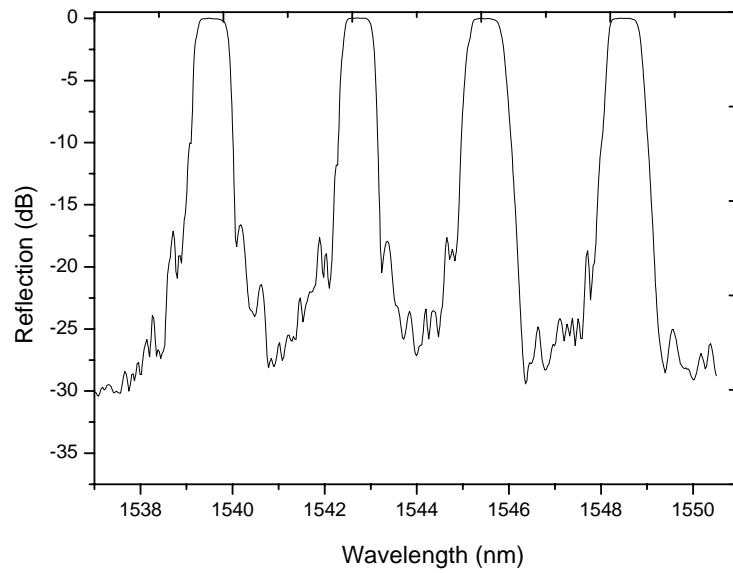


Fig. 4.3 The reflection and transmission spectra of the four channel FBG filter.

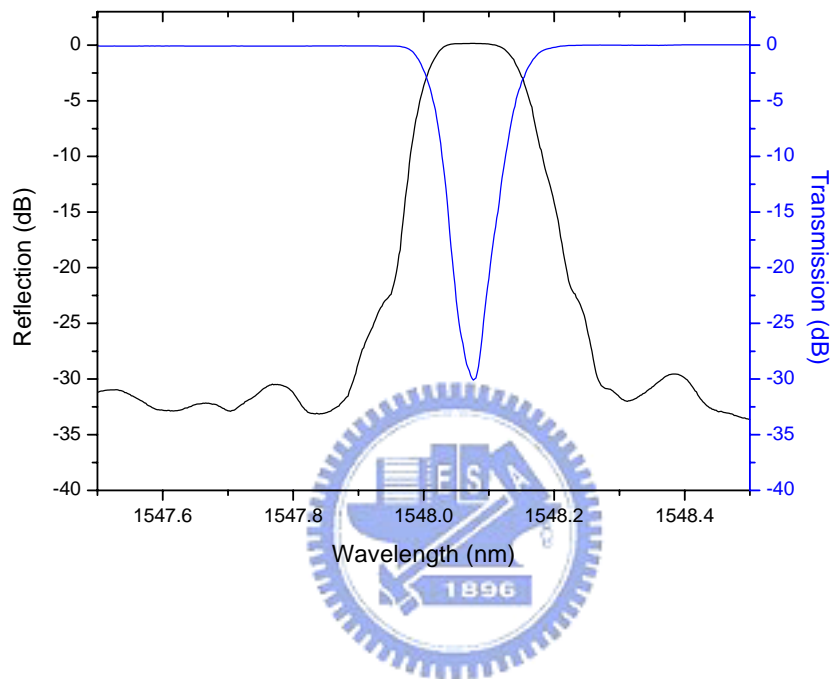


Fig. 4.4 Narrow-band filter by 100 sequences of step writing.

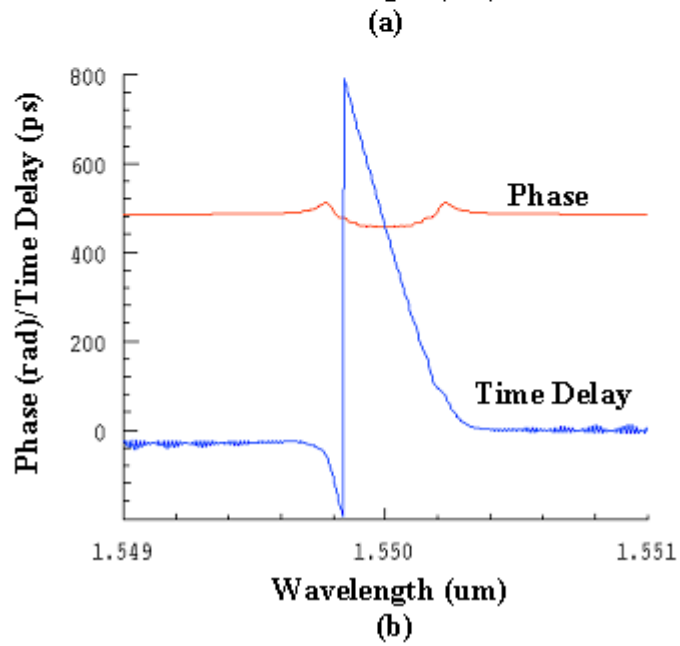
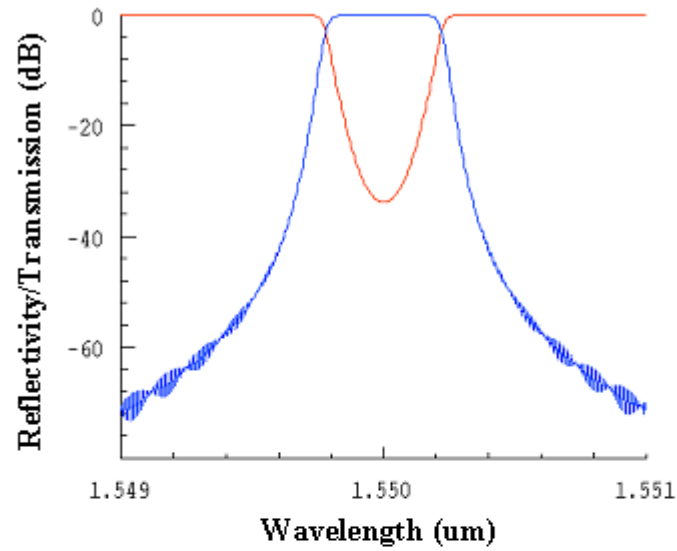


Fig. 4.5 (a) The reflection and transmission spectra, and (b) the phase and time delay of the simulated chirped FBG.

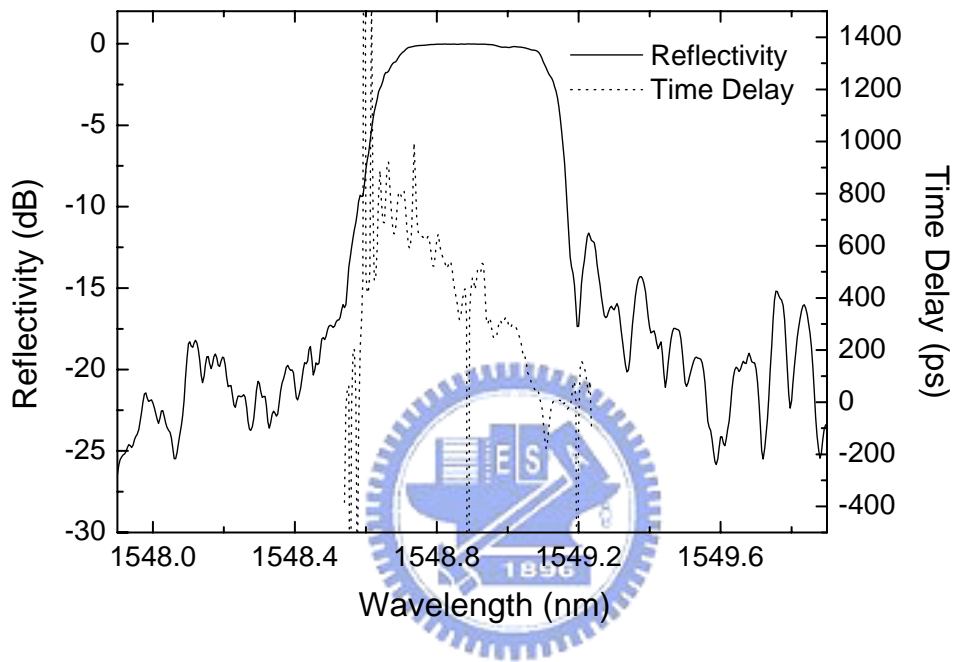


Fig. 4.6 The experimental result of a 10cm long chirped FBG.

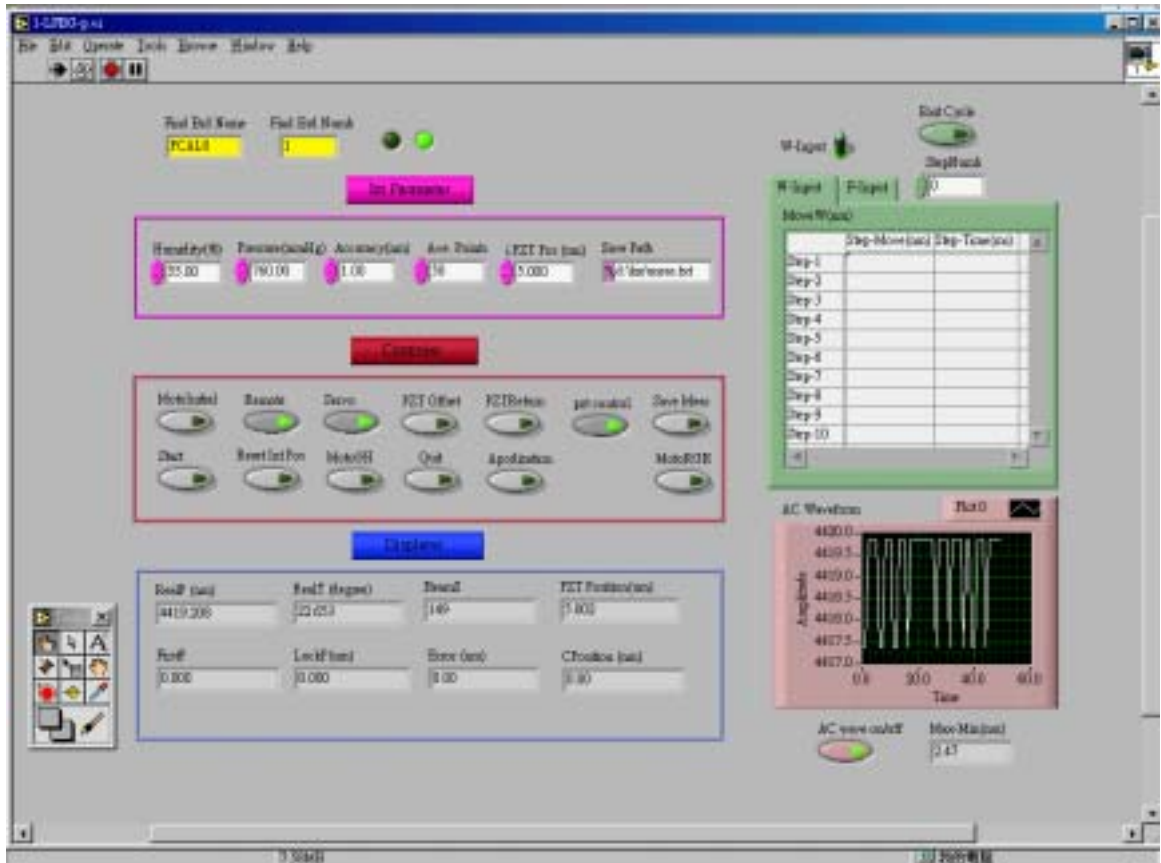


Fig. 4.7 The Labview program for fabricating FBG.

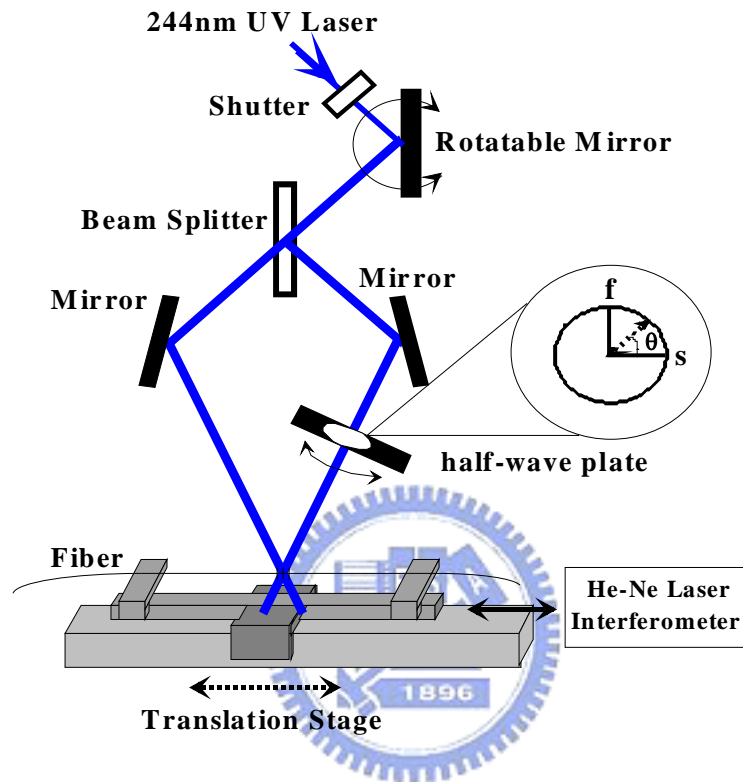


Fig. 4.8 Schematic diagram of fiber Bragg grating fabrication system by using two-beam interferometer method with polarization control.

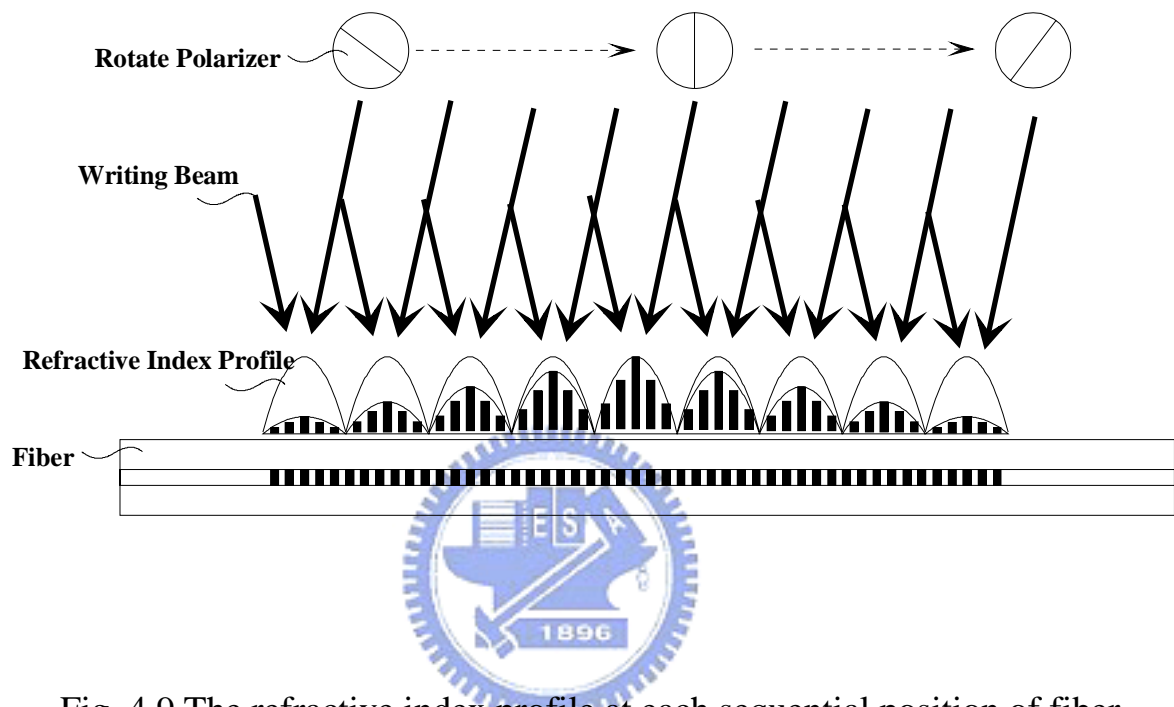


Fig. 4.9 The refractive index profile at each sequential position of fiber.

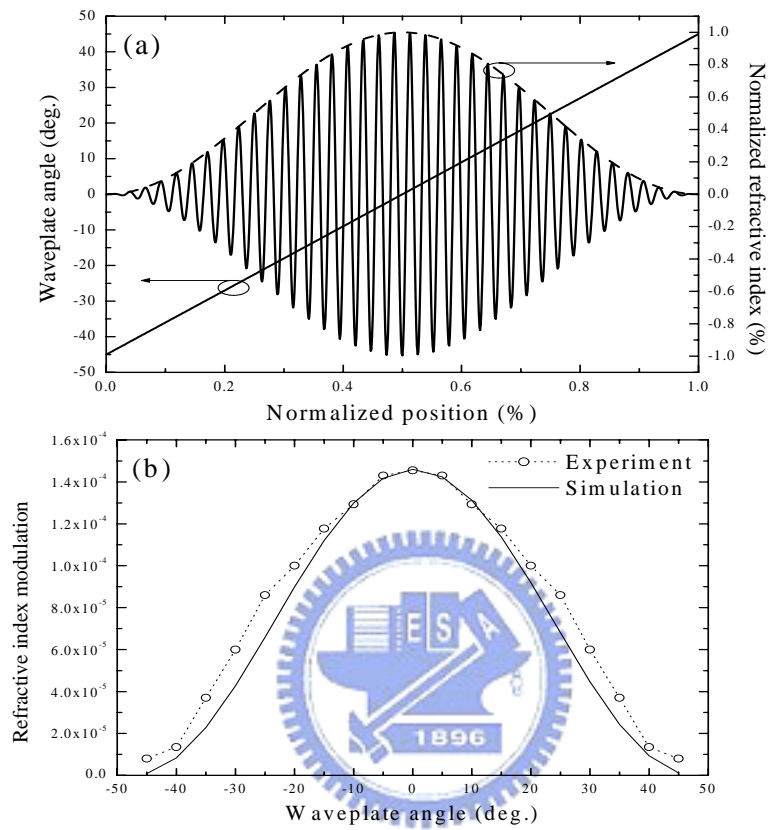


Fig. 4.10 (a) The relation of the half-wave plate angle and the refractive index modulation amplitude along the FBG position and (b) experimental and theoretical results for the refractive index modulation versus the rotation angle of the half-wave plate.

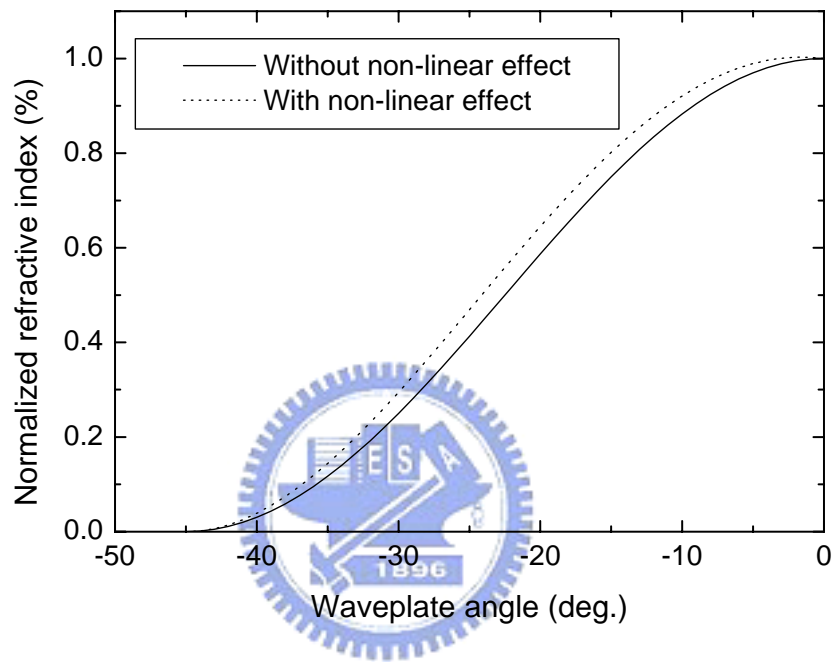


Fig. 4.11 The non-linear effect of refractive index change depends on a power law.

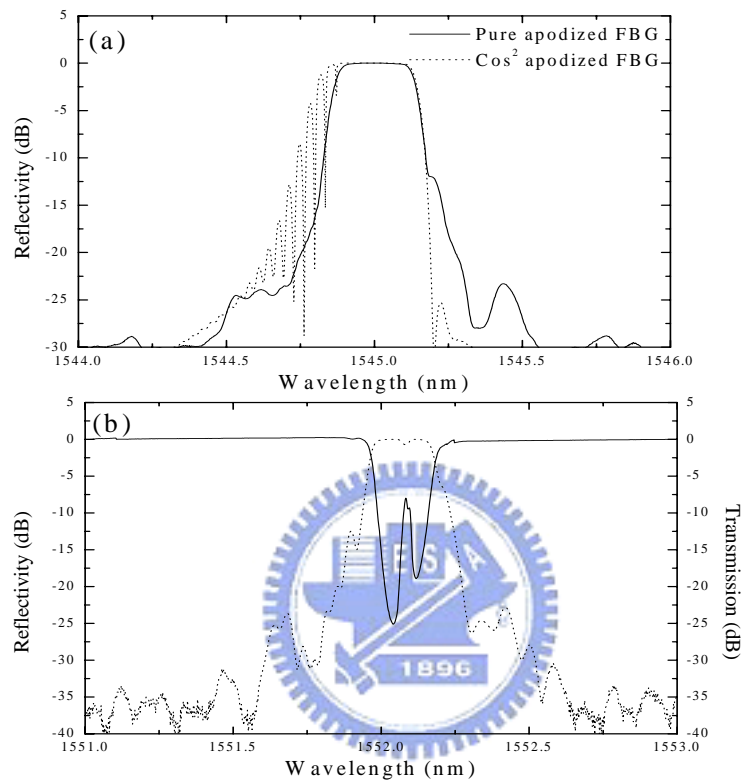


Fig. 4.12 (a) Reflection spectra of the  $\cos^2$  pure apodized (experiment) and ordinarily apodized (simulation) FBGs and (b) reflection and transmission spectra of a  $\pi$ -phase-shifted FBG.

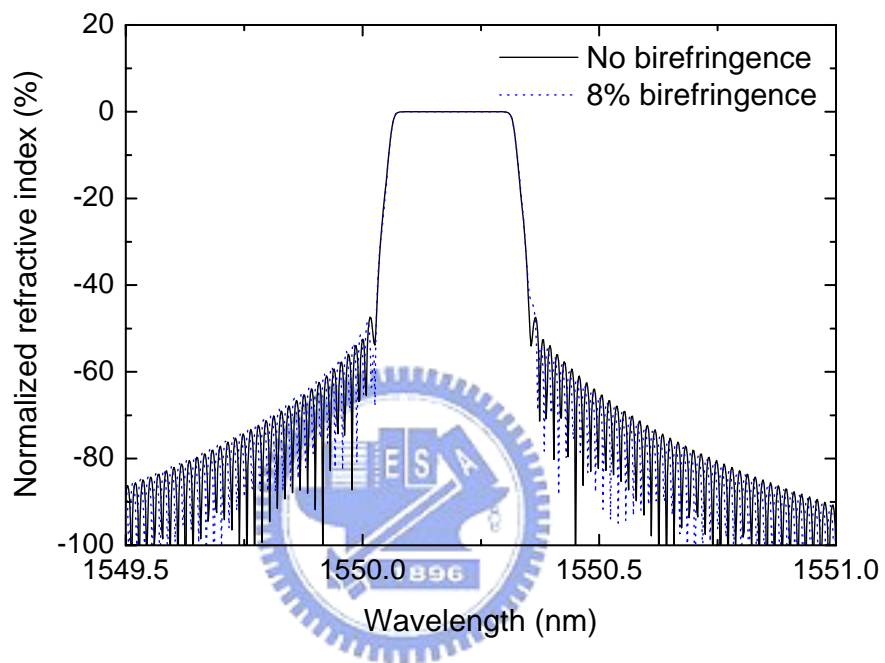


Fig. 4.13 The reflection spectrum of pure gaussian-apodization FBG influences from the UV-induced birefringence.

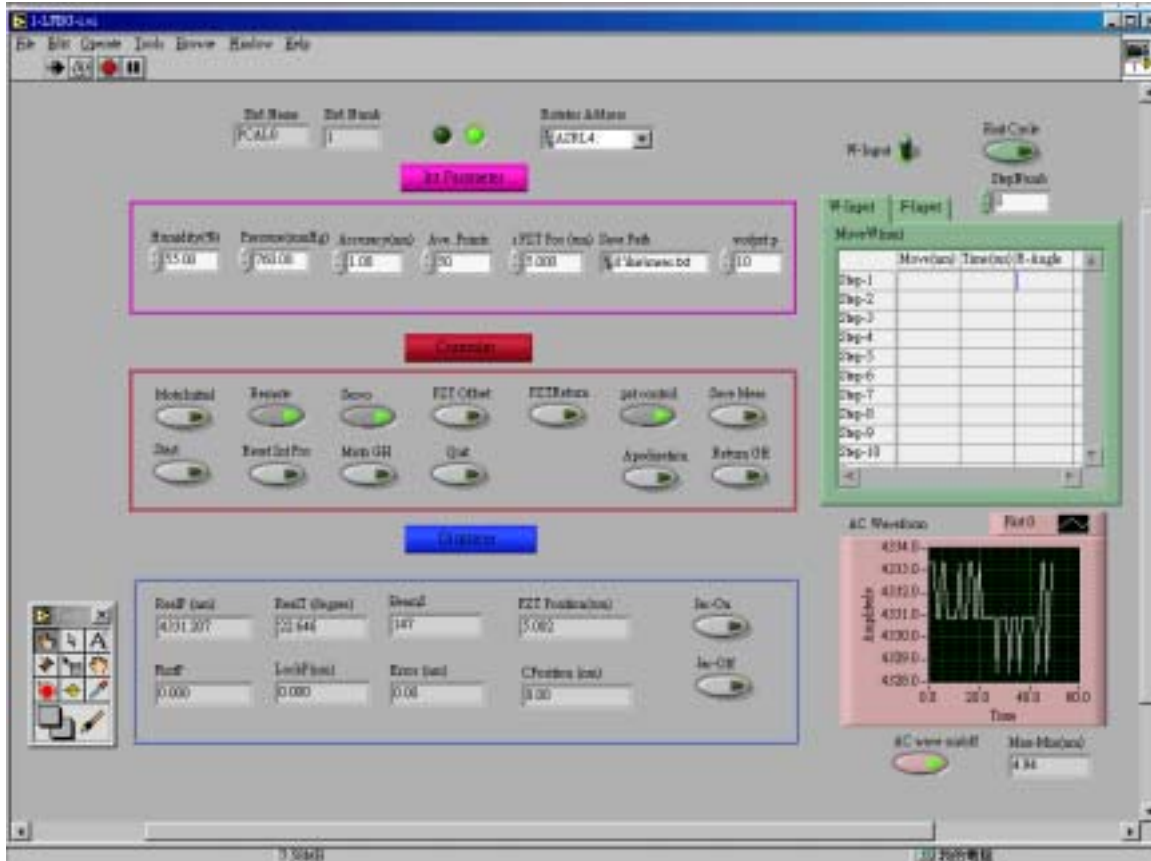


Fig. 4.14 The Labview program is used to control the two-beam interferometer method with the polarization control.

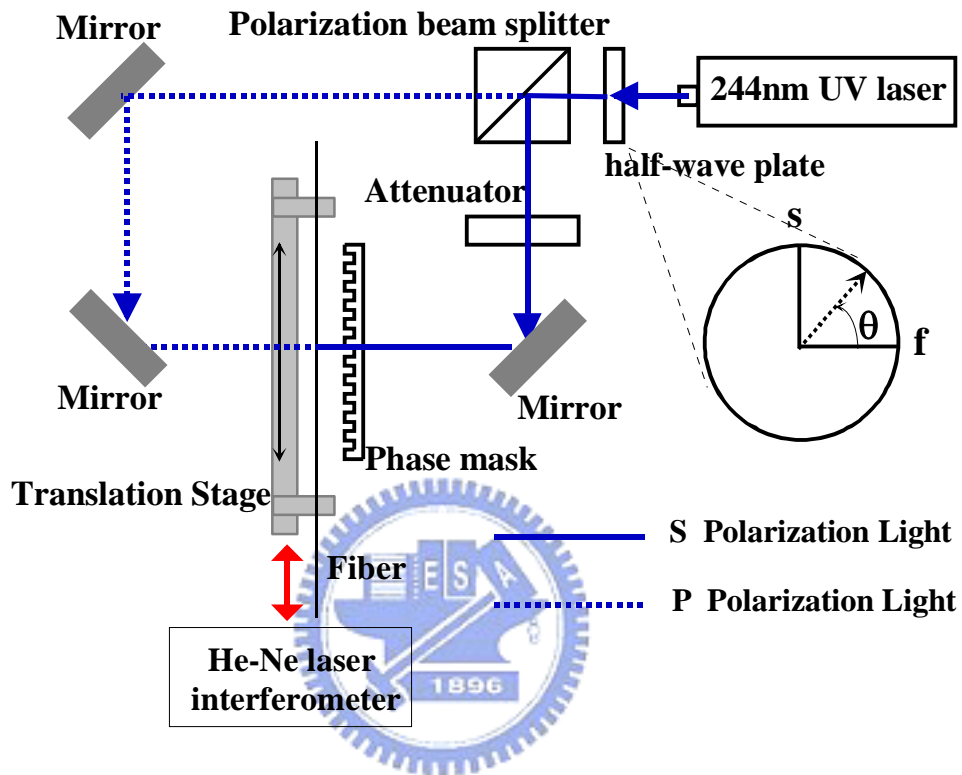


Fig. 4.15 Experimental setup for writing complex fiber grating structures: s and f, slow and fast axes of half-wave plate.

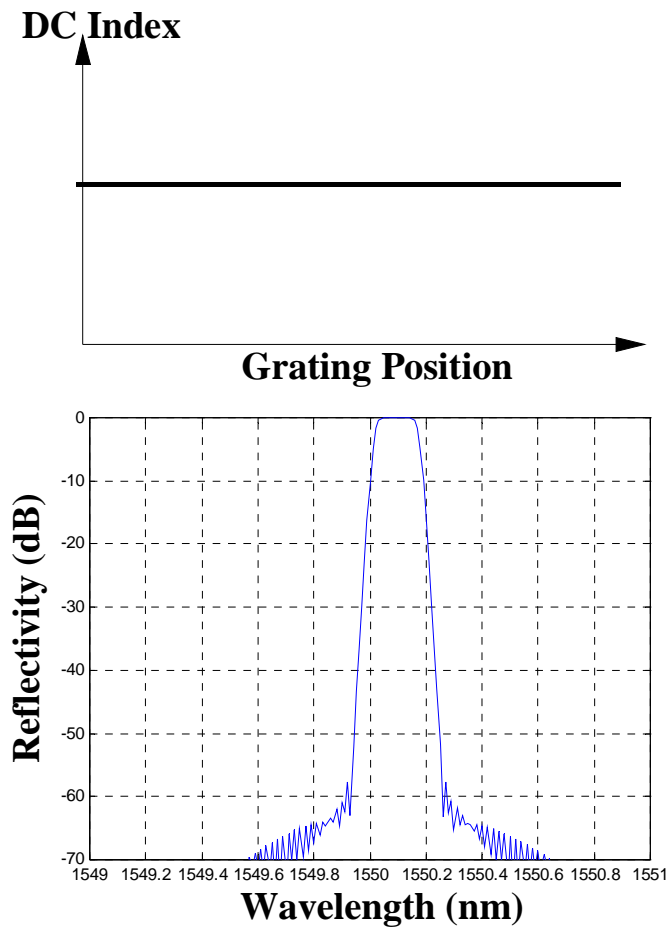


Fig. 4.16 A constant dc-index structure and its reflection spectrum.

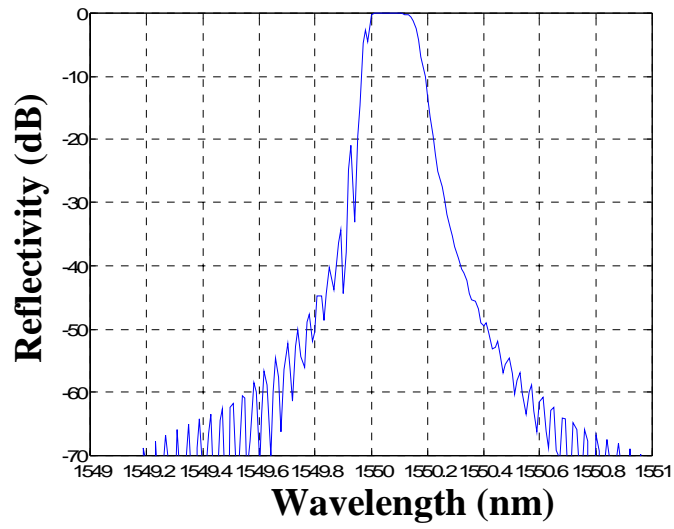
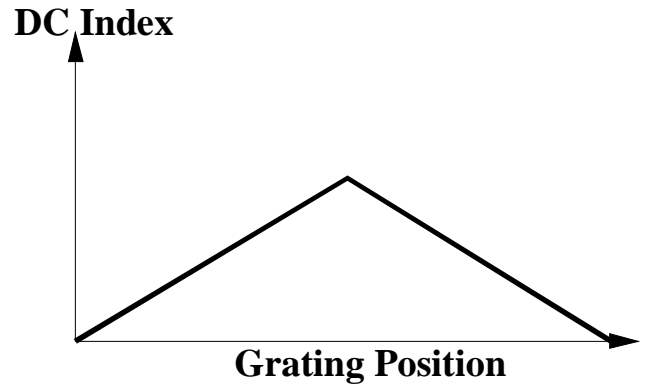


Fig. 4.17 A non-constant dc-index structure and its reflection spectrum.

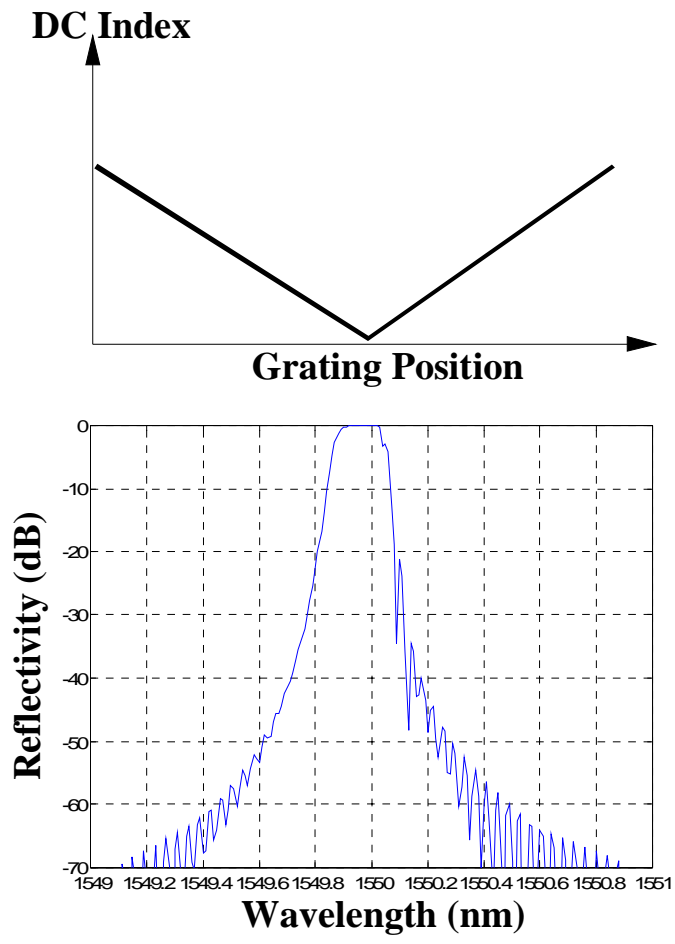


Fig. 4.18 A non-constant dc-index structure and its reflection spectrum.

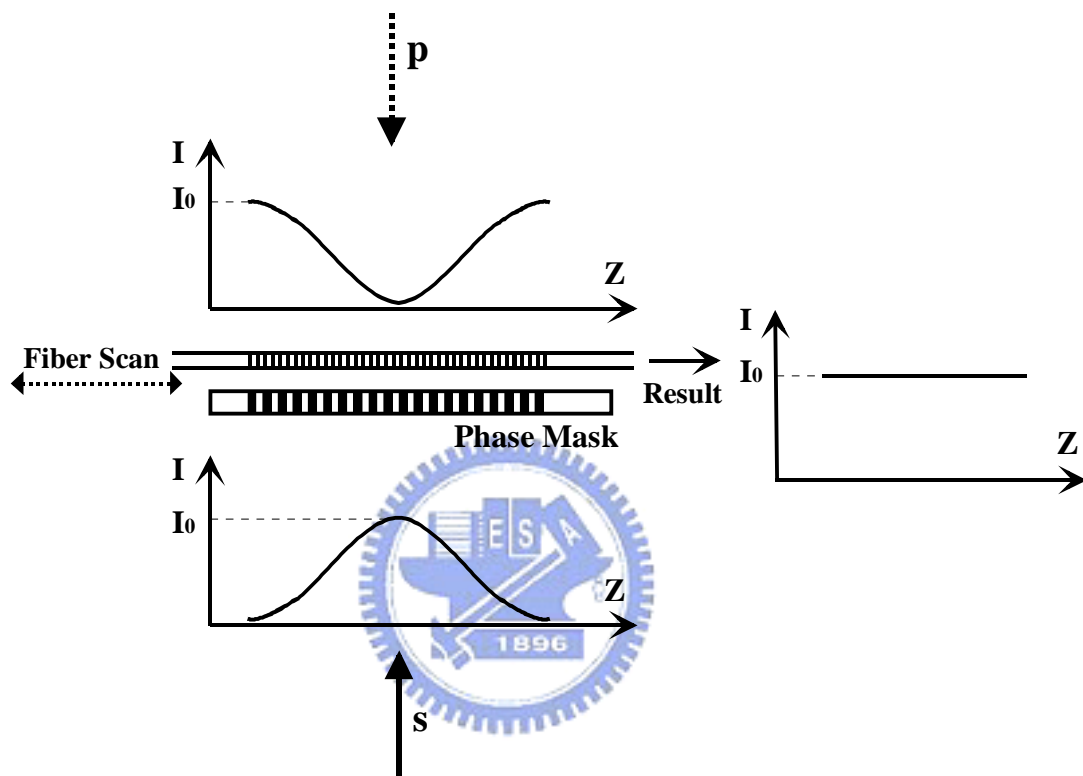


Fig. 4.19 The way of achieving a constant dc refractive index change.

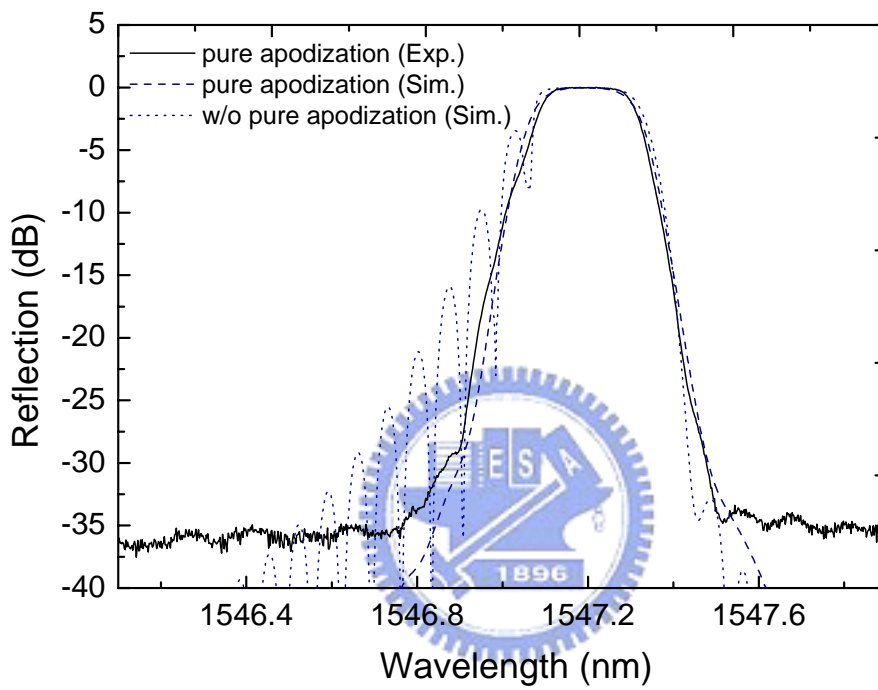


Fig. 4.20 The reflection spectra of a pure apodized FBG and an ordinary apodized FBG with non-constant dc index.

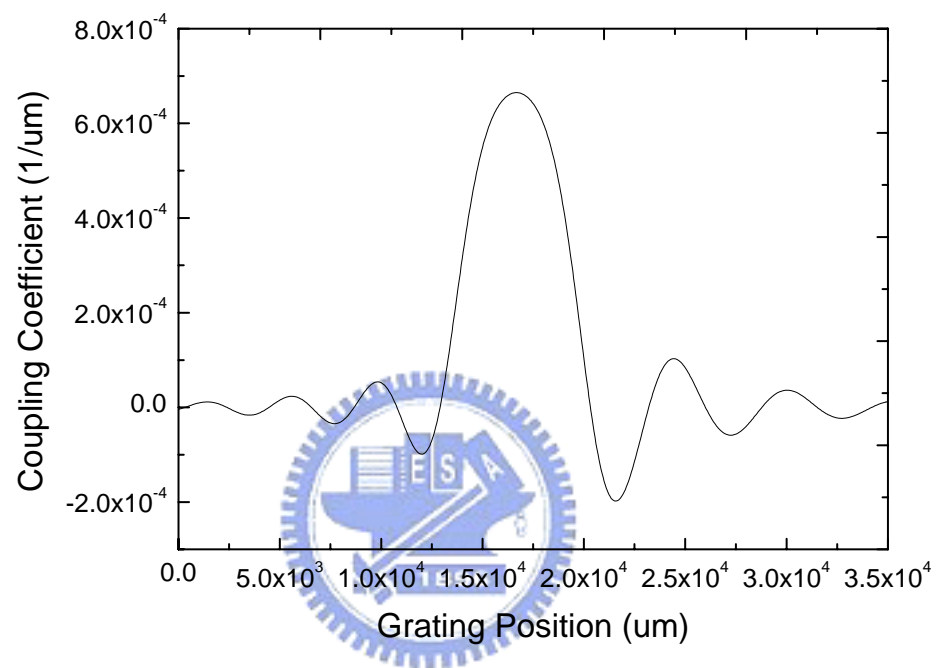


Fig. 4.21 Plots of the coupling coefficient reconstructed from a dispersionless reflection spectrum.

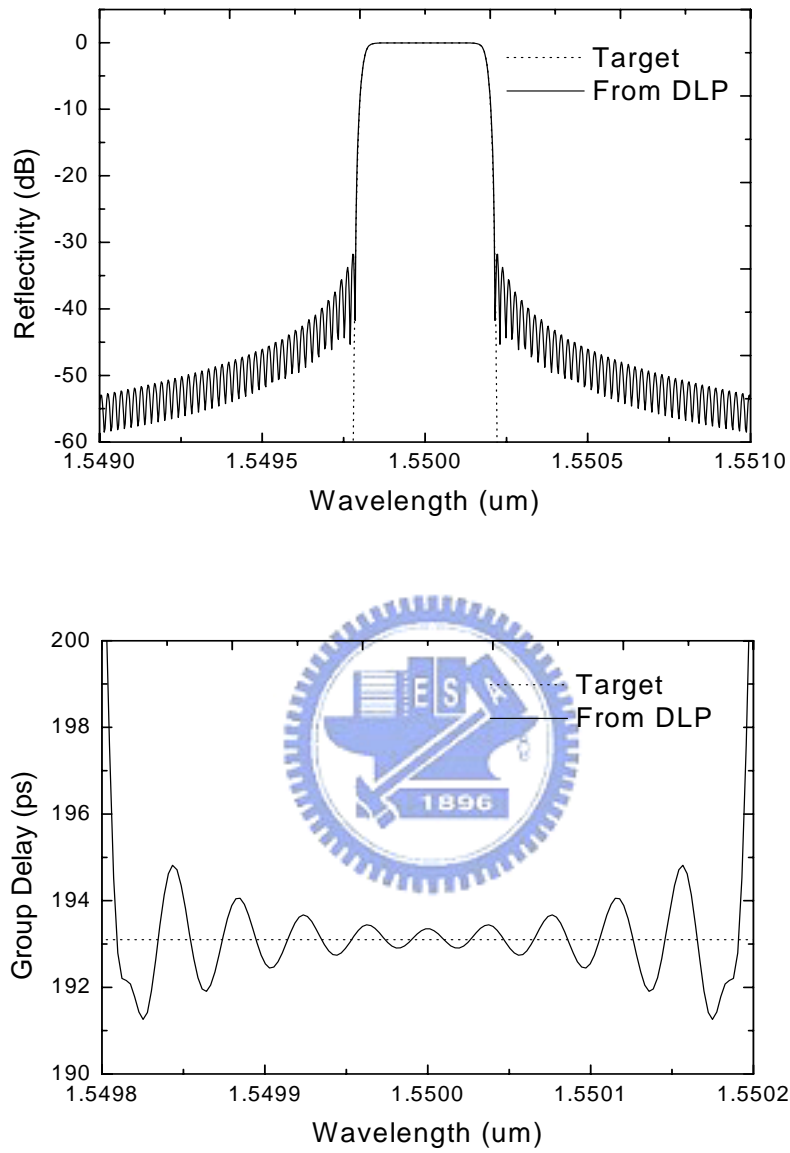


Fig. 4.22 Target and calculated reflection and group delay spectra from DLP.

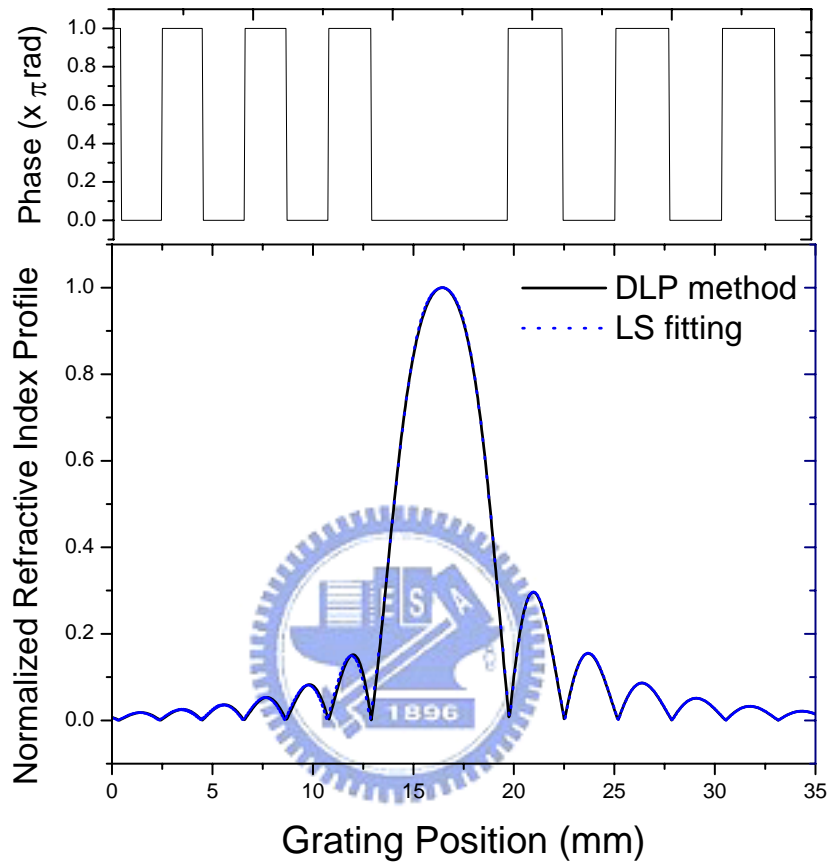


Fig. 4.23 The normalized refractive-index profile and phase of the designed dispersionless FBG.

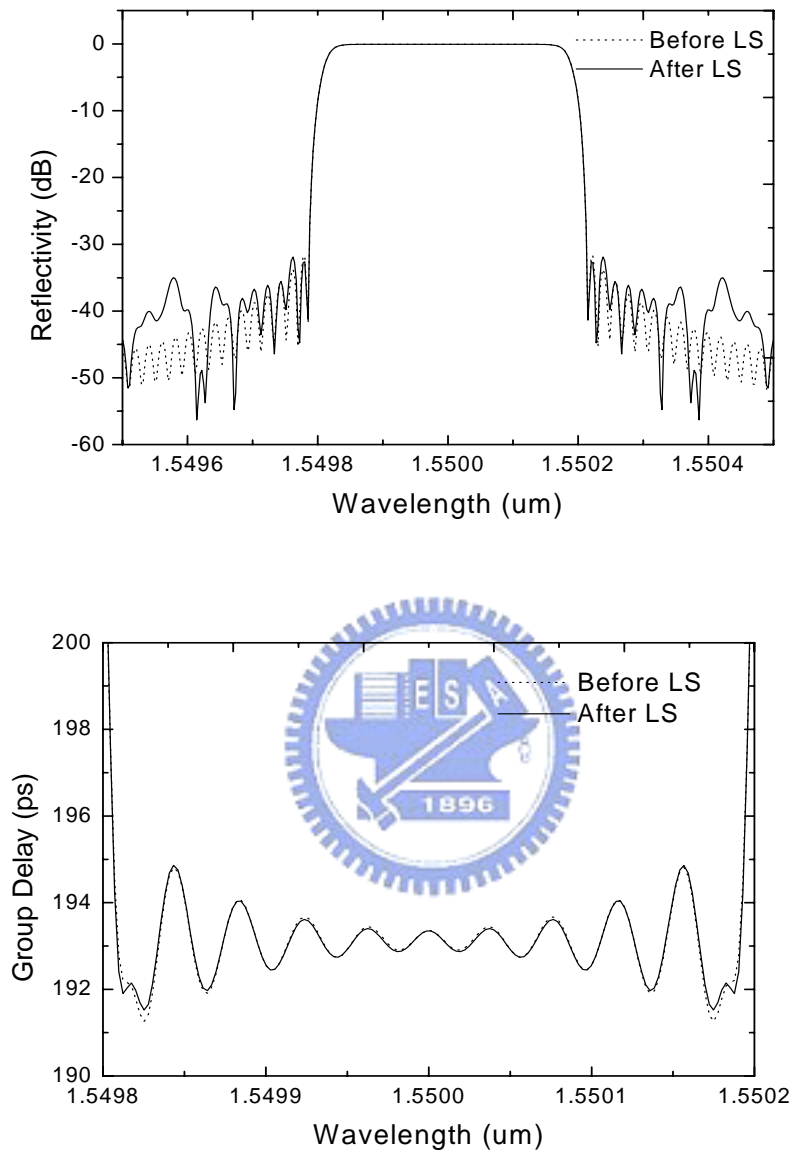


Fig. 4.24 The spectral response calculated from DLP before and after using the least square fitting.

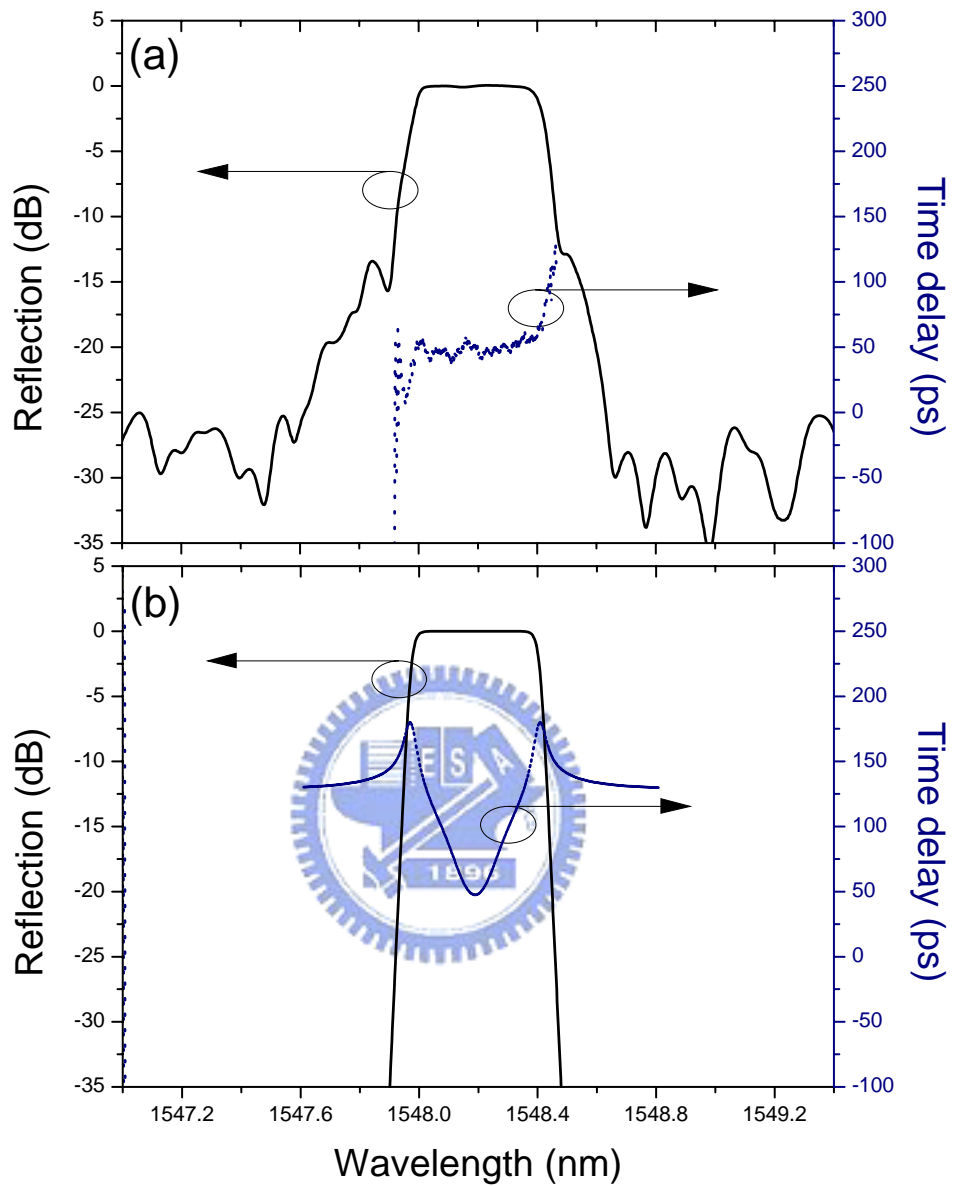


Fig. 4.25 (a) The measured reflection and time delay spectra of the dispersionless FBG and (b) the simulated reflection and time delay spectra of the “standard” Gaussian-apodized FBG.

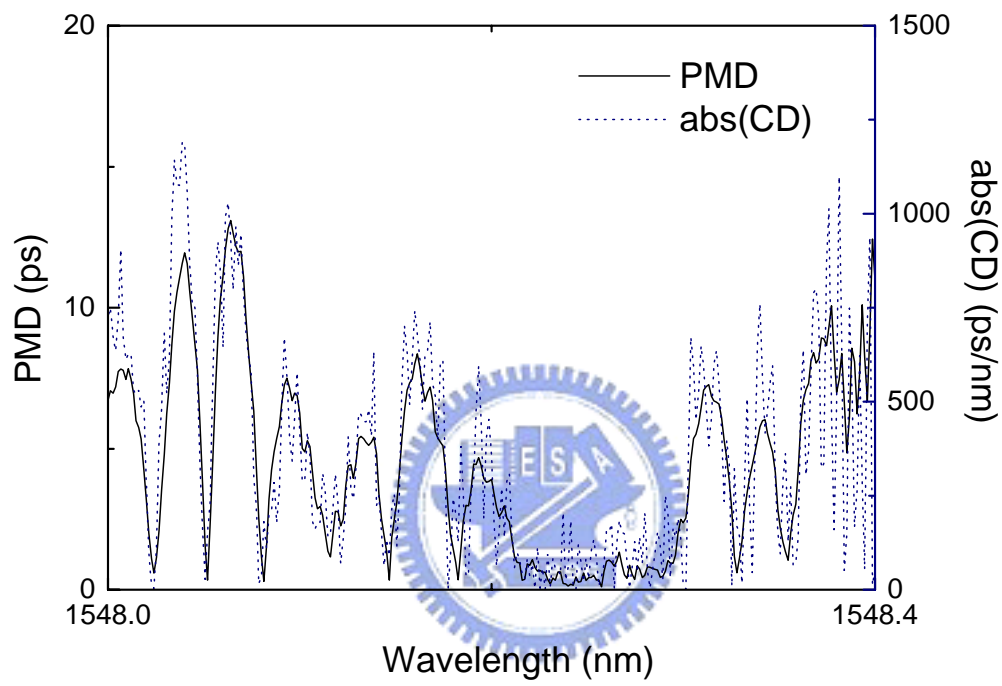


Fig. 4.26 The PMD and CD measurement of the dispersionless FBG.

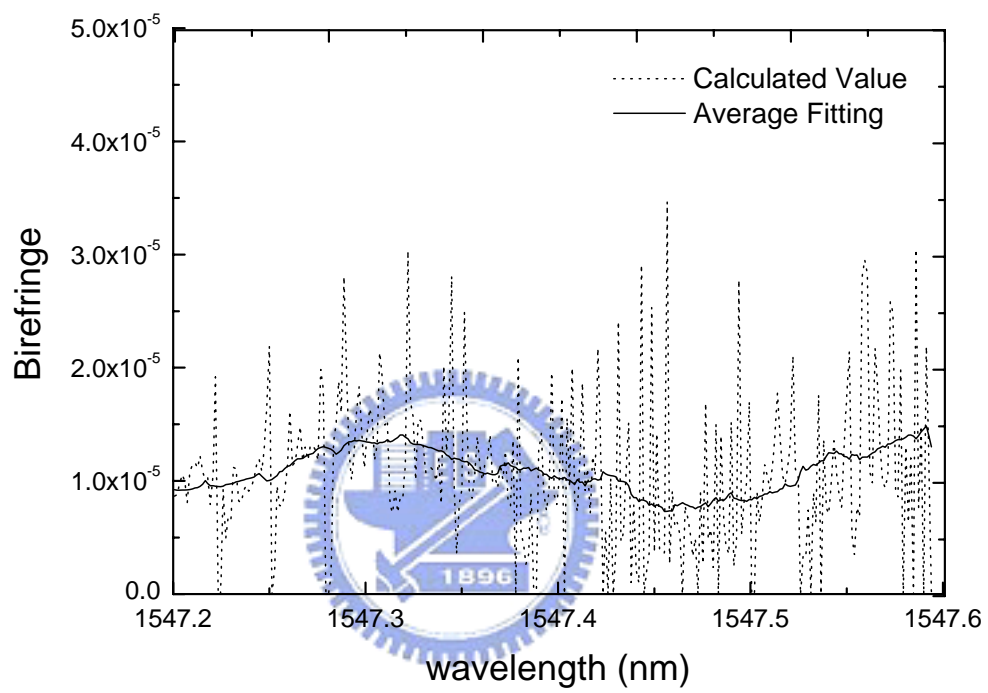


Fig. 4.27 The calculated birefringence from PMD and CD by equation (4.3).



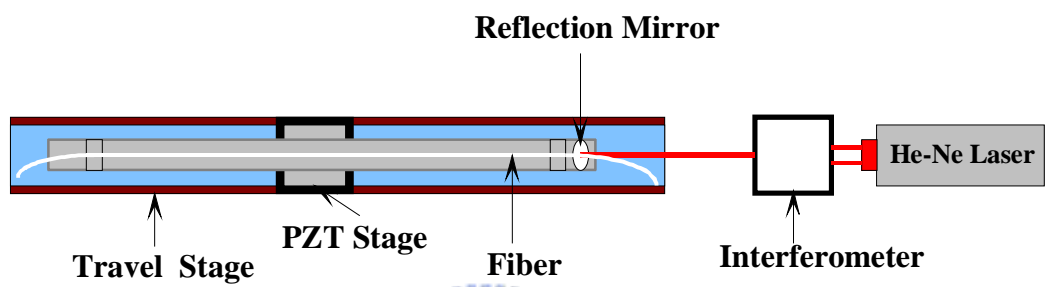


Fig. 4.29 Traditional position monitoring method.



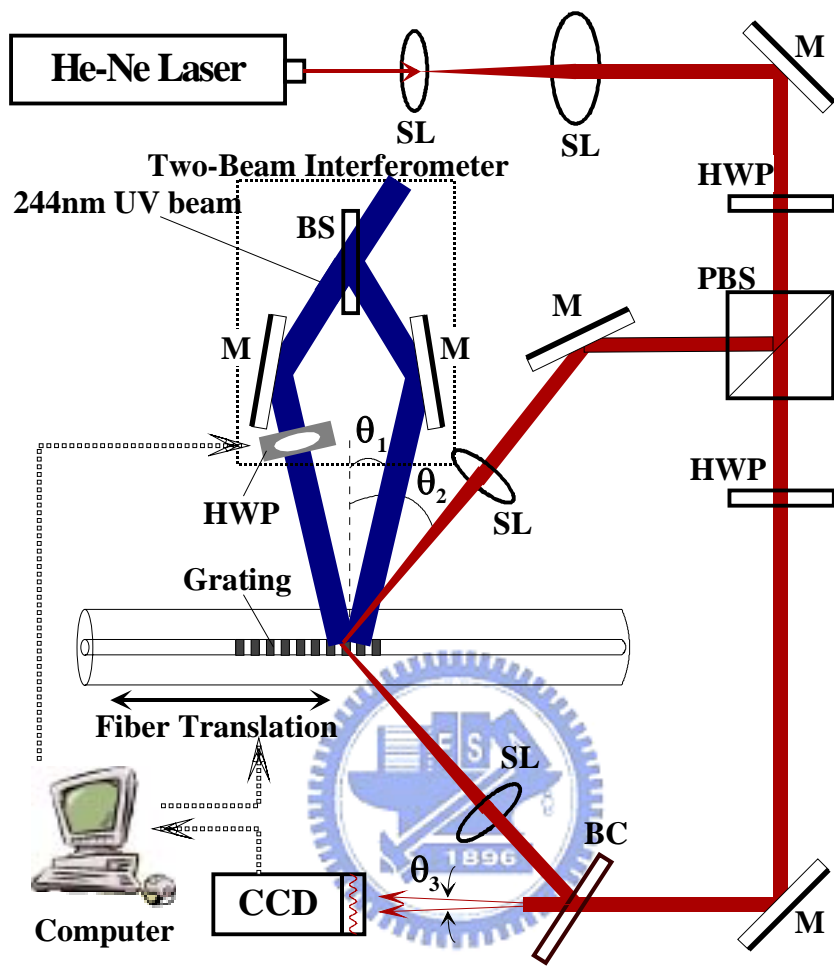


Fig. 4.30 Experimental setup for fabricating and monitoring fiber grating: SL, spherical lens; M, reflecting mirror; BS, beam splitter; PBS, polarization beam splitter; HWP, half-wave plate; BC, beam combiner;  $\theta_1$ , the angle of the FBG writing beams;  $\theta_2$ , the input angle of the probe beam;  $\theta_3$ , the interfering angle of the probe and the reference beams.



Fig. 4.31 The Labview program of side-diffraction monitoring method for fabricating long FBG.

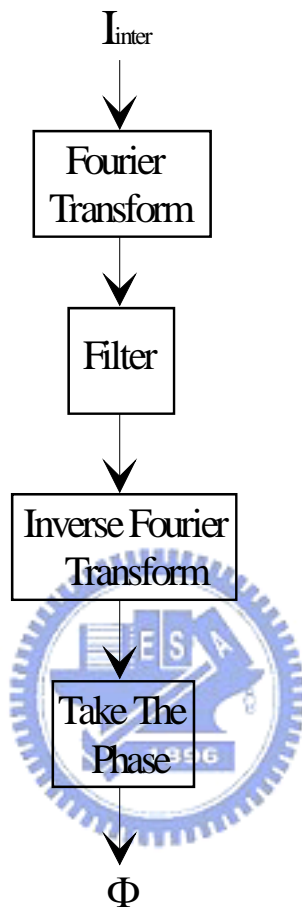


Fig. 4.32 Algorithm for calculating the phase of interference pattern.

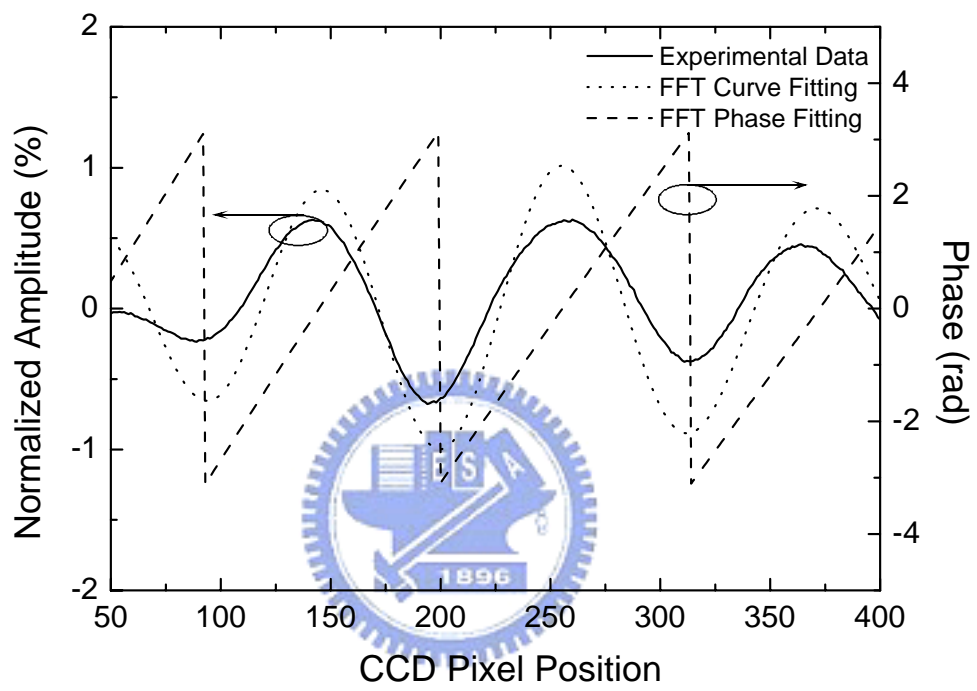


Fig. 4.33 A typical experimental interference pattern and the calculated phase distribution.

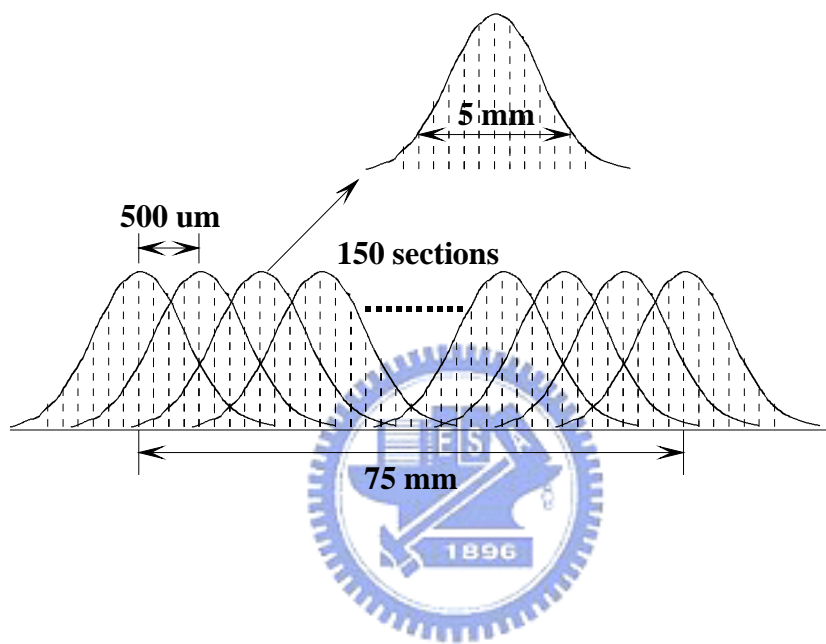


Fig. 4.34 The overlap-step-scan exposure method.

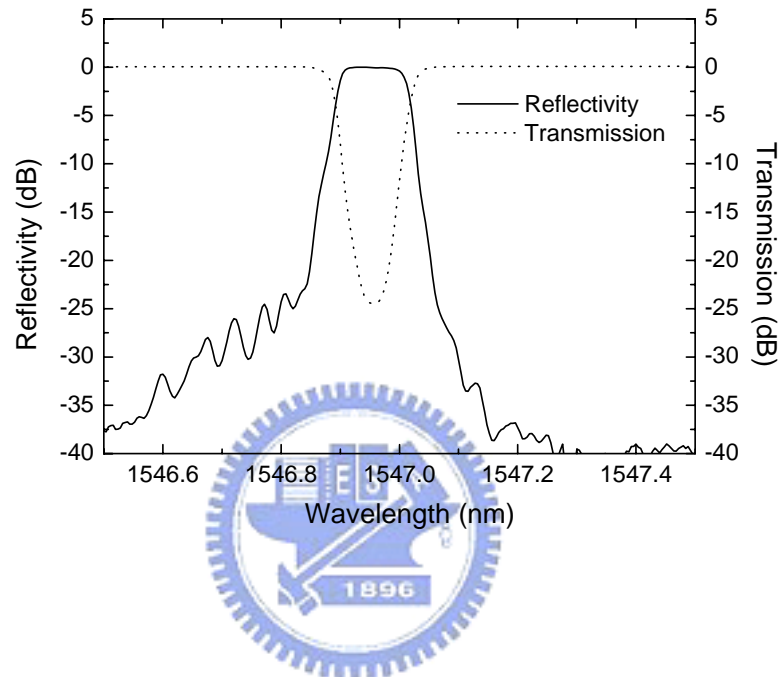


Fig. 4.35 The reflection and transmission spectra of a 75-mm long gaussian apodized FBG with a constant dc refractive index along the whole grating.

## Chapter 5. Conclusions and Future Work

### 5.1 Conclusions

FBGs have become more popular in various applications, which usually need special grating structure to achieve the required properties. For examples, a dispersion-free FBG with the structures of a sinc-index function and multiple- $\pi$  phase shifts has the property of a constant time delay in the stop band. A DFB fiber laser needs a  $\pi$ -phase shift in the middle of the grating structure and usually needs longer grating length for achieving single-mode lasing. For reaching the requirements of these applications, a useful inverse design method, some accurate measurement methods and some flexible fabrication methods have been proposed. In this thesis we firstly review the prior methods for setting the background of our research work. Then we proposed and developed some design, measurement and fabrication methods of the fiber gratings for realizing the advanced fiber grating fabrication.

In chapter 2 we firstly introduce the fundamental of the fiber grating structures, and then introduce the various FBG types for understanding their different properties. The theory of fiber Bragg gratings is based on the coupled-mode theory. From the theory, we studied the inverse scattering problem of finding the grating structure from a desired, complex reflection spectrum. We first applied the layer-peeling algorithm to the problem. The essence of this method is the following causality argument: The impulse response of the grating evaluated at time  $t=0$  corresponds directly to the front end of the coupling coefficient since the light does not have time to propagate deeper into the structure. Since the initial segment of  $q(z)$  can now be determined, one can then propagate the fields to the next section using the coupled-mode equations. In this way one is in the same situation as at the beginning, since the effect of the first layer is “peeled off”. The process is continued until the entire grating

structure is reconstructed. In order to realize the grating structure from the design result of the layer-peeling algorithm, we have used the least square method to find the exposure parameters of using small gaussian UV beams for sequential writing. We expect that these methods will be helpful for the fabrication of advanced FBGs.

In chapter 3 we proposed some methods for measuring the characteristics of the FBGs. These include the measurement of the complex reflection coefficient or the complex coupling coefficient of the grating. Based on the measurement of the phase spectrum which is using the balanced Michelson interferometer method, we have achieved the group time delay measurement with a resolution of about 5 ps. The measurement of the period change and the refractive index modulation is based on the side-diffraction techniques. Combined with these two measurement methods, we can get all of the information of the grating structures. This analysis process will be helpful for improving the fabrication of advanced FBGs.

In chapter 4 we introduced our auto-control exposure system which includes a high resolution position scanning system and other motorized control systems. The operation is controlled with the use of the Labview program to establish the more accurate fabrication process. For the fabrication of complex fiber grating structures, we have proposed three new exposure methods. One is the two-beam interferometer method with the polarization control, and another is the phase mask method with the polarization control. Both of them have the same purpose for achieving controllable ac-index profile in a single scan, and they can also keep the dc-index profile constant during the scan. The third method is the interferometric side-diffraction position monitoring technique for writing long fiber Bragg gratings. In the traditional position monitoring method, the position error would be accumulated. But the proposed method will not have the accumulative error of the fiber position. In this chapter, we have demonstrated that these new methods can indeed realize the long, complex fiber grating structures. They shall provide more options for practically fabricating advanced fiber gratings.

## 5.2 Future Work

In this thesis, we have proposed some new methods on the design, measurement and fabrication of FBGs for realizing the advanced FBG devices. We have also demonstrated that these methods could be combined for fabricating complex structure FBGs. Based on these methods, new integrated techniques need to be developed for achieving higher performance FBG devices in the further work. Some suggestions are given below for further investigation.

### **(1) To develop a more accurate measurement method for improving the FBG fabrication**

In chapter 3, we have shown an analysis method for obtaining the structure parameters of fiber gratings. In this development process, the proposed analysis method hopes not only to measure the accurate grating parameters but also to improve the FBG fabrication process. In order to achieve higher performance FBG devices, a real-time monitoring method of the FBG structure will be needed. Finding a new solution for accurately monitoring the FBG structures will be an important work.

### **(2) A real-time position monitoring technique for fabricating long, complex FBGs**

Although the developed side-diffraction position monitoring method has the ability to fabricate long fiber gratings, this method still has some limits for fabricating complex FBG structures which include the gratings of multiple- $\pi$  phase shifts and of weak index modulation ( $< 5 \times 10^{-6}$ ). How to overcoming these limits for achieving complex FBG fabrication will be a difficult and important research topic.

## List of Publications

### [Journal Paper]

1. Lih-Gen Sheu, **Kai-Ping Chuang**, and Yinchieh Lai, "Fiber Bragg grating dispersion compensator by single-period overlap-step-scan exposure," IEEE Photon. Technol. Lett., vol. 15, pp. 939-941, 2003.
2. **Kai-Ping Chuang**, Lih-Gen Sheu and Yinchieh Lai, "Complex fiber grating structures fabricated by sequential writing with polarization control," Optics Letters, vol. 29, pp. 340-342, 2004.
3. **Kai-Ping Chuang**, Lih-Gen Sheu and Yinchieh Lai, "Pure apodized phase-shifted fiber Bragg gratings fabricated by a two-beam interferometer with polarization control," IEEE Photon. Technol. Lett., vol. 16, pp. 834-836, 2004.

### [Conference Paper]

1. Lin-Gen Sheu, **Kai-Ping Chuang**, and Yinchieh Lai, "Phase-shifted fiber grating as a dispersion compensator," OPT2002, FG4-1, pp. 521-523.
2. Lin-Gen Sheu, **Kai-Ping Chuang**, and Yinchieh Lai, "Multi-channel dispersion compensating fiber grating by single-period overlap-step-scan exposure," CLEO/PR, TH4A-(8)-6, 2003.
3. **Kai-Ping Chuang**, Lih-Gen Sheu and Yinchieh Lai, "Complex fiber grating structures fabricated by use of sequential writing with polarization control," CLEO/PR, W2I-(8)-5, 2003.
4. **Kai-Ping Chuang**, Lih-Gen Sheu and Yinchieh Lai, "Complex fiber grating structures fabricated by using polarization control of the UV exposure beam," OFC, MF25, 2004.
5. **K.-P. Chuang**, I.-L. Wu and Y. Lai, "Interferometric side-diffraction position monitoring technique for writing long fiber Bragg gratings," CLEO/IQEC, CThM6, 2004.

[Patent]

1. **Kai-Ping Chuang**, Lih-Gen Sheu, Meng-Chang Tsai, and Yinchieh Lai “ Fabrication of complex fiber grating structures by use of sequential writing with polarization control,” submit to US patent.
2. **Kai-Ping Chuang**, Lih-Gen Sheu, Meng-Chang Tsai, and Yinchieh Lai “ Fabrication of true apodized fiber Bragg grating using a new two-beam interferometer with polarization control,” submit to US patent.
3. **莊凱評**，許立根，蔡孟璋，賴暎杰 “ 利用控制偏振逐段曝照方法製作複雜的光纖光柵結構 “ 中華民國專利審查中。
4. **莊凱評**，許立根，蔡孟璋，賴暎杰 “ 利用新型偏振控制雙光束干涉儀製造平均折射率係數平坦化之光纖光柵 “ 中華民國專利審查中。

